AN ABSTRACT OF THE THESIS OF

Edward Earnest Meyer for the degree of Doctor of Philosophy in Mechanical Engineering presented on May 3, 1982

Title: An Aeroelastic Analysis of the Darrieus Wind Turbine

Abstract approved: Redacted for privacy

Charles E. Smith

The stability of small oscillations of the troposkein-shaped blade used on Darrieus wind turbines is investigated. The blade is assumed to be attached to a perfectly rigid rotor shaft and spinning in still air. Linear equations of motion are derived which include the effects of in-plane, out-of-plane, and torsional stiffness, mass and aerodynamic center offsets, and the aerodynamic wake. Results presented include the free-vibration characteristics of the rotating blade, stability of the blade rotating in air, and the effects of mass density, mass center offset, and stiffness parameters on the flutter rotation rates. All results are presented in dimensionless form, hence apply to a family of blades.

AN AEROELASTIC ANALYSIS OF THE DARRIEUS WIND TURBINE

by

EDWARD EARNEST MEYER

A THESIS

submitted to

Oregon State University

in partial fulfillment of
the requirements for the
degree of
Doctor of Philosophy

Completed May 3, 1982

Commencement June 1982

APPROVED:

Redacted for privacy

Professor of Mechanical Engineering in charge of major

Redacted for privacy

Head of Department of Mechanical Engineering

Redacted for privacy

Dean of Graduate School

Date thesis is presented May 3, 1982

Typed by Edward Earnest Meyer

ACKNOWLEDGMENTS

I wish to express my deepest graditude to my advisor, Professor Charles Smith, for his inspiration and encouragment throughout the course of this research. I also wish to thank Professor Robert Thresher for his assistance, without which this project would have been impossible. Charles Pratt-Barlow of the Boeing Company has been the source of much inspiration, for which I am very grateful.

Too numerous to mention, but to whom I owe a great deal of appreciation are the many fine teachers I had while at Oregon State.

I would also like to thank the National Science Foundation for supporting me through an Energy Traineeship.

Last, but not least, I wish to thank all the family and friends who encouraged me to seek a higher education.

TABLE OF CONTENTS

LIST OF FIGURES

LIST OF TABLES

PREFACE

Nomenclature

Throughout this thesis **bold** letters indicate vectors (lower case) or matrices (upper case). The term blade axis refers to an imaginary line in the blade which has the shape of a tropo-skien; this is not to be confused with the rotor axis, about which the blades spin.

a	aspect ratio of the area swept by the blade
A	unsteady aerodynamic force matrix
b	semichord of the blade cross-section
b	intrinsic binormal unit vector
c	curvature of the deformed blade
$\underline{c}$	curvature of the undeformed blade
C	centrifugal force matrix $\mathbf{M}_0 + \mathbf{K}_0$
e_a	dimensionless distance from blade axis to the midchord of a cross-section (positive aft) in semichords.
e_m	dimensionless distance from the blade axis to the center of gravity of a cross-section (positive aft) in semichords.
e_r	dimensionless radius of gyration of a cross-section about the blade axis (in semichords)
EA	stiffness constant for blade extension
EI	stiffness constant for bending in the plane of the blade.
g	growth rate coefficient of the oscillations.
g_s	structural damping coefficient
G	gyroscopic matrix
GJ	torsional stiffness constant
h	semispan of the blade

i $(-1)^{\frac{1}{2}}$

k_j $(j=1,2,3)$ stiffness ratios

$\mathbf{K}_j$ $(j=0,1,2,3,4)$ stiffness matrices

k^* reduced frequency ω/Ω

m mass per unit length of the blade

m^* mass density ratio $m/\pi\rho b^2$

$\mathbf{M}$ mass matrix

$\mathbf{M}_0$ centrifugal force matrix

n order of the characteristic equations

$\underline{n}$ number of discretization intervals

$\mathbf{n}$ intrinsic normal unit vector

p characteristic exponent $\omega(\frac{1}{2}g + i)$

p^* dimensionless characteristic exponent $p(mh^4/EI)^{\frac{1}{2}}$

P tension in the undeformed spinning blade

P^* dimensionless tension $P/m\Omega^2h^2$

q torsion of the blade axis

$\mathbf{q}_j$ vector of cubic splines for the j^{th} variable

r dimensionless rotation rate $\Omega(mh^4/EI)^{\frac{1}{2}}$

s arc-length along the deformed blade with origin at mid-span

$\underline{s}$ arc-length along the undeformed blade with origin at mid-span

s^* dimensionless arc-length $\underline{s}/h$

t time

$\mathbf{t}$ intrinsic tangent unit vector

$\mathbf{u}$ vector of generalized coordinates

$\underline{x}_j$ $(j=1,2,3)$ coordinates of the undeformed blade axis

y_j $(j=1,2,3)$ displacements in the x_j directions

θ angular displacement of a cross-section about the local tangent

θ_j $(j=2,3)$ Euler angles describing the orientation of a cross-section

ω frequency of oscillation

Ω rotor spin rate (radians/sec)

ρ density of air

AN AEROELASTIC ANALYSIS OF THE DARRIEUS WIND TURBINE

I. INTRODUCTION

The Darrieus wind turbine is a vertical axis wind powered turbine which has blades formed in the shape known as a troposkien. Figure 1 shows a Darrieus wind turbine with three troposkein-shaped blades. A troposkein is the theoretical shape taken by a perfectly flexible rope with the ends fixed to a spinning shaft. This term was coined by Blackwell (Reference 1) from the greek words tropos (turning) and skeinion (rope). The original concept of this wind turbine dates back to 1931 when G. J. M. Darrieus patented it (Reference 2), although the idea was apparently independently developed by South (Reference 3) in the early 1970's.

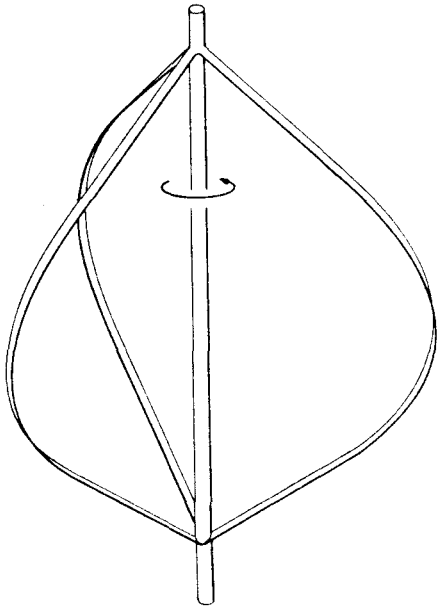

Figure 1. A Three-Bladed Darrieus Rotor

The advantage to troposkein-shaped blades is that the spinning blades are not subjected to bending stresses caused by centrifugal forces, since they have precisely the shape that centrifugal forces would like them to have. Hence the blades are theoretically in pure tension. This is a significant advantage because long, slender blades such as these can easily develop large bending stresses, which tend to fatique the blade, particularly in view of the cyclical nature of the operation of a typical wind turbine. Thus, for example, helicopter blades tend to have relatively short life-spans on account of fatique.

One of the contributing factors to the short fatique life of helicopter blades is vibration. While a certain amount of vibration in helicopter blades is due to the engine, an equally important source is the interaction of the blade with the surrounding air. Under some circumstances, vibrations induced by aerodynamic forces can lead to a catastrophic condition known as flutter. The study of the conditions under which an elastic body flutters is one of the concerns of the field known as aeroelasticity.

The aeroelastic stability of the Darrieus wind turbine has received little attention in the literature, primarily because it was not seriously considered as an alternative to the more conventional horizontal axis wind turbine until the early 1970's. The horizontal axis wind turbine, on the other hand, is similar to a helicopter rotor and although significant differences exist between them, the extensive research which has been done on helicopter rotors over the past thirty years has provided a solid foundation for the aeroelastic analysis of horizontal axis wind turbines. Unfortunately, no such background exists for the Darrieus rotor, so a more basic approach is necessary.

This study then is concerned with the aeroelastic stability of the Darrieus wind turbine with a view towards identifying the parameters which are most important in designing flutter-free blades. Because of the complex geometry of the Darrieus blades it was deemed necessary to use a computer model of the dynamic behavior of the blade; this is in contrast with the only other aeroelastic study of the Darrieus blade (Reference 4) in which simplified equations were developed which resulted in a closed-form analytical solution for the flutter speeds. The scope of the present study is somewhat broader and more detailed.

One of the fundamental questions which an aeroelastic study such as this tries to answer is: how fast can the Darrieus be spun without causing the blades to flutter? Perhaps a more important question in terms of preventing flutter instabilities is: what causes the blade to flutter? Once the mechanism behind the flutter instabilities is known it is of interest to see the effects of varying some of the parameters which describe the model, such as stiffnesses and mass of the blade. Answering these questions is one of the primary objectives of this study.

As mentioned before, a computer model was used to investigate the behavior of the Darrieus blade; no experimental models such as wind tunnel models, were used, nor were the results of any tests available. The primary reason for the lack of available data on flutter in actual working models is that flutter is exceedingly difficult to test for experimentally, largely due to the destructive nature of flutter. These two types of investigation, model or prototype testing and computer modelling, have somewhat different purposes, although they can complement one another. With computer modelling it is usually hoped to gain insight into the phenomenon being studied, rather than actual numbers, whereas model testing is usually concerned with ensuring that a particular configuration is

free from flutter. That is, the results of a computer study can apply to a wide variety of configurations, while a model test is limited to one particular configuration. The purpose of this study then is not to analyse a particular Darrieus wind turbine, but rather to investigate Darrieus wind turbines in general in regards to aeroelastic stability.

Due to the lack of previous analyses of the Darrieus wind turbine, it was necessary to derive equations of motion from basic principles. This is the subject of chapter II and appendix A. The techniques commonly used to solve flutter equations were found to be inadequate in this case, possibly because of the presence of gyroscopic forces. Thus a considerable amount of effort went into developing a method which worked well in this case. The technique, based on the continuation methods of structural mechanics, is described in chapter III and appendix B. Results are presented in chapter IV and conclusions in chapter V.

Throughout this thesis, equations are numbered consecutively within each section; thus equation II.2.25 refers to equation (25) in section II.2.

II. EQUATIONS OF MOTION

II.1 Basic Assumptions

In this chapter linear equations governing the motion of a single Darrieus blade spinning at a constant rotation rate in still air are developed. The equations of motion are derived by developing expressions for the kinetic and potential energy and the aerodynamic forces per unit length of the blade span. An integration along the blade span results in the total kinetic and potential energies and the generalized forces on the blade, which may then be used in Lagrange's equations to arrive at equations of motion.

The cross-section of the blade is assumed to be uniform along the blade span, with the shape of a symmetric airfoil. Furthermore, this cross-sectional shape is assumed to remain undistorted during any motion of the blade. Hence the position and orientation of each element of the blade may be described using four variables: three displacements and one rotation. These four variables are functions of time and distance along the blade, and completely describe the configuration of the blade during any motion.

By retaining only terms which are quadratic or lower order in the displacements, the expressions for kinetic and potential energy will result in equations of motion which are linear in the displacements. In the expressions for aerodynamic forces it is necessary to retain only linear terms in the displacements, or equivalently, quadratic terms in the expression for the virtual work of these forces.

These expressions are differential forms involving partial derivatives with respect to the distance along the blade (s) and time. From these expressions it is possible to develop partial differential equations of motion using Lagrange's equations. In order to obtain a numerical solution of the equations of motion, the spatial dependence is commonly eliminated by discretizing the spatial variable, resulting in ordinary rather than partial differential equations. This method is usually referred to as Galerkin's method (Reference 5). Alternatively, we could discretize the partial differential expressions for kinetic energy, potential energy and the aerodynamic forces before applying Lagrange's equations; this technique is sometimes referred to as the assumed modes method (Reference 5), although because of the close connection between this method and the finite element method it has also been termed the abstract finite element method (Reference 6). These two approaches are completely equivalent, but the second approach is much less cumbersome, hence less prone to error. For this reason we use the second method to develop equations of motion in ordinary differential form. We therefore need only write expressions for kinetic energy, potential energy, and the aerodynamic forces on a differential element of blade, substitute the discretizing functions, and integrate along the blade to obtain expressions involving derivatives with respect to time only. Application of Lagrange's equations results in a system of linear ordinary differential equations describing the motion of the blade. By making the usual assumption of harmonic motion these equations are reduced to a system of complex algebraic characteristic equations known as the flutter equations (Reference 7).

II.2 Geometry

Before deriving equations of motion it is first necessary to describe the blade in geometric terms and define sets of coordinate systems which will make the derivations easier. In addition, we make some assumptions regarding the geometry of the blade.

The undeformed blade is assumed to have the theoretical shape known as a troposkien (Reference 1), with a uniform cross-section along the blade span. The cross-sectional shape is that of a thin, symmetric airfoil with chord length 2b. Furthermore, it is assumed that there is a reference line, hereafter referred to as the blade axis, which remains fixed relative to the blade during any blade motion. This axis is assumed to pass through each cross-section at a fixed point on the chord or line of symmetry of the cross-section. The point of intersection of the axis with a cross-section is referred to as the axis location, and is defined by the distance between this point and the mid-chord of the cross-section. Since the cross-section is constant along the blade and the axis passes through the same point at each cross-section, the axis of the undeformed blade is a plane curve. Stricly speaking, it is the undeformed blade axis which has the shape of a troposkien.

The position of a point on the undeformed axis is described by a vector $\underline{x}$ with components $\underline{x}_1$, $\underline{x}_2$, and $\underline{x}_3$ in the $\mathbf{x}_1$, $\mathbf{x}_2$, and $\mathbf{x}_3$ directions, respectively, as shown in figure 2. $\mathbf{x}_1$ is a unit vector parallel to the wind turbine spin axis, while $\mathbf{x}_2$ is a unit vector which lies in the plane of the undeformed blade and intersects the blade axis at the semi-span of the blade. Thus the undeformed blade lies in the $\mathbf{x}_1$-$\mathbf{x}_2$ plane. $\mathbf{x}_3$ is a unit vector

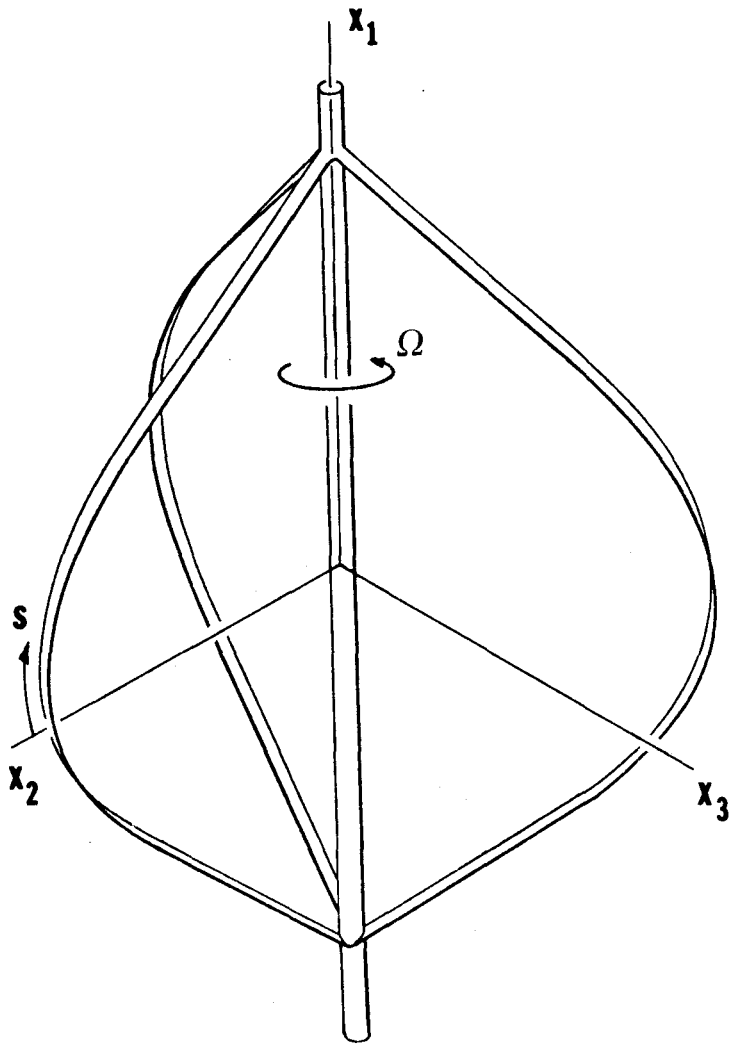

Figure 2. **x** Coordinate System

perpendicular to the x_1-x_2 plane. The x_1-x_2-x_3 coordinate system is thus fixed to the reference frame of the undeformed blade and therefore rotates with the blade.

If we denote the arc-length along the axis with origin at the blade semi-span by $\underline{s}$, then the axis can be described parametrically by $\underline{\mathbf{x}}(\underline{s})$. A point on the axis of the deformed blade is described by a vector

$$\mathbf{x}(\underline{s},t) = \underline{\mathbf{x}}(\underline{s}) + \mathbf{y}(\underline{s},t) \tag{1}$$

where $\mathbf{y}(\underline{s},t)$ is a postion vector relating a point on the deformed blade axis to the corresponding point on the undeformed axis, hence is a function of time and the position on the blade. In component form

$$\mathbf{y}(\underline{s},t) = y_1(\underline{s},t)\mathbf{x}_1 + y_2(\underline{s},t)\mathbf{x}_2 + y_3(\underline{s},t)\mathbf{x}_3 \tag{2}$$

It will prove useful in the sequel to introduce two additional coordinate systems which are based on the geometry of the undeformed and deformed blade axes. These are the so-called intrinsic coordinate systems for space curves (Reference 8).

An arbitrary curve in space has associated with it a set of mutually perpendicular unit vectors known as the tangent, normal, and binormal vectors. If the curve is described in parametric form by

$$\mathbf{x}(s) = x_1(s)\mathbf{x}_1 + x_2(s)\mathbf{x}_2 + x_3(s)\mathbf{x}_3 \tag{3}$$

then the unit tangent vector is defined by

$$\mathbf{t}(s) = \mathbf{x}'(s) = x_1'(s)\mathbf{x}_1 + x_2'(s)\mathbf{x}_2 + x_3'(s)\mathbf{x}_3 \tag{4}$$

The unit normal vector is defined by

$$\mathbf{n}(s) = \frac{1}{c}\,\mathbf{t}'(s) \tag{5}$$

where $c^2 = \mathbf{t}'\cdot\mathbf{t}'$ is the curvature at s. Finally, the unit binormal is defined by

$$\mathbf{b}(s) = \mathbf{t} \times \mathbf{n} = \frac{1}{q}\,(\mathbf{n}' + c\mathbf{t}) \tag{6}$$

where $q = \mathbf{n}'\cdot\mathbf{b}$ is known as the torsion of the curve. The following equations, known as the Frenet formulas, describe the rates of change of these vectors:

$$\begin{aligned} \mathbf{t}' &= c\mathbf{n} \\ \mathbf{n}' &= q\mathbf{b} - c\mathbf{t} \\ \mathbf{b}' &= -q\mathbf{n} \end{aligned} \tag{7}$$

Applying these definitions to the undeformed blade axis we define an intrinsic coordinate system with base vectors $\underline{\mathbf{t}}$, $\underline{\mathbf{n}}$, and $\underline{\mathbf{b}}$. Likewise, at each point on the deformed axis we define an intrinsic coordinate system with base vectors **t**, **n** and **b**. Figure 3 shows the intrinsic base vectors at a typical section of the undeformed and the deformed blade. In addition to the displacement **y**, we allow sections of the blade to rotate about the tangent vector; this rotation is described by the angle θ between the blade chord and the binormal vector (see figure 3). The position and orientation of a section of the blade is completly described by the intrinsic base vectors and θ. It remains to derive expressions for the base vectors in terms of the displacements (**y**); to this end we introduce a sequence of Euler angles (θ_2, θ_3) relating the undeformed and the deformed

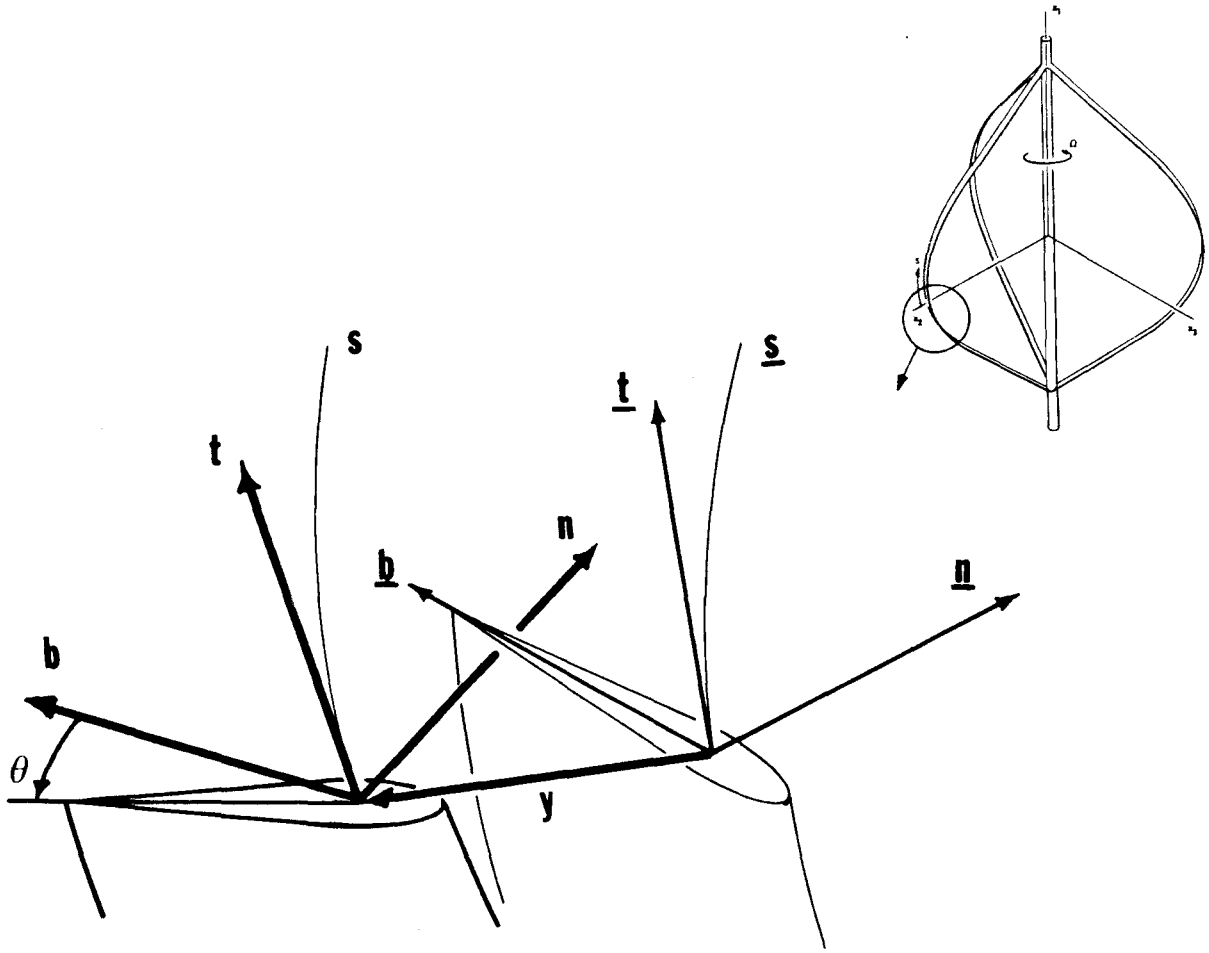

Figure 3. Intrinsic Base Vectors

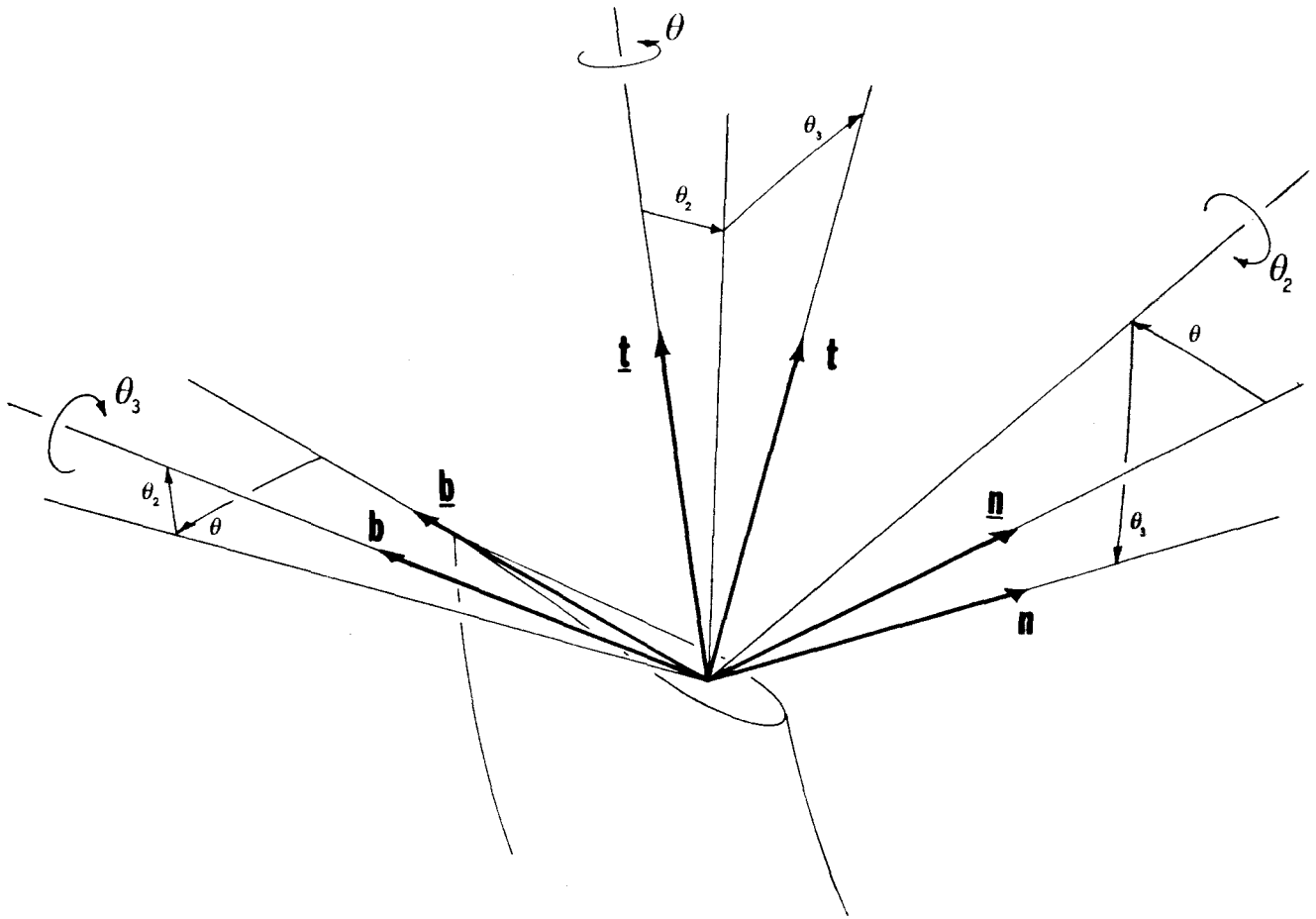

Figure 4. Euler Angles Describing the Orientation of a Section

axis orientations as shown in figure 4.

The axis of the undeformed blade lies in the $\mathbf{x}_1$-$\mathbf{x}_2$ plane, so that

$$\underline{\mathbf{t}}(\underline{s}) = \underline{\mathbf{x}}'(\underline{s}) = \underline{x}_1'(\underline{s})\mathbf{x}_1 + \underline{x}_2'(\underline{s})\mathbf{x}_2 \tag{9}$$

Furthermore, the normal vector

$$\underline{\mathbf{n}}(\underline{s}) = \frac{1}{\underline{c}}\,\underline{\mathbf{t}}'(\underline{s}) = \frac{1}{\underline{c}}\,(\underline{x}_1''(\underline{s})\mathbf{x}_1 + \underline{x}_2''(\underline{s})\mathbf{x}_2) \tag{10}$$

and the binormal vector

$$\underline{\mathbf{b}}(\underline{s}) = \underline{\mathbf{t}}(\underline{s}) \times \underline{\mathbf{n}}(\underline{s}) = \frac{1}{\underline{c}}(\underline{x}_1'\underline{x}_2'' - \underline{x}_1''\underline{x}_2')\mathbf{x}_3 \tag{11}$$

Note that since $\underline{\mathbf{b}} = -\mathbf{x}_3$,

$$\underline{c} = \underline{x}_1''\underline{x}_2' - \underline{x}_1'\underline{x}_2'', \tag{12}$$

and $\underline{\mathbf{b}}' = 0$. Differentiating the relationship

$$\underline{\mathbf{t}}\cdot\underline{\mathbf{t}} = \underline{x}_1'^2 + \underline{x}_2'^2 = 1 \tag{13}$$

results in

$$\underline{x}_1'\underline{x}_1'' + \underline{x}_2'\underline{x}_2'' = 0 \tag{14}$$

which allows us to write (12) as

$$\underline{c} = \underline{x}_2'\underline{x}_1'' + \frac{\underline{x}_1'^2}{\underline{x}_2'}\,\underline{x}_1'' = \frac{\underline{x}_1''}{\underline{x}_2'} \tag{15}$$

and, using (10), (13), and (14) it is easily verified that

$$\underline{\mathbf{n}} = \underline{\mathbf{x}}_2'\mathbf{x}_1 - \underline{\mathbf{x}}_1'\mathbf{x}_2 \tag{16}$$

Thus in terms of the **x** coordinates,

$$\begin{bmatrix} \underline{\mathbf{t}} \\ \underline{\mathbf{n}} \\ \underline{\mathbf{b}} \end{bmatrix} = \begin{bmatrix} \underline{\mathbf{x}}_1' & \underline{\mathbf{x}}_2' & 0 \\ \underline{\mathbf{x}}_2' & -\underline{\mathbf{x}}_1' & 0 \\ 0 & 0 & -1 \end{bmatrix} \begin{bmatrix} \mathbf{x}_1 \\ \mathbf{x}_2 \\ \mathbf{x}_3 \end{bmatrix} \tag{17}$$

The base vectors **t**, **n**, and **b** for the deformed blade axis may be written in terms of the Euler angles and the $\underline{\mathbf{t}}$, $\underline{\mathbf{n}}$, and $\underline{\mathbf{b}}$ vectors as

$$\begin{bmatrix} \mathbf{t} \\ \mathbf{n} \\ \mathbf{b} \end{bmatrix} = \begin{bmatrix} \cos\theta_2\cos\theta_3 & \sin\theta_3 & -\sin\theta_2\cos\theta_3 \\ -\cos\theta_2\sin\theta_3 & \cos\theta_3 & \sin\theta_2\sin\theta_3 \\ \sin\theta_2 & 0 & \cos\theta_2 \end{bmatrix} \begin{bmatrix} \underline{\mathbf{t}} \\ \underline{\mathbf{n}} \\ \underline{\mathbf{b}} \end{bmatrix} \tag{18}$$

which for small angles may be written as

$$\begin{bmatrix} \mathbf{t} \\ \mathbf{n} \\ \mathbf{b} \end{bmatrix} = \begin{bmatrix} 1 & \theta_3 & -\theta_2 \\ -\theta_3 & 1 & 0 \\ \theta_2 & 0 & 1 \end{bmatrix} \begin{bmatrix} \underline{\mathbf{t}} \\ \underline{\mathbf{n}} \\ \underline{\mathbf{b}} \end{bmatrix} \tag{19}$$

Evidently the Euler angles (θ_2, θ_3) are functions of the displacement vector **y**; we next develop explicit expressions for θ_2 and θ_3 in terms of the displacements. From the definition of

the tangent vector,

$$\mathbf{t} = \frac{d}{ds}(\underline{\mathbf{x}} + \mathbf{y}) = \frac{d}{d\underline{s}}(\underline{\mathbf{x}} + \mathbf{y})(\frac{ds}{d\underline{s}})^{-1} = (\underline{\mathbf{t}} + \mathbf{y}')(\frac{ds}{d\underline{s}})^{-1} \tag{20}$$

Recalling the fact that the tangent vector has unit length,

$$(\frac{ds}{d\underline{s}})^2 = 1 + 2\mathbf{t}\cdot\mathbf{y}' + \mathbf{y}'\cdot\mathbf{y}' \tag{21}$$

and writing

$$\begin{aligned}
\mathbf{y}(\underline{s}) &= y_1\mathbf{x}_1 + y_2\mathbf{x}_2 + y_3\mathbf{x}_3 \\
&= (\underline{x}_1'y_1 + \underline{x}_2'y_2)\underline{\mathbf{t}} + (\underline{x}_2'y_1 - \underline{x}_1'y_2)\underline{\mathbf{n}} - y_3\underline{\mathbf{b}}, \\
\mathbf{y}'(\underline{s}) &= y_1'\mathbf{x}_1 + y_2'\mathbf{x}_2 + y_3'\mathbf{x}_3 \\
&= (\underline{x}_1'y_1' + \underline{x}_2'y_2')\underline{\mathbf{t}} + (\underline{x}_2'y_1' - \underline{x}_1'y_2')\underline{\mathbf{n}} - y_3'\underline{\mathbf{b}}
\end{aligned} \tag{22}$$

results in

$$(\frac{ds}{d\underline{s}})^2 = 1 + 2(\underline{x}_1'y_1' + \underline{x}_2'y_2') + y_1'^2 + y_2'^2 + y_3'^2 \tag{23}$$

which expresses the elongation of the deformed blade axis in terms of the displacements. Substituting (22) into (20) and linearizing yields

$$\mathbf{t} = \underline{\mathbf{t}} + (\underline{x}_2'y_1' - \underline{x}_1'y_2')\underline{\mathbf{n}} - y_3'\underline{\mathbf{b}} \tag{24}$$

Comparing (19) and (24) we conclude that

$$\theta_2 = y_3' \tag{25}$$

$$\theta_3 = \underline{x}_2'y_1' - \underline{x}_1'y_2'$$

Hence the transformation from the undeformed intrinsic base vectors to the deformed base vectors is

$$\begin{bmatrix} \mathbf{t} \\ \mathbf{n} \\ \mathbf{b} \end{bmatrix} = \begin{bmatrix} 1 & \underline{x}_2'y_1' - \underline{x}_1'y_2' & -y_3' \\ -(\underline{x}_2'y_1' - \underline{x}_1'y_2') & 1 & 0 \\ y_3' & 0 & 1 \end{bmatrix} \begin{bmatrix} \underline{\mathbf{t}} \\ \underline{\mathbf{n}} \\ \underline{\mathbf{b}} \end{bmatrix} \tag{26}$$

or in terms of the $\mathbf{x}_1$, $\mathbf{x}_2$, $\mathbf{x}_3$ base vectors,

$$\begin{bmatrix} \mathbf{t} \\ \mathbf{n} \\ \mathbf{b} \end{bmatrix} \begin{bmatrix} T_{11} & T_{12} & T_{13} \\ T_{12} & T_{22} & 0 \\ \underline{x}_1'y_3' & \underline{x}_2'y_3' & -1 \end{bmatrix} \begin{bmatrix} \mathbf{x}_1 \\ \mathbf{x}_2 \\ \mathbf{x}_3 \end{bmatrix} \tag{27}$$

where

$$T_{11} = \underline{x}_1' + \underline{x}_2'(x_2'y_1' - x_1'y_2')$$

$$T_{12} = \underline{x}_2' - \underline{x}_1'(\underline{x}_2'y_1' - \underline{x}_1'y_2')$$

$$T_{22} = -\underline{x}_1' - \underline{x}_2'(\underline{x}_2'y_1' - \underline{x}_1'y_2')$$

II.3 Strain Energy

The potential energy of the blade consists of strain energy due to linear elastic deformations. Expressions for the elastic strain energy will be derived using engineering beam theory; that is, it is assumed that plane cross-sections which are initially normal to the axis tangent remain plane and normal to the axis tangent. This hypothesis, known as the Euler-Bernoulli hypothesis, implies that a cross-section of the blade which is initially in the plane of the intrinsic normal and binormal vectors remains in the plane of the normal and binormal vectors of the deformed blade axis. In addition, we allow plane sections to rotate about the tangent to the axis through an angle θ. Thus the strain energy of the blade will consist of strain energy due to elongation of longitudinal fibers and twisting of the blade about the local tangent. For the torsional strain energy we use St-Venant's theory which states that the torsional strain energy is proportional to the square of the rate of twist with respect to $\underline{s}$.

Although others have treated the problem of strain energy in a curved beam, there are two characteristics which have apparently not been previously accounted for: centrifugal forces due to spinning, and the troposkien shape. Ojalvo (Reference 9) treated out-of-plane and twisting vibrations in inextensible, incomplete (semi-circular) rings. Fettahlioglu and Mayers (Reference 10) dealt with in-plane bending and axis extension in beams of constant curvature, and Archer (Reference 11) studied the in-plane vibrations of inextensible, incomplete rings. In order to include the effects of axis extension, centrifugal forces and the geometry of the troposkien-shaped blade, it is therefore necessary to develop an expression for

the strain energy from basic principles.

Apart from the strain energy induced by vibratory deformations, the spinning blade will have a certain strain energy due to centrifugal forces. Ideally, these centrifugal forces will result in strictly axial deformations in the troposkien-shaped blade. Indeed, the fact that the troposkien shape results in no bending moments (in the absence of vibration) is one of the prime advantages to this shape. Here we assume that the undeformed spinning blade is in a state of pure tension, so the extension of a fiber in the vibrating blade is the sum of the extension due to the initial centrifugal tension ($P(\underline{s})$) and the extension due to the displacement and twist of the section ($\mathbf{y},\theta$).

The strain energy per unit length of the blade due to elongation of blade fibers and torsion about the axis will have the form

$$V'(\underline{s}) = \iint E(e_0 + e)^2 \, dA + GJ\theta_t^2$$

$$= \iint Ee_0^2 dA + 2\iint Ee_0 e \, dA + \iint Ee^2 \, dA + GJ\theta_t^2 \quad (1)$$

where E is the modulus of elasticity, e_0 is the elongation due to centrifugal tension, e is the elongation of a fiber, G is the shear modulus, J is the St-Venant torsion constant, θ_t is the twist rate, and the integrals are over the cross-sectional area of the blade. Once again, ()' denotes differentiation with respect to $\underline{s}$, the arc-length along the undeformed blade axis. The first integral on the right-hand side of (1) is not a function of the displacements, hence will not appear in the equations of motion. It will prove useful in deriving an expression for the potential energy in terms of the

displacements to investigate the form of (1) and make further assumptions regarding the strain energy in the blade.

The most important assumption we make regarding the strain energy is that the blade is very thin relative to both the span and the radius of curvature at any point on the blade. We therefore assume a linear distribution of strain throughout the cross-section. Locating the fibers relative to the axis by a vector

$$\underline{\rho}(\underline{s}) = \underline{\rho}_2\underline{n} + \underline{\rho}_3\underline{b} \tag{2a}$$

allows us to write the elongation of a fiber in the form

$$e = e_1 + e_2\underline{\rho}_2/h + e_3\underline{\rho}_3/h \tag{2b}$$

where h is the blade semi-span. Furthermore, if we locate the blade axis such that

$$\iint E\underline{\rho}_2 dA = \iint E\underline{\rho}_3 dA = \iint E\underline{\rho}_2\underline{\rho}_3 dA = 0 \tag{2c}$$

and define

$$\iint E\underline{\rho}_2^2 dA = EI$$

$$\iint E\underline{\rho}_3^2 dA = k_1 EI$$

$$k_2 = EI/GJ \tag{2d}$$

$$EA = k_3 EI/h^2$$

$$P(\underline{s}) = \iint Ee_0 dA$$

where EI is the stiffness constant for in-plane bending, k_1 is the ratio of out-of-plane to in-plane bending stiffnesses, P is the tension, and k_3 is the ratio of axial to in-plane stiffnesses, then the strain energy expression (1) may be written as

$$V'(\underline{s}) = 2Pe_1 + k_3 EIe_1^2 + EIe_2^2/h^2 + k_1 EIe_3^2/h^2 + k_2 EI\theta_t^2 \qquad (2e)$$

From this equation we see that if the potential energy is to contain no higher than second order terms in the displacements, then e_1 may have quadratic displacement terms, but e_2 and e_3 must be linear. Moreover, the twist rate must also be linear in the displacements.

To derive an expression for the elongation of an arbitrary fiber, consider the following four arcs as shown in figure 5:

1) an arc along the undeformed blade axis with arc-length $\underline{s}$.
2) an arc along a fiber in the undeformed blade which intersects a cross-section at $\underline{\mathbf{x}} + \underline{\mathbf{p}}$ and has arc-length $\underline{s}^+$.
3) an arc along the deformed blade axis with arc-length s.
4) an arc along the same blade fiber as in 2) in the deformed blade with arc-length s^+.

The extension of an arbitrary fiber is then given by

$$2e = \left(\frac{ds^+}{d\underline{s}^+}\right)^2 - 1 = \left(\frac{ds^+}{ds}\right)^2 \left(\frac{ds}{d\underline{s}}\right)^2 \left(\frac{d\underline{s}}{d\underline{s}^+}\right)^2 - 1 \qquad (3)$$

The derivatives in this expression may be evaluated by considering the tangent vectors to the arcs in (2 - 4) above.

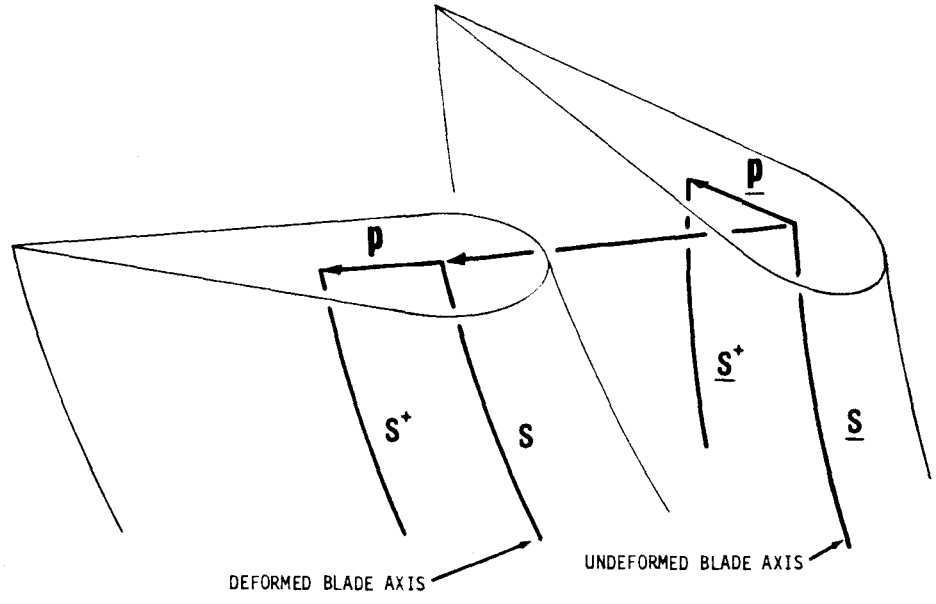

Figure 5. Blade Fibers

2) Undeformed blade fiber

The intersection of an arbitrary blade fiber with a cross-section in the undeformed blade is located by

$$\underline{\mathbf{x}}^{+}(\underline{s}) = \underline{\mathbf{x}}(\underline{s}) + \underline{\mathbf{p}} = \underline{\mathbf{x}} + \underline{p_2}\underline{\mathbf{n}} + \underline{p_3}\underline{\mathbf{b}} \tag{4}$$

Thus the tangent vector to the fiber is

$$\underline{\mathbf{t}}^{+} = \frac{d}{d\underline{s}^{+}}(\underline{\mathbf{x}}^{+}) = \frac{d}{d\underline{s}}(\underline{\mathbf{x}} + \underline{\mathbf{p}})(\frac{d\underline{s}}{d\underline{s}^{+}}) = \underline{\mathbf{t}}(1 - \underline{cp_2})(\frac{d\underline{s}}{d\underline{s}^{+}}) \tag{5}$$

Since $\underline{\mathbf{t}}^{+} \cdot \underline{\mathbf{t}}^{+} = 1$,

$$(\frac{d\underline{s}}{d\underline{s}^{+}})^2 = (1 - \underline{cp_2})^{-2} = 1 + 2\underline{cp_2} \tag{6}$$

where it is assumed that $\underline{cp_2}$ is much less than 1; that is, the radius of curvature of the blade is much larger than the section thickness.

3) Deformed axis

Equation (II.2.23) expresses the second of the derivatives in terms of the displacements:

$$(\frac{d\underline{s}}{d\underline{s}})^2 = 1 + 2(\underline{x}_1' y_1' + \underline{x}_2' y_2') + y_1'^2 + y_2'^2 + y_3'^2 \tag{7}$$

4) Deformed blade fiber

A fiber which intersects a cross-section in the undeformed blade at $\mathbf{x}^{+} = \underline{\mathbf{x}} + \underline{\mathbf{p}}$ will intersect the cross-section in the deformed blade at

$$\mathbf{x}^{+} = \underline{\mathbf{x}} + \mathbf{y} + \mathbf{p} \tag{8}$$

where $\mathbf{p}$ locates the intersection relative to the deformed blade axis. The assumption that plane cross-sections remain plane and perpendicular to the blade axis implies that

$$\mathbf{p} = (\underline{p}_2\cos\theta - \underline{p}_3\sin\theta)\mathbf{n} + (\underline{p}_3\cos\theta + \underline{p}_2\sin\theta)\mathbf{b} = p_2\mathbf{n} + p_3\mathbf{b} \quad (9)$$

The tangent to the deformed blade fiber is defined as

$$\mathbf{t}^+ = \frac{d\mathbf{x}^+}{ds^+} = \frac{d}{ds}(\underline{\mathbf{x}} + \mathbf{y} + \mathbf{p})(\frac{ds^+}{ds})^{-1}$$

$$= (\mathbf{t} + \frac{d\mathbf{p}}{ds})(\frac{ds^+}{ds})^{-1} \quad (10)$$

Recalling the transformation (II.2.26) and neglecting the effect of axis elongation (i.e. $\frac{ds}{d\underline{s}} = 1$),

$$\frac{d\mathbf{p}}{ds} = \frac{d}{d\underline{s}}(p_2\mathbf{n} + p_3\mathbf{b})(\frac{ds}{d\underline{s}})^{-1} \quad (11)$$

$$= \frac{d}{d\underline{s}}\left\{ p_2\underline{\mathbf{n}} - p_2(\underline{x}_2'y_1' - \underline{x}_1'y_2')\underline{\mathbf{t}} + p_3(\underline{\mathbf{b}} + y_3'\underline{\mathbf{t}}) \right\}$$

$$= p_2'\underline{\mathbf{n}} - p_2\underline{c\mathbf{t}} - p_2'(\underline{x}_2'y_1' - \underline{x}_1'y_2')\underline{\mathbf{t}}$$

$$- p_2(\underline{x}_2''y_1' + \underline{x}_2'y_1'' - \underline{x}_1''y_2' - \underline{x}_1'y_2'')\underline{\mathbf{t}}$$

$$- p_2(\underline{x}_2'y_1' - \underline{x}_1'y_2')\underline{c\mathbf{n}}$$

$$+ p_3'(\underline{\mathbf{b}} + y_3'\underline{\mathbf{t}}) + p_3(y_3''\underline{\mathbf{t}} + y_3'\underline{c\mathbf{n}})$$

Making use of equations II.2.14 and II.2.15,

$$\underline{x}_2''y_1' - \underline{x}_1''y_2' = -\frac{\underline{x}_1'}{\underline{x}_2'}\underline{x}_1''y_1' - \underline{x}_1''y_2'$$

$$= - \frac{\underline{x}_1''}{\underline{x}_2'} (\underline{x}_1'y_1' + \underline{x}_2'y_2') \qquad (12)$$

$$= - \underline{c}(\underline{x}_1'y_1' + \underline{x}_2'y_2')$$

Retaining only linear terms in θ,

$$\begin{aligned} p_2 &= \underline{p}_2 - \underline{p}_3\theta \\ p_2' &= - \underline{p}_3\theta' \\ p_3 &= \underline{p}_3 + \underline{p}_2\theta \\ p_3' &= \underline{p}_2\theta' \end{aligned} \qquad (13)$$

Neglecting terms according to (2),

$$\begin{aligned} \frac{d\mathbf{p}}{ds} = &- \underline{p}_3\theta'\underline{\mathbf{n}} - \underline{c}\underline{p}_2\underline{\mathbf{t}} + \underline{c}\underline{p}_3\theta\underline{\mathbf{t}} + \underline{c}\underline{p}_2(\underline{x}_1'y_1' + \underline{x}_2'y_2')\underline{\mathbf{t}} \\ &- \underline{p}_2(\underline{x}_2'y_1'' - \underline{x}_1'y_2'')\underline{\mathbf{t}} - \underline{c}\underline{p}_2(\underline{x}_2'y_1' - \underline{x}_1'y_2')\underline{\mathbf{n}} \\ &+ \underline{p}_2\theta'\underline{\mathbf{b}} + \underline{p}_3y_3''\underline{\mathbf{t}} + \underline{c}\underline{p}_3y_3'\underline{\mathbf{n}} \end{aligned} \qquad (14)$$

So that

$$\begin{aligned} (\frac{ds^+}{ds})\mathbf{t}^+ = &\{ 1 - \underline{c}\underline{p}_2 + \underline{c}\underline{p}_3\theta + \underline{c}\underline{p}_2(\underline{x}_1'y_1' + \underline{x}_2'y_2') \\ &- \underline{p}_2(\underline{x}_2'y_1'' - \underline{x}_1'y_2'') + \underline{p}_3y_3'' \}\ \underline{\mathbf{t}} \\ &+ \{ - \underline{p}_3\theta' - \underline{c}\underline{p}_2(\underline{x}_2'y_1' - \underline{x}_1'y_2') + \underline{c}\underline{p}_3y_3' \}\ \underline{\mathbf{n}} \\ &+ \underline{p}_2\theta'\underline{\mathbf{b}} \end{aligned} \qquad (15)$$

Hence, using the fact that $\mathbf{t}^+$ has unit length,

$$\left(\frac{ds^+}{ds}\right)^2 = 1 - 2\underline{c}p_2 + 2\underline{c}p_3\theta + 2\underline{c}p_2(\underline{x}_1'y_1' + \underline{x}_2'y_2') - 2p_2(\underline{x}_2'y_1'' - \underline{x}_1'y_2'') + p_3y_3'' \tag{16}$$

Substituting (6), (7), and (16) into (3) and again neglecting terms according to (2) results in

$$2e = y_1'^2 + y_2'^2 + y_3'^2 + 2\underline{c}(\underline{x}_1'y_1' + \underline{x}_2'y_2')p_2 + 2(\underline{x}_1'y_2'' - \underline{x}_2'y_1'')p_2 + 2(\underline{c}\theta + y_3'')p_3 \tag{17}$$

Comparing (17) with (2b) we conclude that

$$e_1 = y_1'^2 + y_2'^2 + y_3'^2$$

$$e_2 = 2hc^*(\underline{x}_1'y_1' + \underline{x}_2'y_2') + 2h(\underline{x}_1'y_2'' - \underline{x}_2'y_1'')$$

$$e_3 = 2(c^*\theta + hy_3'')$$

where $c^* = \underline{c}h$ is the dimensionless blade curvature.

The rate of twist of the blade about the axis can be obtained by considering a unit vector which is fixed relative to a cross-section. The rate of change of $\mathbf{m}$ with respect to s is given by

$$\frac{d\mathbf{m}}{ds} = \theta_t \mathbf{t} \times \mathbf{m}$$

Without loss of generality we can assume the vector is in the direction of the chord and coincides with the binormal when the blade is undeformed:

$$\mathbf{m} = -\sin\theta\,\mathbf{n} + \cos\theta\,\mathbf{b} = -\theta\mathbf{n} + \mathbf{b} \tag{18}$$

Neglecting elongation of the axis, the rate of change of this vector with respect to s is

$$\frac{d\mathbf{m}}{ds} = -\theta'\mathbf{n} - \theta(q\mathbf{b} - c\mathbf{t}) - q\mathbf{n} = \theta_t\mathbf{t}\times(\mathbf{b} - \theta\mathbf{n}) \tag{19}$$

$$= -\theta_t(\mathbf{n} + \theta\mathbf{b})$$

where q is the torsion of the deformed axis. From the $\mathbf{n}$ component of (19) we conclude that the twist rate is

$$a = q + \theta' \tag{20}$$

Now from the Frenet formulas

$$q = -\frac{d\mathbf{b}}{ds}\cdot\mathbf{n} \tag{21}$$

Recalling equation II.2.26, neglecting elongation of the axis and retaining only linear displacement terms,

$$q = -\frac{d}{d\underline{s}}(y_3'\underline{\mathbf{t}} + \underline{\mathbf{b}})\cdot(\underline{\mathbf{n}} - (\underline{x}_2'y_1' - \underline{x}_1'y_2')\underline{\mathbf{t}}$$

$$= -(y_3''\underline{\mathbf{t}} + \underline{c}y_3'\underline{\mathbf{n}})\cdot\underline{\mathbf{n}} \tag{22}$$

$$= -\underline{c}y_3'$$

Thus the twist rate is

$$\theta_t = \theta' - \underline{c}y_3' \tag{23}$$

The total strain energy per unit length can now be written as

$$\begin{aligned}\frac{2h^2V'}{EI} &= k_2(c^*y_3' - h\theta')^2 \\ &+ \frac{Ph^2}{EI}(y_1'^2 + y_2'^2 + y_3'^2) + \frac{Ph^2}{EI}(\underline{x}_1'y_1' + \underline{x}_2'y_2') \\ &+ k_3(\underline{x}_1'y_1' + \underline{x}_2'y_2')^2 + k_1(y_3'' + \underline{c}\theta)^2 \\ &+ h^2(\underline{x}_1'y_2'' - \underline{x}_2'y_1'')^2 + 2hc^*(\underline{x}_1'y_2'' - \underline{x}_2'y_1'') \\ &+ c^*(\underline{x}_1'y_1' + \underline{x}_2'y_2')^2\end{aligned} \tag{24}$$

where $c^* = \underline{c}h$ is the dimensionless curvature.

II.4 Kinetic Energy

An expression for the kinetic energy of the blade can be derived by writing the kinetic energy per unit length at a typical cross-section, then integrating along the blade span for the total kinetic energy. This section then is concerned with deriving an expression for the kinetic energy per unit length of blade span.

A typical section of the blade, as shown in figure 3, will have a mass center on the chord-line of the section, located relative to the axis by $be_m(\underline{b} - \theta\underline{n})$, where b is the semichord of the blade section. Assuming the cross-section has the shape of a thin airfoil we can neglect the rotary inertia about the chord-line and let the rotary inertia about the axis tangent and normal be $mb^2e_r^2$, where m is the mass per unit length of the blade and be_r is the radius of gyration of the cross-section. The kinetic energy for a typical section will then have the form (Reference 12)

$$\frac{2}{m}T'(\underline{s}) = \dot{\mathbf{x}}\cdot\dot{\mathbf{x}} + be_m\dot{\mathbf{x}}\cdot\dot{\boldsymbol{\theta}} \times (\underline{b} - \theta\underline{n}) + b^2e_r^2(\dot{\theta}^2 + \dot{\theta}_2^2) \qquad (1)$$

where

$$\dot{\boldsymbol{\theta}} = (\Omega\underline{x}_1' + \dot{\theta})\underline{t} + (\Omega\underline{x}_2 + \dot{\theta})\underline{n} + \dot{\theta}_3\underline{b} \qquad (2)$$

is the angular velocity of the section and

$$\theta_2 = y_3'$$

$$\theta_3 = \underline{x}_2'y_1' - \underline{x}_1'y_2' \qquad (3)$$

are the Euler angles defined in section II.2. The velocity of a point on the deformed axis is

$$\mathbf{x} = \dot{y}_1\mathbf{x}_1 + (\dot{y}_2 - \Omega y_3)\mathbf{x}_2 + \Omega(\underline{x}_2 + y_2)\mathbf{x}_3 + \dot{y}_3\mathbf{x}_3$$

$$= (\underline{x}_1'\dot{y}_1 + \underline{x}_2'\dot{y}_2 - \Omega\underline{x}_2'y_3)\underline{t} + (\underline{x}_2'\dot{y}_1 - \underline{x}_1'\dot{y}_2 + \Omega\underline{x}_1'y_3)\underline{n}$$

$$- \Omega(\underline{x}_2 + y_2)\mathbf{b} + \dot{y}_3\underline{b} \qquad (4)$$

When (2), (3), and (4) are substituted into (1), a number of terms result which are linear in the displacements (y_1, y_2, y_3, and θ). These terms appear as constants in the final equations of motion, thus contribute only to the equilibrium configuration of the blade. That is, the linear terms are related to the static deflections of the blade due to centrifugal forces. Since these deflections will have little influence on the vibration characteristics of the blade, the linear terms in the kinetic energy expression will be ignored. As with the potential energy, we also ignore terms which are higher than quadratic in the displacements; hence the kinetic energy will be strictly quadratic in the displacements and derivatives of the displacements. The kinetic energy expression may thus be written as

$$\frac{2}{m} T' = \dot{y}_1^2 + \dot{y}_2^2 + \dot{y}_3^2$$

$$+ 2\Omega(y_2\dot{y}_3 - y_3\dot{y}_2) + \Omega^2(y_3^2 + y_2^2)$$

$$+ be_m \{ x_1'\dot{y}_1\dot{y}_3' + x_2'\dot{y}_2\dot{y}_3' - x_2'\dot{y}_1\dot{\theta} + x_1'\dot{y}_2\dot{\theta}$$

$$+ \Omega(- x_2'y_3\dot{y}_3' - x_1'y_3\dot{\theta} + x_2\theta\dot{\theta} + x_2y_3'\dot{y}_3' \qquad (5)$$

$$+ x_1'\theta\dot{y}_3 + x_2'y_3'\dot{y}_3)$$

$$+ \Omega^2(x_1'\theta y_2 + x_2'y_3'y_2) \}$$

$$+ b^2e_r^2(\dot{\theta}^2 + \dot{y}_3'^2)$$

Note that this equation consists of terms which have no time derivatives, only one time derivative, and terms with two time derivatives. It will prove useful to write the kinetic energy in the form

$$T' = T_0' + T_1' + T_2' \qquad (6a)$$

where

$$\frac{2}{m\Omega^2} T_0' = y_2^2 + y_3^2 + be_m(\underline{x}_1'y_2\theta + \underline{x}_2'y_2y_3') \qquad (6b)$$

consists of terms associated with centrifugal forces,

$$\frac{1}{m^2} T_1' = y_2\dot{y}_3 - y_3\dot{y}_2 + be_m(x_1'\theta + x_2'y_3')\dot{y}_3 + be_m(x_2y_3' - x_2'y_3)\dot{y}_3' + be_m(x_2\theta - x_1'y_3)\dot{\theta} \tag{6c}$$

is associated with coriolis forces, and

$$\frac{2}{m} T_2' = \dot{y}_1^2 + \dot{y}_2^2 + \dot{y}_3^2 + be_m(x_1'\dot{y}_1 + x_2'\dot{y}_2)\dot{y}_3' + be_m(x_1'\dot{y}_2 - x_2'\dot{y}_1)\dot{\theta} + b^2e_r^2(\dot{y}_3'^2 + \dot{\theta}^2) \tag{6d}$$

consists of terms quadratic in the velocities.

II.5 Aerodynamic Forces

A Darrieus blade spinning in still air will experience drag forces opposing the spinning motion, but no aerodynamic forces normal to the line of direction (lift forces). The absence of lift forces is due to the fact that the Darrieus blade has a symmetric airfoil section which is at zero angle of attack in the absence of wind or deformation of the blade. Vibration of the blade, however, causes an angle of attack with respect to the surrounding air, thereby inducing lift forces in the plane of the blade. In addition, the air causes a moment on the blade which tends to twist the blade about the axis. The study of such interactions between the unsteady aerodynamic forces on the one hand and the elastic and inertia forces of the structure on the other hand is known as aeroelasticity. Under certain conditions these forces can cause the vibrations to become unstable, a potentially serious problem known as flutter. It is the purpose of this section to derive expressions for the unsteady aerodynamic forces acting on a harmonically vibrating blade with a view towards finding the conditions under which the blade will flutter.

Unsteady aerodynamics is a very difficult phenomenon to treat mathematically, primarily due to the fact that in general, motion of the structure at one point induces aerodynamic disturbances which are felt at all other points of the structure. Indeed, one of the few cases where explicit expressions for the aerodynamic forces on an airfoil have been obtained is the classic solution of Theodorsen (Reference 7) for the lift and moment acting on a two-dimensional airfoil section oscillating at zero mean angle of attack in a steady, incom-

pressible fluid stream. In the two-dimensional problem, it is assumed that there is no aerodynamic interaction between adjacent sections of the airfoil; this assumption is evidently valid in the case of a straight wing of infinite span with the fluid flowing perpendicular to the axis. Since the Darrieus blade is neither straight nor infinitly long the two-dimensional assumption is not strictly valid in this case. Despite this fact, it is reasonable to assume that each section of the Darrieus blade acts as a two-dimensional section for the following reasons:

1) relative to the thickness of the airfoil section, the blade has a small curvature and is very long. In addition, the ends of the blade have very low velocity, hence small aerodynamic forces.
2) since the blade is symmetric about the mid-span, there will be no flow along the blade near the mid-span, which is the region of highest velocity, hence the greatest aerodynamic forces. The lack of flow along the span of the blade reduces the three-dimensional nature of the problem to interactions due to the curvature of the blade.

Perhaps a more important consideration is the fact that the vibrating blade will shed vortices which, in the absence of wind, will interfere with the next blade. Here it is assumed that the vortices will dissipate entirely before the next blade passes; that is, we assume the airstream to be free from turbulence.

Theodorsen's solution for the unsteady aerodynamic forces on a thin, two-dimensional airfoil assumes that the section moves in pitch (θ) and translation (z) as shown in figure 6. Moreover, the motion is assumed to be steady-state and harmonic

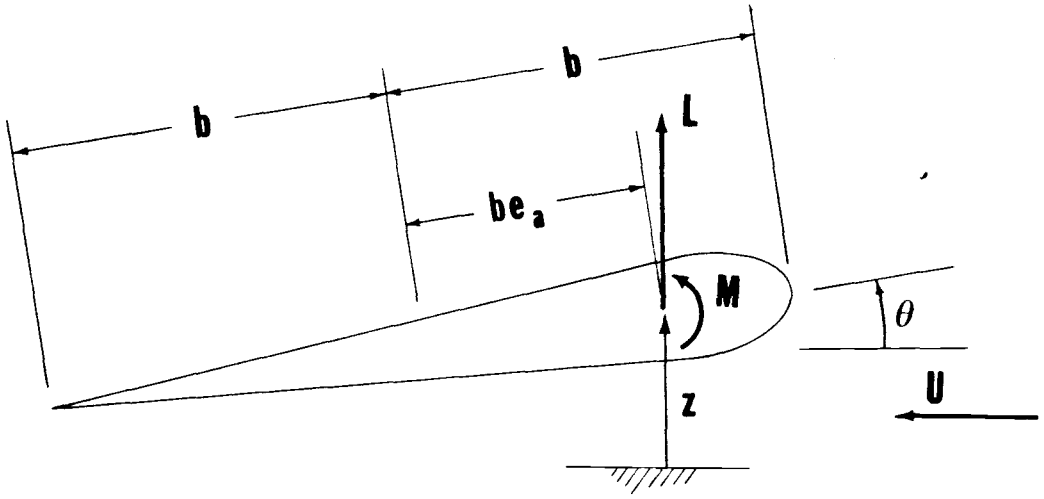

Figure 6. Aerodynamic Forces on a Two-Dimensional Airfoil Section

with frequency ω. Thus the motion of the airfoil section may be represented in the complex form

$$z = z_0 e^{i\omega t}$$

$$\theta = \theta_0 e^{i\omega t},$$

in which z_0 and θ_0 are complex amplitudes and, as usual, it is tacitly agreed that the actual motion is represented by the real part of these expressions. In a steady airstream with velocity U the aerodynamic forces on the section will consist of a lift force acting perpendicular to the airstream, and a moment about the pitch axis, as illustrated in figure 6. As shown in References 7 and 13, the lift may be written as

$$L = \pi\rho b(L_1 + L_2 + L_3) \tag{1a}$$

where

$$L_1 = b(be_a\ddot{\theta} - \ddot{z}) \tag{1b}$$

is the lift due to the apparent mass of the section, e_a is the distance from the axis to the midchord divided by the semichord,

$$L_2 = bU\dot{\theta} \tag{1c}$$

represents lift due to circulation caused by rotation of the airfoil, and

$$L_3 = 2UC(k)\left[U\theta - \dot{z} + b(\tfrac{1}{2} - e_a)\dot{\theta}\right] \tag{1d}$$

is the lift due to the apparent angle of attack, modified by a dimensionless factor C(k) which accounts for the time lag between motion of the airfoil and the resulting change in the vorticity distribution and accompanying lift. C(k), known as Theodorsen's function, is complex valued, thus accounting for the phase shift between the oscillatory motion and the lift force. Theodorsen's function depends only on the real, dimensionless parameter $k = \omega b/U$, known as the reduced frequency, and may be expressed in terms of modified Bessel functions as

$$C(k) = \frac{K_1(ik)}{K_0(ik) + K_1(ik)} \tag{2}$$

The following rational approximation to Theodorsen's function, given in reference 13, will be used here

$$C(k) = 1 - \frac{0.165}{1 - \frac{0.0455}{k} i} - \frac{0.335}{1 - \frac{0.3}{k} i} \tag{3}$$

Note that when $k = 0$, $C = 1$; this is the so-called quasi-steady case, sometimes used to simplify the resulting expressions for aerodynamic forces when the reduced frequency is small.

According to Theodorsen's solution, the moment about the axis is

$$M = - e_a L_1 - b(\tfrac{1}{2} + e_a)L_2 + b(\tfrac{1}{2} - e_a)L_3 + M_1 \tag{4a}$$

where

$$M_1 = - \frac{1}{8} \pi \rho b^4 \ddot{\theta} \tag{4b}$$

is due to the apparent moment of inertia. From equation (4a) it is apparent that L_1 acts at the mid-chord, while L_2 acts at the 3/4 chord and L_3 acts at the ¼ chord.

These expressions for lift and moment may be applied to the Darrieus by setting

$$z = \underline{x}_2' y_1 - \underline{x}_1' y_2$$
$$U = \Omega \underline{x}_2, \tag{5}$$

resulting in

$$\frac{L'}{\pi\rho b} = b(e_a\ddot{\theta} + \underline{x}_1\ddot{y}_2 - \underline{x}_2'\ddot{y}_1) + \Omega\underline{x}_2 b\dot{\theta}$$
$$+ 2\Omega\underline{x}_2 C(k)(x_1'\dot{y}_2 - x_2'\dot{y}_1 + \Omega\underline{x}_2\theta + \tfrac{1}{2}b\dot{\theta} + e_a\dot{\theta}) \tag{6}$$

$$\frac{M'}{\pi\rho b} = -e_a b(e_a\ddot{\theta} + \underline{x}_1'\ddot{y}_2 - x_2'\ddot{y}_1)$$
$$- b(\tfrac{1}{2}b + e_a)\Omega\underline{x}_2\dot{\theta} - \frac{b^3}{8}\ddot{\theta} \tag{7}$$
$$+ (b - 2e_a)\Omega\underline{x}_2 C(k)(x_1'\dot{y}_2 - \underline{x}_2'\dot{y}_1 + \Omega\underline{x}_2\theta + \tfrac{1}{2}b\dot{\theta} + e_a\dot{\theta})$$

Recalling equation II.2.17, the generalized forces acting on the generalized coordinates y_1, y_2, y_3, and θ, respectively, are

$$f_1'(\underline{s}) = \underline{x}_2' L' \tag{8a}$$

$$f_2'(\underline{s}) = -x_1' L' \tag{8b}$$

$$f_3'(\underline{s}) = 0 \tag{8c}$$

$$f_4'(\underline{s}) = M' \tag{8d}$$

The expressions (6) and (7) for the lift and moment assume that the motion is steady and harmonic. Thus solutions to the equations of motion are, strictly speaking, only valid at neutral stability (flutter) points. This limitation is perfectly acceptable here, since we are primarily concerned with the conditions under which the blade is neutrally stable.

II.6 Boundary Conditions

Boundary conditions for the Darrieus blade consist of the geometric and force compatability conditions at the ends of the blade, at the points where the blade is fastened to the rotor axis. In this study it is assumed that the blade is pinned to the rotor axis, thus allowing the transmission of force in all three directions, moment about the x_1 and x_2 axes, but no moment about the x_3 axis. In terms of the displacements the geometric or essential boundary conditions are

$$\begin{aligned} y_k(\pm h,t) &= 0 \qquad\qquad k = 1, 2, 3 \\ \theta(\pm h,t) &= 0 \\ y_3'(\pm h,t) &= 0 \end{aligned} \tag{1}$$

while the natural boundary conditions of zero moment about the x_3 axis at the ends leads to

$$\underline{x}_1'y_2'' - \underline{x}_2'y_1'' + \underline{c}(\underline{x}_1'y_1' + \underline{x}_2'y_2')\Big|_{\underline{s}=\pm h} = 0 \tag{2}$$

II.7 Blade Shape

In this section we derive equations describing the troposkien shape. The troposkien shape is defined as the shape of a perfectly flexible, inextensible rope which is spinning in the absence of gravity. It will be shown that this shape is independent of the spin rate; moreover, the shape is a function only of the height-to-width ratio, hereafter referred to as the aspect ratio of the blade. A set of ordinary differential equations which describe the troposkien shape can be derived using the previously derived expressions for potential and kinetic energy (suitably modified to model a perfectly flexible rope) in conjunction with Lagrange's equations.

The kinetic energy for a spinning rope is simply

$$T' = \tfrac{1}{2}m\Omega^2(\underline{x}_2 + y_2)^2 \tag{1}$$

With $E = G = y_3 = 0$, the potential energy (equation II.3.24) becomes

$$V' = \tfrac{1}{2}P(y_1'^2 + y_2'^2) + P(\underline{x}_1'y_1' + \underline{x}_2'y_2) \tag{2}$$

Thus the Lagrangian for the spinning rope is

$$2L' = 2(T' - V') = m\Omega^2(\underline{x}_2 + y_2)^2 - 2P(\underline{x}_1'y_1' + \underline{x}_2'y_2') - P(y_1'^2 + y_2'^2) \tag{3}$$

The Euler-Lagrange equations in this case have the form

$$\frac{\partial L'}{\partial y_1} - \frac{d}{d\underline{s}}\left(\frac{\partial L'}{\partial y_1'}\right) = 0 \qquad j = 1, 2 \tag{4}$$

Substituting (3) into (4) and setting $y_1 = y_2 = 0$ results in the following two ordinary differential equations for $\underline{x}_1$, $\underline{x}_2$ and P:

$$P'\underline{x}_1' + P\underline{x}_1'' = 0 \tag{5a}$$

$$m\Omega^2\underline{x}_2 + P'\underline{x}_2' + P\underline{x}_2'' = 0 \tag{5b}$$

Since these two equations contain three unknowns it is necessary to add at least one more equation; recalling equation II.2.13,

$$\underline{x}_1'^2 + \underline{x}_2'^2 = 1 \tag{5c}$$

Denoting the aspect ratio by a, the boundary conditions for this system of three ordinary differential equations are

$$\underline{x}_1(0) = \underline{x}_2'(0) = \underline{x}_2(h) = 0 \tag{6a}$$

$$\underline{x}_1(h) = a\underline{x}_2(0) \tag{6b}$$

$$\underline{x}_1'(0) = 1 \tag{6c}$$

Thus we have a two-point boundary value problem for $\underline{x}_1$, $\underline{x}_2$ and P between $\underline{s} = 0$ and $\underline{s} = h$; the lower half of the blade can be completed by symmetry. A common technique for solving such a system of equations is the shooting method (Reference 14), whereby the differential equations are integrated starting at one end, say $\underline{s} = 0$, using guesses for the missing initial conditions. The differences between the final values and the actual boundary conditions are then considered to be functions of

the guessed initial conditions; hence the problem is reduced to the solution of a system of nonlinear equations for the missing initial conditions.

In order to recast the problem as a shooting problem it is first necessary to put the differential equations into first order form. To this end let

$$s^* = \underline{s}/h$$

$$z_1(s^*) = x_1^*(s^*) = \underline{x}_1/h \qquad z_1'(s^*) = \underline{x}_1'(\underline{s})$$

$$z_2(s^*) = \underline{x}_1'(\underline{s}) = z_1'(s^*)$$

$$z_3(s^*) = x_2^*(s^*) = \underline{x}_2(\underline{s})/h \qquad z_3'(s^*) = \underline{x}_2'(\underline{s})$$

$$z_4(s^*) = \underline{x}_2'(\underline{s}) = z_3'(s^*)$$

$$z_5(s^*) = P^* = P/m\Omega^2h^2$$

and write equations (5) as

$$z_5'z_2 + z_5z_2' = 0 \tag{7a}$$

$$z_3 + z_5'z_4 + z_5z_4' = 0 \tag{7b}$$

$$z_2^2 + z_4^2 - 1 = 0 \tag{7c}$$

with boundary conditions

$$z_1(0) = 0 \tag{8a}$$

$$z_4(0) = 0 \tag{8b}$$

$$z_3(1) = 0 \tag{8c}$$

$$z_1(1) = az_3(0) \tag{8d}$$

$$z_2(0) = 1 \tag{8e}$$

Differentiating (7c) gives

$$z_2z_2' + z_4z_4' = 0 \tag{7c}$$

which, when substituted into (7a) and (7b) results in

$$z_5' = - z_3z_4 \tag{9}$$

$$z_4' = - z_2^2z_3/z_5 \tag{10}$$

Thus in a form suitable for numerical integration the equations are

$$z_1' = z_2 \tag{11a}$$

$$z_2' = z_2z_3z_4/z_5 \tag{11b}$$

$$z_3' = z_4 \tag{11c}$$

$$z_4' = - z_2^2z_3/z_5 \tag{11d}$$

$$z_5' = - z_3z_4 \tag{11e}$$

In addition, the curvature can be written as

$$c^* = hc = h\underline{x}_1''/x_2' = z_2 z_3/z_5 \tag{12}$$

Considering the boundary conditions we see that (8a), (8b), and (8e) are initial conditions, (8c) is a final condition, and (8d) involves both initial and final conditions. At this point, the shooting method assumes that a good guess is available for the missing initial conditions, namely

$$z_3(0) = u_1 \tag{13a}$$

$$z_5(0) = u_2 \tag{13b}$$

Clearly the final values are dependent on the values u_1 and u_2 chosen for the missing initial conditions; this dependence is expressed by defining functions

$$\begin{aligned} f_1(u_1,u_2) &= z_1(1) - az_3(0) = z_1(1) - au_1 \\ f_2(u_1,u_2) &= z_3(1) \end{aligned} \tag{14}$$

Note that the evaluation of these functions requires integrating from $s^* = 0$ to $s^* = 1$ using the current value of u_1 and u_2 as the missing initial conditions. This system of two nonlinear equations in two unknowns can be solved numerically using any of a variety of algorithms (Reference 15). Results for an aspect ratio of 1 are shown in figure 7.

The rotation rate of the Darrieus blade is limited by the strength of the blade material in tension. If the yeild strain of the material in tension is

$$e_y = \frac{P}{EA} = P^* r^2 / k_3$$

where

$$r^2 = \Omega^2 \frac{mh^4}{EI}$$

and the maximum value of P* from figure 7 is approximately .46, then the maximum dimensionless rotation rate is

$$r^2_{max} = 2.2 k_3 e_y$$

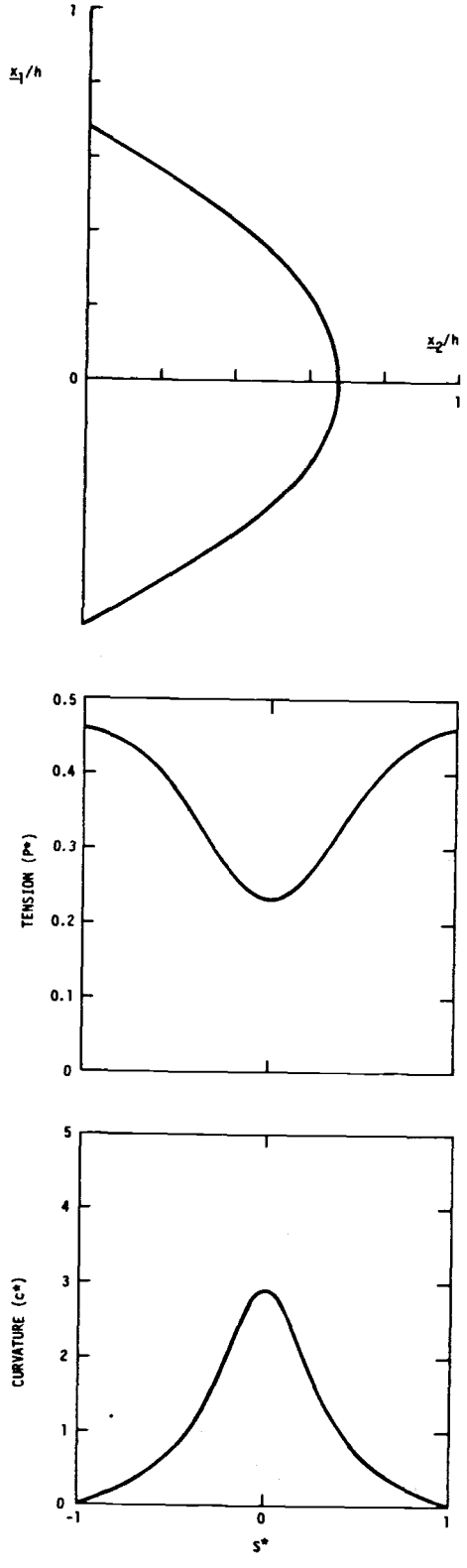

Figure 7. Troposkein Shape Functions

II.8 Discretization

At this point in the development of equations of motion, we have expressions for kinetic energy, potential energy and generalized forces, each of which are functions of time and arc-length along the blade axis. If applied to these expressions, Lagrange's equations would result in partial differential equations of motion. Since the aim here is to derive equations suitable for numerical study, it is necessary at some point to discretize the spatial variable $\underline{s}$. For our purposes it is most convenient to discretize the kinetic energy, potential energy, and generalized forces at this point.

Virtually all discretization methods for linear systems start by assuming the following form for the displacements:

$$\begin{aligned} y_1(\underline{s},t) &= he^{pt}\mathbf{u}_1^T\mathbf{q}_1(s^*) \\ y_2(\underline{s},t) &= he^{pt}\mathbf{u}_2^T\mathbf{q}_2(s^*) \\ y_3(\underline{s},t) &= he^{pt}\mathbf{u}_3^T\mathbf{q}_3(s^*) \\ \theta(\underline{s},t) &= e^{pt}\mathbf{u}_4^T\mathbf{q}_4(s^*) \end{aligned} \tag{1}$$

where $\mathbf{u}_k$ is a complex vector of generalized coordinates,

$$\mathbf{q}_k(s^*) = (q_k^1 \quad q_k^2 \quad \cdots \quad q_k^{n_k})^T \qquad (k=1,2,3,4) \tag{2}$$

is a vector of discretization functions, $s^* = \underline{s}/h$, and the usual assumption of harmonic motion with complex characteristic exponent p has been made. It is tacitly assumed, of course, that the actual displacements are represented by the real part

of these complex quantities.

There are two aspects to projection methods such as Galerkin's or the Rayleigh-Ritz method: the inner-product used, and the choice of basis function. Here the inner-product is simply

$$(f,g) = \int f(s^*)g(s^*)ds^* \tag{3}$$

Possibilities for the basis functions are many; we could use, for instance orthogonal functions such as the Chebyshev polynomials or trigonometric functions. The only requirements on the functions is that they be twice continuously differentiable (since the potential energy contains second derivatives) and that they meet the boundary conditions. Currently very popular are <u>local</u> basis functions, each of which is defined only on a subinterval of the interval of interest. One such type of function is the Hermite cubic polynomial, which results in the finite element method (Reference 6). The primary advantages to using locally defined basis functions are 1) it is generally much easier to satisfy boundary conditions with local functions than with globally defined functions, 2) the resulting coefficient matrices tend to be highly banded, and 3) local functions tend to have better numerical properties, as illustrated by the well-known Runge phenomenon (Reference 16). Hermite cubics are twice differentiable, although the second derivative is not continuous at the ends of each subinterval. We could use Hermite cubics even though it would mean integrating across the second derivative discontinuities (this is exactly what is done in the finite element method), but it turns out that by using piecewise cubic polynomials which <u>do</u> have continuous second derivatives results in the same degree of approximation with

fewer functions (i.e. fewer subintervals). The main drawback to adding the extra continuity is that the functions are not as local; that is, they are non-zero over more subintervals than the Hermite cubics, resulting in larger bandwidths in the coefficient matrices and more complexity in meeting the boundary conditions. Adding second derivative continuity results in a so-called cubic spline (Reference 16).

A cubic spline is the mathematical representation of the elastic ruler used by draftsmen, also known as a spline. A draftsmen's spline is used to draw smooth curves by holding the spline down with weights at various points along the curve called knots, and bending the spline to produce the desired curve. Modeling the spline as a beam simply supported at the knots results in a series of cubic polynomials, each defined between two knots. Although the first and second derivatives of this representation will be continuous even at the knots, the third derivative will have discontinuities at the knots. This set of piecewise cubic polynomials then is a cubic spline in the mathematical sense. It can be shown that any cubic spline can be expressed as a linear combination of the cardinal basis or B-splines (Reference 16). If we divide the interval (-1,1) into $\underline{n}$ equal subintervals with knots at

$$s_j = -h + \frac{2j}{\underline{n}} \qquad j = 0, 1, 2, \ldots \underline{n}, \tag{4}$$

there will be $\underline{n} + 3$ B-splines which are non-zero over this interval. The situation is illustrated in figure 8 for four subintervals. In the case of equal subintervals, each B-spline is defined as

$$B_j(s^*) = \begin{cases} v_{j-2}^3 & 0 < v_{j-2} < 1 \\ 1 + 3v_{j-1} + 3v_{j-1}^2 - 3v_{j-1}^3 & 0 < v_{j-1} < 1 \\ 1 + 3v_{j+1} + 3v_{j+1}^2 + 3v_{j+1}^3 & -1 < v_{j+1} < 0 \\ -v_{j+2}^3 & 0 < v_{j+2} < 1 \\ 0 & \text{otherwise} \end{cases} \qquad (5)$$

where $v_j = \underline{n}(s^* - s_j)/2$. Table 1 gives values of B_j and its derivatives at the knots.

TABLE 1

	s_{j-2}	s_{j-1}	s_j	s_{j+1}	s_{j+2}
B_j	0	¼	1	¼	0
B_j'	0	$3\underline{n}/8$	0	$-3\underline{n}/8$	0
B_j''	0	$3\underline{n}^2/8$	$-3\underline{n}^2/4$	$3\underline{n}^2/8$	0

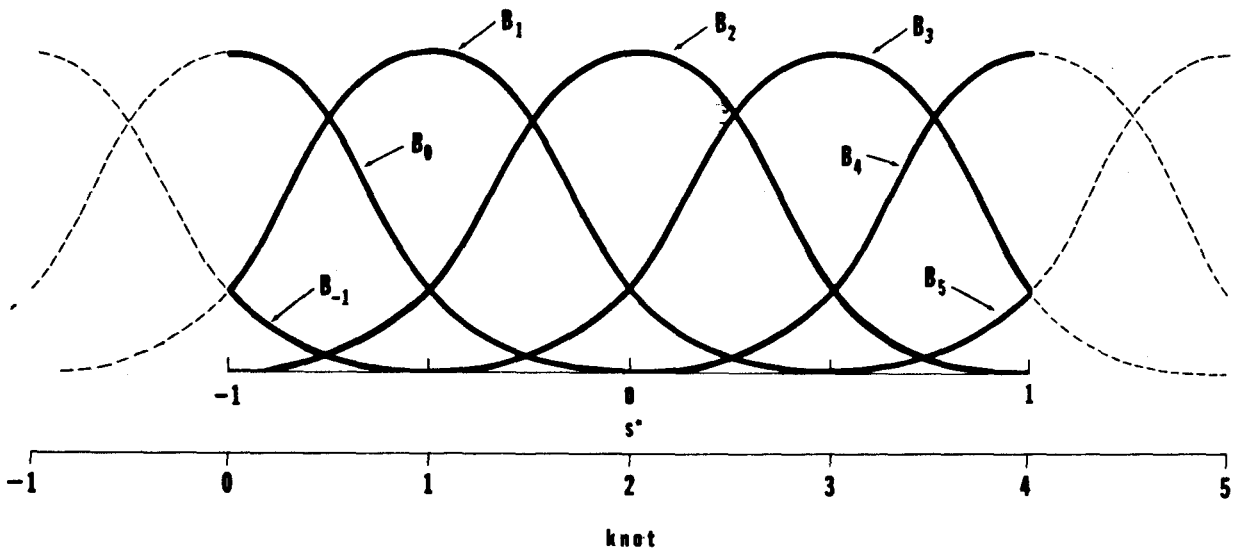

Figure 8. B-Splines

Before applying the B-splines to our problem it is necessary to take into consideration the boundary conditons. That is, we want to define the discretization functions as linear combinations of the B-splines such that the boundary conditions are met. Each boundary condition reduces the number of functions by one, hence for the variables y_1, y_2 and θ, which are required only to have zero displacement at the ends, there will be $\underline{n}$ + 1 splines, while y_3 will have $\underline{n}$ - 1 due to the requirement of zero slope at the ends. It is easily verified that combinations of the B-splines which meet the boundary conditions are

a) zero displacement (y_1, y_2, and θ)

$$q_k^1(s^*) = B_0 - 4B_{-1} \qquad k = 1, 2, 4 \tag{6a}$$

$$q_k^2(s^*) = B_0 - 4B_1 \qquad k = 1, 2, 4 \tag{6b}$$

$$q_k^j(s^*) = B_{j-1} \qquad (j = 3, 4, \ldots \underline{n}-1) \quad (k = 1, 2, 4) \tag{6c}$$

$$q_k^{\underline{n}}(s^*) = B_{\underline{n}} - 4B_{\underline{n}+1} \qquad (k = 1, 2, 4) \tag{6d}$$

$$q_k^{\underline{n}+1}(s^*) = B_{\underline{n}} - 4B_{\underline{n}-1} \qquad (k = 1, 2, 4) \tag{6e}$$

b) zero displacement and zero slope (y_3)

$$q_3^1(s^*) = B_{-1} - \tfrac{1}{2}B_0 + B_1 \tag{7a}$$

$$q_3^j(s^*) = B_{j+1} \qquad (j = 2, 3, \ldots \underline{n}-2) \tag{7b}$$

$$q_{\frac{1}{3}}^{n-1}(s^*) = B_{\underline{n}+1} - \tfrac{1}{2}B_{\underline{n}} + B_{\underline{n}-1} \tag{7c}$$

The two types of discretization functions a) and b) are illustrated for four intervals in figure 9. Note that each function has been normalized so that the maximum value is 1.

Substitution of equation (1) into equation II.3.24 results in an expression for the potential energy per unit length in terms of the generalized coordinates. Likewise, substitution into equation II.4.6 results in the discretized kinetic energy, and substitution into II.5.6 and II.5.7 yeilds the discretized aerodynamic forces. An integration with respect to s* then results in matrix expressions for the potential energy, kinetic energy, and the aerodynamic forces. The terms of these matrices are presented in Appendix A. A typical term of the potential energy in this form is

$$k_2(c^*\mathbf{u}_3^T\mathbf{q}_3' - \mathbf{u}_4^T\mathbf{q}_4)^2 e^{2pt}$$

$$= k_2 \{\mathbf{u}_3^T(c^{*2}\mathbf{q}_3'\mathbf{q}_3'^T)\mathbf{u}_3 - \mathbf{u}_3^T(c^*\mathbf{q}_3'\mathbf{q}_4^T)\mathbf{u}_4$$

$$- \mathbf{u}_4^T(c^*\mathbf{q}_4\mathbf{q}_3'^T)\mathbf{u}_3 + \mathbf{u}_4^T(\mathbf{q}_4\mathbf{q}_4^T)\mathbf{u}_4 \} \tag{8}$$

The terms within parentheses are matrix functions of s* which can be numerically integrated from s* = - 1 to s* = 1 to give the total potential energy in the following form:

$$\frac{2h}{EI} V = \mathbf{u}^T(r^2\mathbf{K}_0 + k_1\mathbf{K}_1 + k_2\mathbf{K}_2 + k_3\mathbf{K}_3 + \mathbf{K}_4)\mathbf{u}e^{pt} \tag{9}$$

where

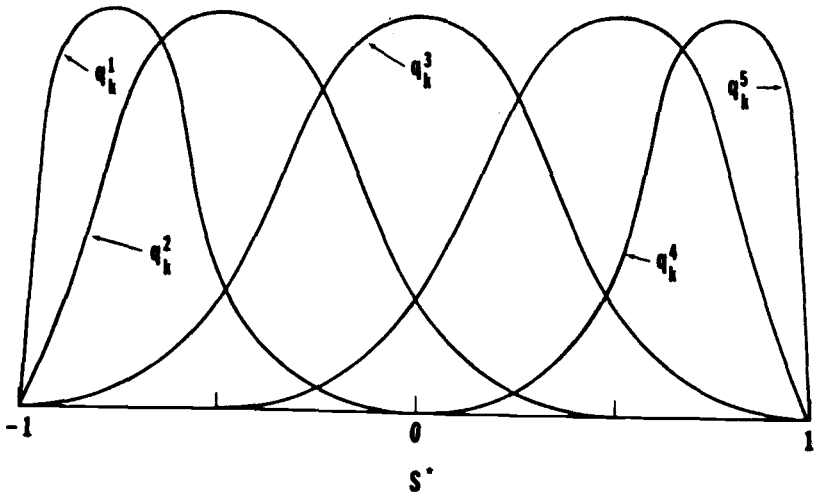

a) functions for y_1, y_2, and θ

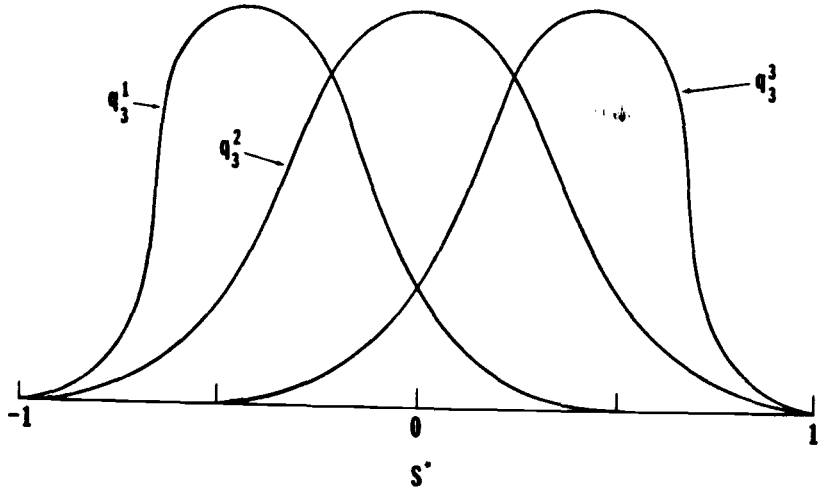

b) functions for y_3

Figure 9. Discretization Functions

$$\mathbf{u} = \begin{Bmatrix} u_1 \\ u_2 \\ u_3 \\ u_4 \end{Bmatrix} \tag{10}$$

Matrix $\mathbf{K}_0$ arises from the blade tension terms in the strain energy and is associated with centifugal stiffening of the blade; hence it is multiplied by the dimensionless rotation rate

$$r = \Omega\sqrt{\frac{mh^4}{EI}} \tag{11}$$

Matrices $\mathbf{K}_0$, $\mathbf{K}_1$, $\mathbf{K}_2$, $\mathbf{K}_3$, and $\mathbf{K}_4$ contain the strain energy terms for out-of-plane bending, twisting, stretching, and in-plane bending, respectively.

Two problems which arise when discretizing a curved beam such as this is that a) there are no longer rigid body displacement modes which do not induce in-plane bending and stretching, and b) there are no longer allowable in-plane displacement patterns which do not induce stretching (Reference 17). This can be seen by considering expressions for the additional curvature

$$c(\underline{s}) = \underline{x}_1'y_2'' - \underline{x}_2'y_1'' + \underline{c}(\underline{x}_1'y_1' + \underline{x}_2y_2') \tag{12}$$

and for the axial stretch

$$e(\underline{s}) = \underline{x}_1'y_1' + \underline{x}_2'y_2' \tag{13}$$

The general rigid body in-plane displacement of the unconstrained blade is

$$\mathbf{y}^r = (d_1^r - \theta_3^r \underline{x}_2)\mathbf{x}_1 + (d_2^r + \theta_3^r \underline{x}_1)\mathbf{x}_2 = y_1^r \mathbf{x}_1 + y_2^r \mathbf{x}_2 \qquad (14)$$

where d_1^r, d_2^r, and θ_3^r are arbitrary constants. By substituting (14) into (12) and (13) it is easily verified that this displacement pattern yields no in-plane bending or stretching. Note that $\mathbf{y}^r$ is not representable by cubic polynomials, due to the presence of $\underline{x}_1$ and $\underline{x}_2$. Thus when y_1 and y_2 are discretized with cubic polynomials it is no longer possible to exactly represent rigid body displacements. Likewise, due to the presence of $\underline{x}_1$ and $\underline{x}_2$ in the expressions for additional curvature and extension it is not, in general, possible to represent zero-extension bending displacement patterns. Most solutions to this problem involve approximating $\underline{x}_1$ and $\underline{x}_2$ with low-order polynomials (Reference 17); here we take a different approach and approximate the additional curvature and extension with cubic splines. That is, we let

$$c(s^*) = \mathbf{c}^T \mathbf{q}(s^*) \qquad (15)$$

$$e(s^*) = \mathbf{e}^T \mathbf{q}(s^*) \qquad (16)$$

where $\mathbf{q} = (B_{-1} \quad B_0 \quad B_1 \ \ldots \ B_{\underline{n}+1})^T$ is a vector of cubic splines with no end conditions. By approximating the curvature as cubic functions of the generalized coordinates $\mathbf{u}_1$ and $\mathbf{u}_2$, the rigid body mode and zero-extension bending conditions will automatically be satisfied. Thus we need to express the coefficients $\mathbf{c}$ and $\mathbf{e}$ in terms of $\mathbf{u}_1$ and $\mathbf{u}_2$. Since there are $\underline{n}$ + 3 coefficients (elements of $\mathbf{c}$ or $\mathbf{e}$) and $2\underline{n}$ + 2 "unknowns" ($\mathbf{u}_1$ and $\mathbf{u}_2$), expressing $\mathbf{c}$ and $\mathbf{e}$ in terms of $\mathbf{u}_1$ and $\mathbf{u}_2$ will necessarily be an approximation; here we choose to approximate in a least-squares sense. To this end multiply (13) and (14) by $\mathbf{q}$

and integrate from $s^* = -1$ to $s^* = 1$. This results in the following linear expressions for the coefficients **c** and **e** in terms of $\mathbf{u}_1$ and $\mathbf{u}_2$:

$$\mathbf{Qc} = \mathbf{C}_1\mathbf{u}_1 + \mathbf{C}_2\mathbf{u}_2 \tag{17}$$

$$\mathbf{Qe} = \mathbf{E}_1\mathbf{u}_1 + \mathbf{E}_2\mathbf{u}_2 \tag{18}$$

where

$$\mathbf{Q} = \int \mathbf{q}\mathbf{q}^T ds^*, \tag{19}$$

the so-called Gram matrix, is positive definite and symmetric (Reference 16), and

$$\mathbf{C}_1 = \int (\underline{c}\mathbf{x}_1'\mathbf{q}\mathbf{q}_1'^T - \underline{x}_2'\mathbf{q}\mathbf{q}_1''^T) ds^* \tag{20}$$

$$\mathbf{C}_2 = \int (\underline{c}\mathbf{x}_2'\mathbf{q}\mathbf{q}_2'^T + \underline{x}_1'\mathbf{q}\mathbf{q}_2''^T) ds^* \tag{21}$$

$$\mathbf{E}_1 = \int \underline{x}_1'\mathbf{q}\mathbf{q}_1'^T ds^* \tag{22}$$

$$\mathbf{E}_2 = \int \underline{x}_2\mathbf{q}\mathbf{q}_2'^T ds^* \tag{23}$$

are (n+3,n+1) real matrices. The additional curvature can now be written as

$$c(s^*) = \mathbf{q}^T(s^*)\mathbf{Q}^{-1}\mathbf{C}_1\mathbf{u}_1 + \mathbf{q}^T(s^*)\mathbf{Q}^{-1}\mathbf{C}_2\mathbf{u}_2 \tag{24}$$

and the extension as

$$e(s^*) = \mathbf{q}^T(s^*)\mathbf{Q}^{-1}\mathbf{E}_1\mathbf{u}_1 + \mathbf{q}^T(s^*)\mathbf{Q}^{-1}\mathbf{E}_2\mathbf{u}_2 \tag{25}$$

Recalling the definition of the Gram matrix (19) the strain energy due to additional curvature then becomes

$$\frac{2h}{EI} V_c = \int c^2(s^*)ds^*$$

$$= u_1^T C_1^T Q^{-T} Q Q^{-1} C_1 u_1 + u_1^T C_1^T Q^{-T} Q Q^{-1} C_2 u_2 \qquad (26)$$

$$+ u_2^T C_2^T Q^{-T} Q Q^{-1} C_1 u_1 + u_2^T C_2^T Q^{-T} Q Q^{-1} C_2 u_2$$

and the strain energy due to extension becomes

$$\frac{2h}{EI} V_e = k_3 \int e^2(s^*)ds^*$$

$$= u_1^T E_1^T Q^{-T} Q Q^{-1} E_1 u_1 + u_1^T E_1^T Q^{-T} Q Q^{-1} E_2 u_2 \qquad (27)$$

$$+ u_2^T E_2^T Q^{-T} Q Q^{-1} E_1 u_1 + u_2^T E_2^T Q^{-T} Q Q^{-1} E_2 u_2$$

Thus matrix K_3 in equation (9) has the form

$$K_3 = \begin{bmatrix} E_1^T Q^{-1} E_1 & E_1^T Q^{-1} E_2 & 0 & 0 \\ E_2^T Q^{-1} E_1 & E_2^T Q^{-1} E_2 & 0 & 0 \\ 0 & 0 & 0 & 0 \\ 0 & 0 & 0 & 0 \end{bmatrix} \qquad (28)$$

and matrix K_4 becomes

$$K_4 = \begin{bmatrix} C_1^T Q^{-1} C_1 & C_1^T Q^{-1} C_2 & 0 & 0 \\ C_2^T Q^{-1} C_1 & C_2^T Q^{-1} C_2 & 0 & 0 \\ 0 & 0 & 0 & 0 \\ 0 & 0 & 0 & 0 \end{bmatrix} \tag{29}$$

The discretized kinetic energy may be written as

$$\frac{2h}{EI} T = u^T (p^{*2} M + p^* r G + r^2 M_0) u e^{pt} \tag{30}$$

where M is a real, symmetric matrix arising from the quadratic velocity terms, G is a real, skew-symmetric matrix of coriolis or gyroscopic terms arising from terms linear in the velocities, and M_0 is a real, symmetric matrix of centrifugal force terms. The dimensionless characteristic exponent

$$p^* = p\sqrt{\frac{mh^4}{EI}} \tag{31}$$

can be written in terms of the frequency of oscillation and growth rate

$$p^* = \omega(\tfrac{1}{2}g + i)\sqrt{\frac{mh^4}{EI}} \tag{32}$$

While this definition of growth rate (g) may seem awkward, it corresponds to the traditional way in which damping rates are measured in the flutter literature; this point will be discussed further in a later section.

Finally, the aerodynamic forces become

$$\frac{h}{EI}\,\mathbf{f} = \frac{r^2}{m^*}\,\mathbf{Au} \tag{33}$$

where **A** is a complex matrix of aerodynamic terms, the elements of which are nonlinear functions of the reduced frequency $k^* = \omega/\Omega$, and

$$m^* = \frac{m}{\pi\rho_b{}^2} \tag{34}$$

is the mass density ratio.

The order of each of the above matrices is equal to the sum of the number of splines used for each variable; thus the order is

$$n = (\underline{n} + 1) + (\underline{n} + 1) + (\underline{n} - 1) + (\underline{n} + 1)$$

$$n = 4\underline{n} + 2 \tag{35}$$

Using the discretized expressions for kinetic energy, potential energy, and aerodynamic forces, and considering Lagrange's equations results in a system of n complex characteristic equations known as the flutter equations:

$$\mathbf{Du} = \mathbf{0} \tag{36}$$

where

$$\mathbf{D} = p^{*2}\mathbf{M} + p^{*}r\mathbf{G} + r^{2}(\mathbf{M}_0 + \mathbf{K}_0)$$

$$+ k_1\mathbf{K}_1 + k_2\mathbf{K}_2 + k_3\mathbf{K}_3 + \mathbf{K}_4 - \frac{r^2}{m^*}\mathbf{A}$$

Solutions to these equations are sufficient to determine the stability of linear motions of the Darrieus blade.

III. SOLUTION TECHIQUE

III.1 Form of the Equations

The stability of linear motions of the Darrieus blade spinning in still air is determined by solutions to the system of complex algebraic equations

$$\mathbf{Du} = \{\ p^{*2}\mathbf{M} + p^{*}r\mathbf{G} + r^{2}\mathbf{C} + (1 + ig_{s})\mathbf{K} - \frac{r^{2}}{m^{*}}\mathbf{A}(k^{*})\ \}\ \mathbf{u} = \mathbf{0}, \tag{1}$$

where

$$\mathbf{K} = k_1\mathbf{K}_1 + k_2\mathbf{K}_2 + k_3\mathbf{K}_3 + \mathbf{K}_4$$

and

$$\mathbf{C} = \mathbf{M}_0 + \mathbf{K}_0,$$

known as the flutter equations. This system of equations is quadratic in the characteristic exponent (p^*) and rotation rate (r), linear in the stiffness ratios (k_1, k_2, and k_3) and generalized coordinates (u), and nonlinear in the so-called reduced frequency (k^*). Note that the reduced frequency is not necessarily an independent parameter since we can write

$$k^{*} = \frac{\mathrm{Im}(p^{*})}{r} \tag{2}$$

In the next chapter the results of four types of solution to (1) will be presented:

a) free-vibration solutions at zero rotation rate obtained

by setting the density of air and the rotation rate to zero in (1)

b) free-vibration solutions at non-zero rotation rates obtained using a few of the low-frequency mode shapes obtained in (a) as generalized coordinates,

c) flutter stability solutions using generalized coordinates as in (b),

d) variations in the neutral-stability rotation rates with system parameters.

Free-vibration solutions at zero rotation rate involve a generalized symmetric eigenvalue problem, for which there are fast, reliable solution techniques (Reference 1). Solutions to (b), (c), and (d) on the other hand are much more difficult to obtain, as there are no reliable methods available.

The aerodynamics matrix **A** is a nonlinear function of the reduced frequency k*, and as such must be evaluated for each value of k* which is required in the solution process. Since it is not generally known beforehand which values of k* will be needed, the usual procedure is to compute **A** at a few values of k*, then interpolate for intermediate values (Reference 20). Here we evaluate **A** at a number of values of k* between 0 and 10, then compute cubic spline interpolants for each term, resulting in four complex matrix spline coefficients per interval between 0 and 10. The real and imaginary parts of each term of **A** are interpolated individually as real functions of the real variable k*.

III.2 Free-Vibration at Zero Rotation Rate

At zero rotation rate in a vacuum the flutter equations reduce to

$$(p^{*2}\mathbf{M} + \mathbf{K})\mathbf{u} = \mathbf{0}, \tag{1}$$

which is a symmetric generalized eigenvalue problem for the n pair of eigenvalues and eigenvectors $(p^*_j, \mathbf{u}_j)$. Provided $\mathbf{M}$ is positive definite, the eigenvalues will all be real and negative, hence the frequencies will all be positive (Reference 19). In addition, the eigenvectors are necessarily real and satisfy the orthogonality relations

$$\mathbf{u}_j^T \mathbf{M} \mathbf{u}_k = 0 \qquad k \neq j \tag{2}$$

Solutions to the eigenvalue problem (1) are easily obtained using, for example, routines in the EISPACK library (Reference 21).

A common method for reducing the order of the flutter equations for subsequent analyses is to use the free-vibration eigenvectors as a basis for generalized coordinates; that is, set

$$\mathbf{u} = \mathbf{U}\mathbf{z} \tag{3}$$

where $\mathbf{U}$ is an (n,m) matrix of the eigenvectors of (1) corresponding to the m lowest frequencies, and $\mathbf{z}$ is a new set of generalized coordinates. Transforming to the new generalized

coordinates results in

$$\mathbf{D^*z} = \mathbf{U}^T\mathbf{DUz} = \mathbf{0} \tag{4}$$

This process of reducing the order of the equations is known as modal analysis (Reference 5). In practice it is usually sufficient to use a small number of free-vibration modes to reduce the flutter equations. The effect of using different number of modes will be discussed in a later section.

There have been doubts expressed as to the validity of using normal modes of the non-rotating structure as generalized coordinates in a rotating structure (Reference 22). Clearly, if all normal modes were used (m = n), there would be no error introduced; the fear is that a very large number of normal modes need to be retained if the normal modes are of the non-rotating structure. In Reference 23, Meirovitch shows that these doubts are unwarrented because the free-vibration frequencies of a rotating structure satisfy a stationarity principle similar to Rayleigh's quotient. Thus the convergence characteristics of a rotating structure with regard to the number of normal modes used in the reduction will be similar to those of the non-rotating structure. Numerical experiments with the Darrieus flutter problem using both rotating and non-rotating-blade modes have confirmed Meirovitch's theory. In this study it has proven to be advantageous to use modes of the non-rotating blade as generalized coordinates, both from a computational standpoint and by the fact that modes of the non-rotating blade have no gyroscopic coupling between the in-plane and out-of-plane motions, hence the modes are purely in-plane or out-of-plane, making interpretation of the flutter results much easier.

A further reduction in the order of the problem is realized by noting that due to the symmetry of the blade about the x_2 axis, the motions of the blade may be split into symmetric and antisymmetric modes. More precisely, a symmetric mode is one in which

$$\begin{aligned} y_1(\underline{s},t) &= - y_1(-\underline{s},t), \\ y_2(\underline{s},t) &= y_2(-\underline{s},t), \\ y_3(\underline{s},t) &= y_3(-\underline{s},t), \\ \theta(\underline{s},t) &= \theta(-\underline{s},t), \end{aligned} \tag{5}$$

whereas an antisymmetric mode is one in which

$$\begin{aligned} y_1(\underline{s},t) &= y_1(-\underline{s},t), \\ y_2(\underline{s},t) &= -y_2(-\underline{s},t), \\ y_3(\underline{s},t) &= -y_3(-\underline{s},t), \\ \theta(\underline{s},t) &= -\theta(-\underline{s},t). \end{aligned} \tag{6}$$

The corresponding symmetric ($\mathbf{U}_s$) and antisymmetric eigenvectors ($\mathbf{U}_a$) not only satisfy the $\mathbf{M}$-orthogonality property (2), but also satisfy

$$\mathbf{U}_s^T \mathbf{U}_a = \mathbf{0} \tag{7}$$

That is, the set of symmetric eigenvectors is orthogonal (in the ordinary sense) to the set of antisymmetric eigenvectors. Thus we may split the reduced problem (4) into symmetric and antisymmetric problems, resulting in a substantial savings in effort in subsequent analyses.

III.3 Solutions at Non-Zero Rotation Rates

The problems posed in (b), (c), and (d) in section 2 above are essentially the same: to solve a system of non-linear equations for a range of values of a parameter of the system. In (b) and (c) the parameter is the rotation rate and the equations are nonlinear functions of the characteristic exponent; the parameter in (d) can be any of the system parameters such as mass density ratio or stiffness ratios.

By far the most common method of solution of flutter equations (at least in the United States) is known as the V-g method. In the V-g method the solution is assumed to consist of steady harmonic oscillations; that is, p^* is assumed to be imaginary. The structural damping coefficient (g_s) is then assumed to be such that the oscillations are steady and harmonic; for decaying oscillations this requires g_s to be negative, while for growing oscillations g_s must be positive. Normally the structural damping coefficient must be positive to be physically meaningful, so in a V-g solution this added structural damping is reffered to as artificial or added structural damping. The V-g solution proceeds by dividing the flutter equations by p^{*2} resulting in

$$\mathbf{M} + \frac{i}{k^*}\mathbf{G} + \frac{1 + ig_s}{\omega^*}\mathbf{K} - \frac{1}{m^* k^{*2}}\mathbf{A}(k^*) \qquad (1)$$

where $\omega^* = \mathrm{Im}(p^*)$. For a particular value of k^* this is simply a complex generalized eigenvalue problem in which $(1 + ig_s)/\omega^*$ is the eigenvalue. Having computed the eigenvalues, the corresponding rotation rate is simply $r = \omega^*/k^*$. This process is repeated for a number of values of k^* in the range of interest. Points of neutral stability are then determined by

interpolating the results to find rotation rates where $g_s = 0$.

There are a number of disadvantages to the V-g solution technique. The most serious in our case is the fact that a V-g solution has little physical significance unless g_s is small; when g_s becomes large not only does the damping lose physical meaning, but the corresponding generalized coordinates also tend to become unrealistic, making it difficult to interpret how a particular mode shape changes as the rotation rate is increased (Reference 24). As we shall see later, the behavior of the mode shape with rotation rate is very important in understanding the cause of flutter in the Darrieus blade.

It is generally agreed that far more meaningful results are obtained using the so-called p-k solution technique. In the p-k method the characteristic exponent is assumed to be complex and no artificial damping is assumed. The flutter equations are thus viewed as a system of nonlinear algebraic equations to be solved over a range of rotation rates for the characteristic exponent and generalized coordinates. The real part of the characteristic exponent then may be interpreted as the rate of growth of the oscillations. More specifically, since we have defined

$$g = \frac{2\mathrm{Re}(p)}{\omega}$$

it can be shown (Reference 24) that

$$g = \ln(a_{j+1}/a_j)/\pi$$

where a_{j+1}/a_j is the ratio of amplitudes of successive cycles of oscillation. It can also be shown that g corresponds closely in value to the g_s which would be obtained in a V-g solution,

provided g is small. Appendix B contains an example of the difference in results obtained using the V-g and p-k methods. The most serious disadvantage to the p-k formulation of the flutter equations and the reason that this method is not often used is that this formulation involves the solution of a system of nonlinear equations, for which there are no solution techniques which are as reliable as the eigenvalue solution techniques used with the V-g formulation. For this reason it was necessary to develop a method by which the p-k formulation of the flutter equations could be solved as reliably as possible.

The method used here to solve the p-k formulation of the flutter equations is known as a continuation method. A continuation method is merely a method for solving a system of nonlinear equations which depends on a parameter; that is, each value of the parameter results in a different set of nonlinear equations to solve. Starting with a known solution, solutions to the problem at each increment of the parameter is obtained using, for instance, Newton's method with the solution at the previous step as an initial guess. If the parameter is taken to be the rotation rate, the solution is a p-k flutter solution for the neutral-stability points; the same method may be used to compute variations in the neutral-stability rotation rates with a system parameter such as mass density ratio or stiffness. Appendix B contains a description of the method used to compute solutions to problems (b), (c), and (d).

III.4 Computer Program

Computer programs were written to carry out the calculations described in previous sections. In this section we give a brief outline of the programs.

The calculations were divided into two separate programs to take advantage of the two very different computers which were available: a) a CDC 175 and b) a PDP 11/70. The CDC 175 is a very fast, high capacity machine, whereas the PDP 11/70 is a small mini-computer with limited memory. Thus the program for the CDC was written to perform the calculations which required large amounts of memory, and the PDP was used for those calculations which could be done with limited memory. Basically, the calculations were divided as follows:

A) CDC program

1) the locations of points for Gauss numerical integration (Reference 25) of the flutter matrices are calculated.
2) integrate equations II.7.11 for the values of the blade shape parameters at the Gauss integration points.
3) form matrices $\mathbf{M}$, $\mathbf{G}$, $\mathbf{C}$, $\mathbf{K}_1$, $\mathbf{K}_2$, $\mathbf{K}_3$, and $\mathbf{K}_4$ by integrating the expressions given in appendix A using 4 point Gauss quadrature over each interval.
4) evalutate the aerodynamics matrix at a specified number (usually 4) values of reduced frequency k*
5) compute natural frequencies and eigenvectors at zero rotation rate using equation III.2.2.
6) use the eigenvectors computed in (4) to reduce the matrices computed in (2) and (3)

7) compute coeffiecient matrices of the spline interpolant which interpolates the aerodynamics matrices.
8) write the reduced matrices onto a file for transfer to the PDP computer.

B) PDP program

1) read the file created with program A.
2) read a file of execution options
3) compute natural frequencies of the spinning blade by setting $1/m^* = 0$ and using the method of appendix B.
4) perform a p-k flutter solution by computing p^* and **u** at intervals of r.
5) using the neutral-stability points found in (4), compute solutions varying m^*, k_1, and k_2

Although the accuracy of the PDP 11/70 is limited by a word length of only 16 bits, the accuracy and stability of the solution process was found to be quite acceptable. The LINPACK library along with the BLAS (Reference 26) were used extensively with double precision accumulation of inner-products in the PDP version of the BLAS.

IV. RESULTS

IV.1 Parameters

The flutter equations

$$\mathbf{Du} = \Big[\, p^{*2}\mathbf{M} + p^{*}r\mathbf{G} + r^{2}\mathbf{C} + (1 + ig_s)(k_1\mathbf{K}_1 + k_2\mathbf{K}_2 + k_3\mathbf{K}_3 + \mathbf{K}_4) - \frac{r^2}{m^*}\mathbf{A}(k^*) \,\Big]\, \mathbf{u} = \mathbf{0} \qquad (1)$$

contain a number of dimensionless parameters, allowing us to present the results of solutions to (1) in dimensionless form. This has the advantage that the results presented will apply to a one-parameter family of Darrieus wind turbines, rather than a particular configuration. The parameters contained explicitly in the flutter equations are:

1) characteristic exponent $p^* = \omega(\tfrac{1}{2}g + i)\sqrt{\frac{mh^4}{EI}}$

2) rotation rate $r = \Omega\sqrt{\frac{mh^4}{EI}}$

3) reduced frequency $k^* = \omega/\Omega$

4) chordwise to flatwise stiffness ratio k_1

5) torsional to flatwise stiffness ratio k_2

6) axial to flatwise stiffness ratio k_3

7) density ratio $m^* = \frac{m}{\pi\rho b^2}$

8) structural damping g_s

Implicit in (1) are the following parameters:

1) aspect ratio $a = \underline{x}_1(h)/\underline{x}_2(0)$
2) cubic spline intervals $\underline{n}$
3) radius of gyration (in semichords) e_r
4) axis to midchord distance (in semichords) e_a
5) axis to center of gravity (in semichords) e_m
6) semichord $b^* = b/h$

Of these parameters, a number will remain fixed for all cases presented here unless otherwise noted; they are

a)	aspect ratio a	=	1
b)	semichord b^*	=	.02
c)	radius of gyration e_r	=	.5
d)	density ratio m^*	=	50
e)	cubic spline intervals $\underline{n}$	=	15
f)	chordwise/flatwise stiffness ratio k_1	=	50
g)	torsional/flatwise stiffness ratio k_2	=	1
h)	axial/flatwise stiffness ratio k_3	=	10^6
i)	axis to midchord e_a	=	.5
j)	axis to c.g. e_m	=	0
k)	structural damping g_s	=	0

IV.2 Accuracy and Convergence

As a means of verifying the equations of motion used in this study a comparison was made with results published for the in-plane and out-of-plane vibrations of semi-circular arcs. Ojalvo (Reference 9) presents natural frequencies of the out-of-plane vibrations of a circular arc clamped at the ends, while Archer (Reference 11) presents natural frequencies for the in-plane vibrations of a clamped semi-circular arched beam. For this comparison it was necessary to replace the definition of the troposkien blade shape with that of a circular arc, and change the boundary conditions to clamped. Both of these differences involve only minor changes to the computer program used to generate the results. The results of this comparison are presented in Table 2 (also included are natural frequencies computed for the corresponding troposkien-shaped arc). Note that the results for out-of-plane vibrations compare better than the in-plane vibrations; this is due to the problem of discretizing curved beams as discussed in section II.8.

TABLE 2. Natural frequencies of a circular arc

$\omega_j \frac{mh^4}{EI}$ with $k_1 = 5$, $k_2 = 1$

j	present study	Ref. 1	Ref. 2	troposkein
1	9.022	9.018		9.002
2	10.96		10.81	11.81
3	24.84		23.81	27.15
4	26.19	26.18		26.89
5	46.66		44.24	46.92
6	56.06	55.94		57.03
7	77.16		67.86	71.44
8	98.55	100.2		98.88

A solution to the problem of extensional deformations induced by in-plane bending of a curved beam was presented in section II.8. The technique presented involved discretization of the strains in additon to the displacements. Of interest is how this technique effects the convergence of the natural frequencies with respect to the number of spline intervals used. Figure 10 illustrates the convergence behavior of the first 10 natural frequencies with and without discretization of the strains. Clearly the convergence is much better with discretization of the strains.

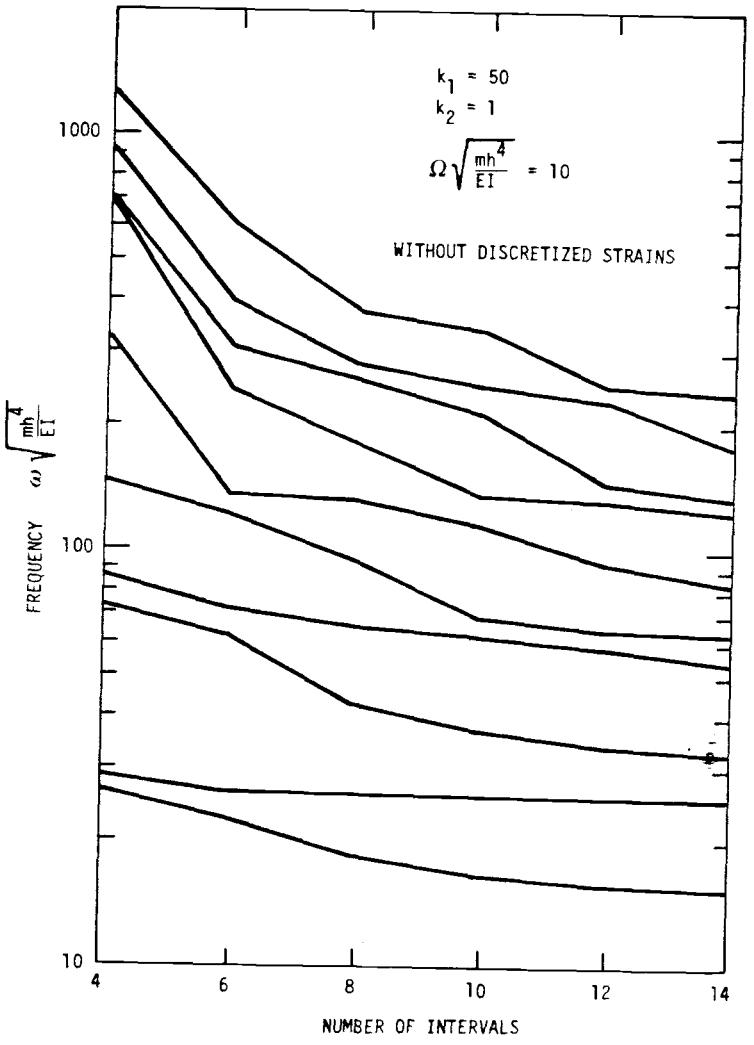

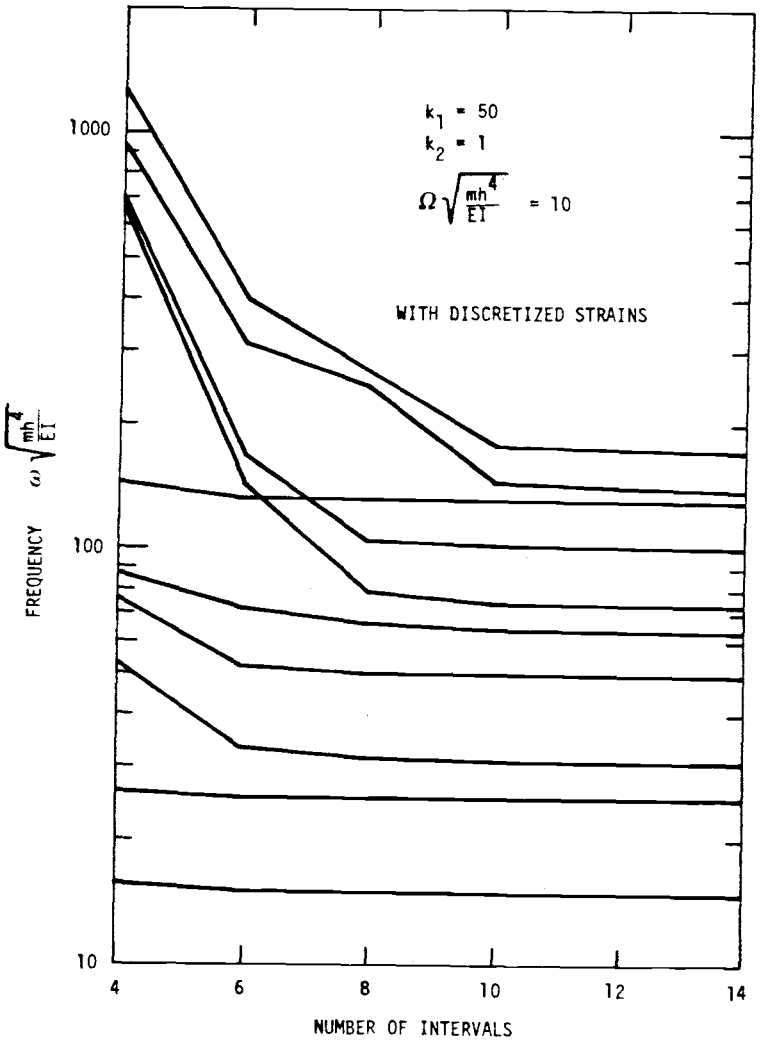

Figure 10. Convergence of Natural Frequencies

IV.3 Zero Rotation Rate

The primary interest in solutions at zero rotation rate is in reducing the size of the problem for subsequent analyses of the spinning blade. As mentioned in III.2, the reduction involves computing a few low-frequency normal modes of the blade at zero rotation rate, then using these modes in conjunction with generalized coordinates for analyzing the general case. Also mentioned was the fact that the normal modes consist of symmetric and antisymmetric modes, and that the flutter equations can be split into equations for symmetric and antisymmetric motion.

Solution of the eigenvalue problem

$$(p^{*2}\mathbf{M} + \mathbf{k})\mathbf{u} = \mathbf{0}, \tag{1}$$

where $\mathbf{K} = k_1\mathbf{K}_1 + k_2\mathbf{K}_2 + k_3\mathbf{K}_3 + \mathbf{K}_4$, yeilds n pair of natural frequencies and eigenvectors for the non-rotating blade. Equations II.8.1 and II.8.10 then allow us to transform the eigenvectors to physical displacements of the blade. Figure 11 illustrates the first few symmetric and antisymmetric normal modes at zero rotation rate. Note that the torsional displacements (θ) in the out-of-plane modes are not all to the same scale. Considering the symmetric modes (figure 11(a)), it can be seen that mode 1 is an in-plane bending mode, while mode 2 is an out-of-plane bending and torsion mode, modes 3 and 4 are in-plane bending modes, and mode 5 is a torsion mode. The antisymmetric modes (figure 11(b)) consist of two in-plane bending modes followed by an out-of-plane bending mode (mode 3), two more in-plane bending modes (4 and 5), and finally a

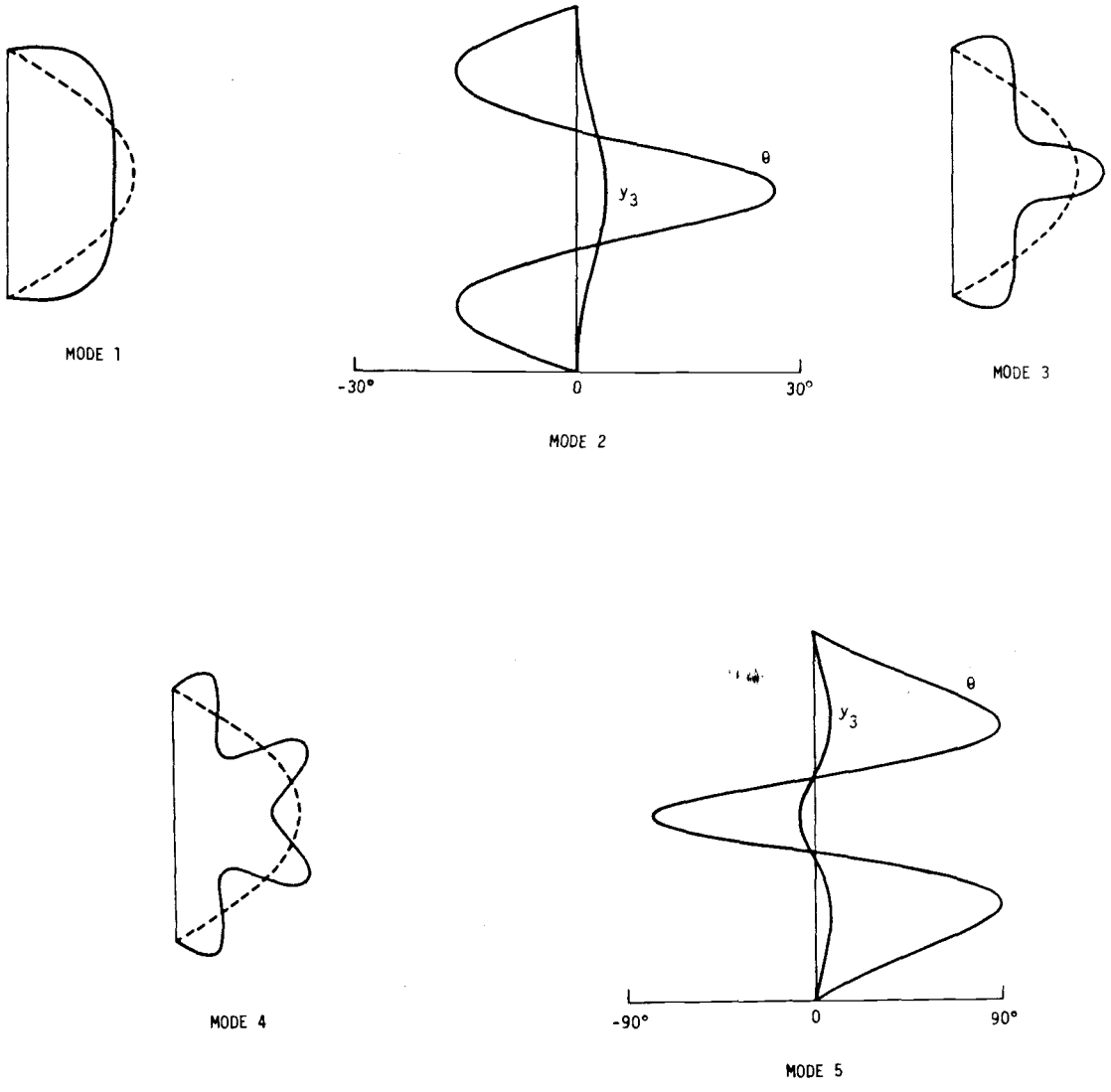

Figure 11a. Normal Modes of the Non-Rotating Blade
Symmetric Modes

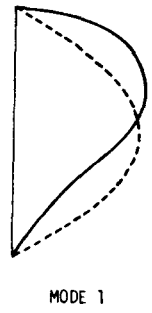

MODE 1

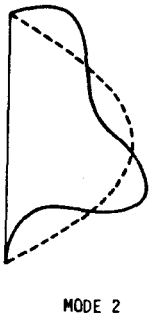

MODE 2

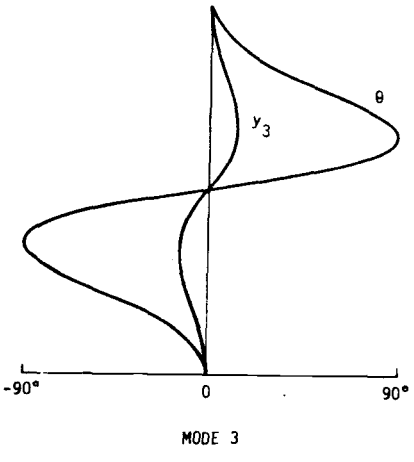

MODE 3

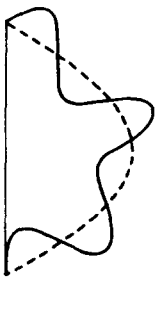

MODE 4

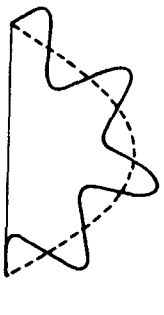

MODE 5

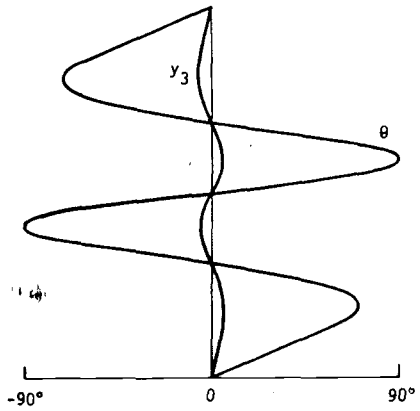

MODE 6

Figure 11b. Normal Modes of the Non-Rotating Blade
Antisymmetric Modes

torsion mode. For the reduction to normal-mode generalized coordinates, these 5 symmetric modes and 6 antisymmetric modes were found to be sufficient for flutter analyses. The reason for using 6 antisymmetric modes instead of 5 as in the symmetric case is to include the torsion mode (mode 6). It will prove convenient in subsequent discussions to refer to the j^{th} generalized coordinate (either symmetric or antisymmetric) as GCj.

A point regarding symmetric mode 2 should be made since the displacement patterns in this mode appear anomolous. Intuitively one might expect y_3 and θ to have similar displacement patterns, and indeed they do for all but this particular mode. Not only are the displacement patterns for y_3 and θ different in this mode, but θ has a reverse twist very much like symmetric mode 5, which has a much higher frequency. The fact that this behavior is possible can be proven with the following experiment: bend a piece of thin metal or plastic such as strapping material into a semi-circular arc and fasten the ends to a board; then by pushing out-of-plane on the center of the arc a displacement pattern similar to the second symmetric mode will result. The amount of reverse twist depends on the ratio of out-of-plane stiffness to in-plane stiffness.

IV.4 Free-Vibration of the Spinning Blade

Free-vibration frequencies of the spinning blade can be computed by setting the air density to zero, resulting in

$$(p^{*2}\mathbf{M} + p^{*}r\mathbf{G} + r^{2}\mathbf{C} + \mathbf{K})\mathbf{u} = \mathbf{0} \qquad (1)$$

The presence of the gyroscopic matrix **G** prevents us from solving this equation as a generalized eigenvalue problem. Meirovitch (Reference 27) shows how gyroscopic equations such as this can be treated as a $2n^{th}$ order generalized eigenvalue problem with 2n pure imaginary complex conjugate eigenvalues (p*). A more convenient approach here is to use the same technique which will be used for flutter analyses, as outlined in Appendix B. Figures 12(a) and 12(b) show the natural frequencies of the spinning blade for symmetric and antisymmetric motions, respectively. At low rotation rates the natural frequencies depend primarily on the blade stiffnesses; as the spin rate increases centrifugal and coriolis forces effectively stiffen the blade, increasing the natural frequencies. At very high spin rates the frequencies become directly proportional to the rotation rate as can be seen by dividing (1) by r^2, which for large r results in

$$(w^{2}\mathbf{M} + w\mathbf{G} + \mathbf{C})\mathbf{u} = \mathbf{0} \qquad (2)$$

where $w = p^*/r$. This eigenvalue problem yields the asymptotic frequencies:

$$p_j = w_j r \qquad (j = 1, 2, .. n) \qquad \text{as } r \to \infty$$

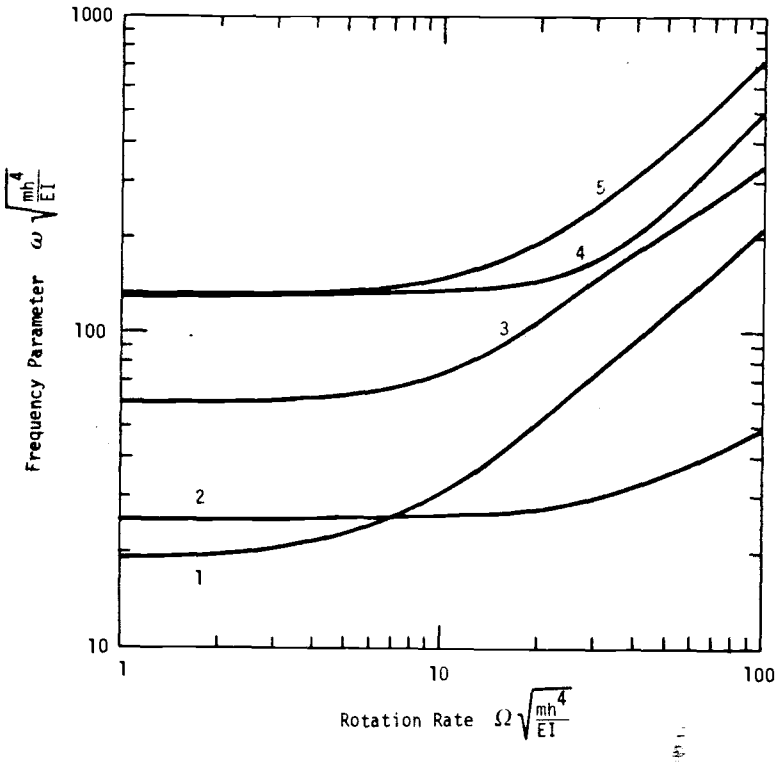

a) symmetric

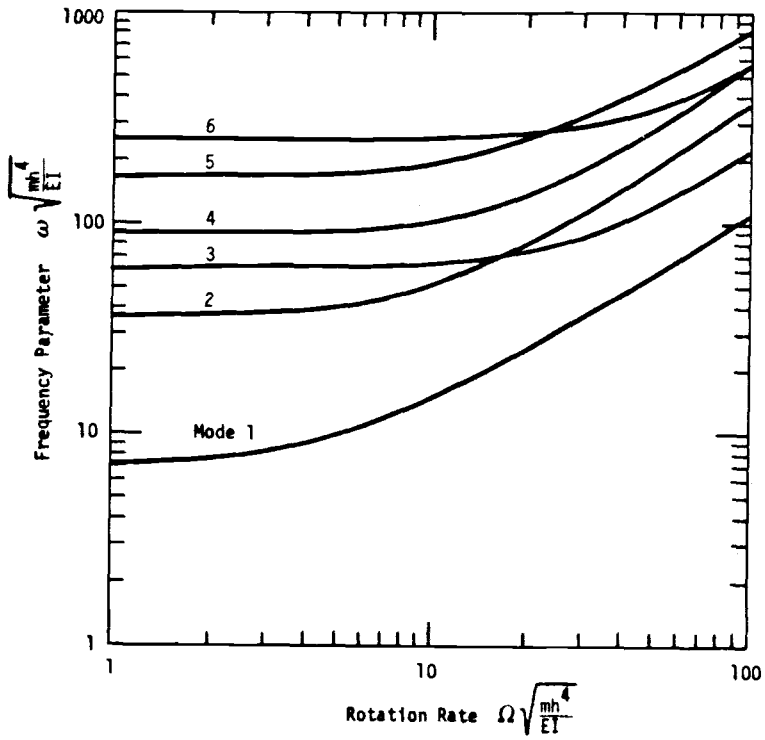

b) antisymmetric

Figure 12. Natural Frequencies of the Spinning Blade

Particularly significant in figure 12 is the fact that the frequencies of some modes increase more rapidly than others, resulting in frequency curves which cross. For instance, the frequencies of symmetric modes 1 and 2 cross at a dimensionless rotation rate of about 6.5. The reason for the different rates of increase in frequency is that the in-plane bending modes, such as symmetric mode 1, are effected much more by centrifugal forces than the out-of-plane bending modes, such as symmetric mode 2. It is interesting to note that instabilities are possible in a conservative gyroscopic system such as this, and that a necessary condition for such instability is the coalescence of free-vibration frequencies (References 28 and 29); however, no instabilities were encountered in the free-vibration case even with the frequency crossing seen in figure 12.

Free-vibration mode shapes of the spinning Darrieus blade likewise exhibit characteristics peculiar to gyroscopic systems. For instance, an in-plane bending vibration mode such as symmetric mode 1 will, due to gyroscopic coupling, induce motion out-of-plane. This behavior can be seen in a plot of the generalized coordinates for the free-vibration modes. Figure 13 shows the generalized coordinate amplitudes for symmetric modes 1 and 2 and antisymmetric mode 1. The generalized coordinates are normalized so that the sum of the squares of the amplitudes is one. At zero rotation rate symmetric mode 1 (figure 13(a)) consists of generalized coordinate 1, the first in-plane symmetric bending mode. As the rotation rate increases gyroscopic coupling increases the imaginary part of GC2, the out-of-plane bending mode. Recalling that in the complex

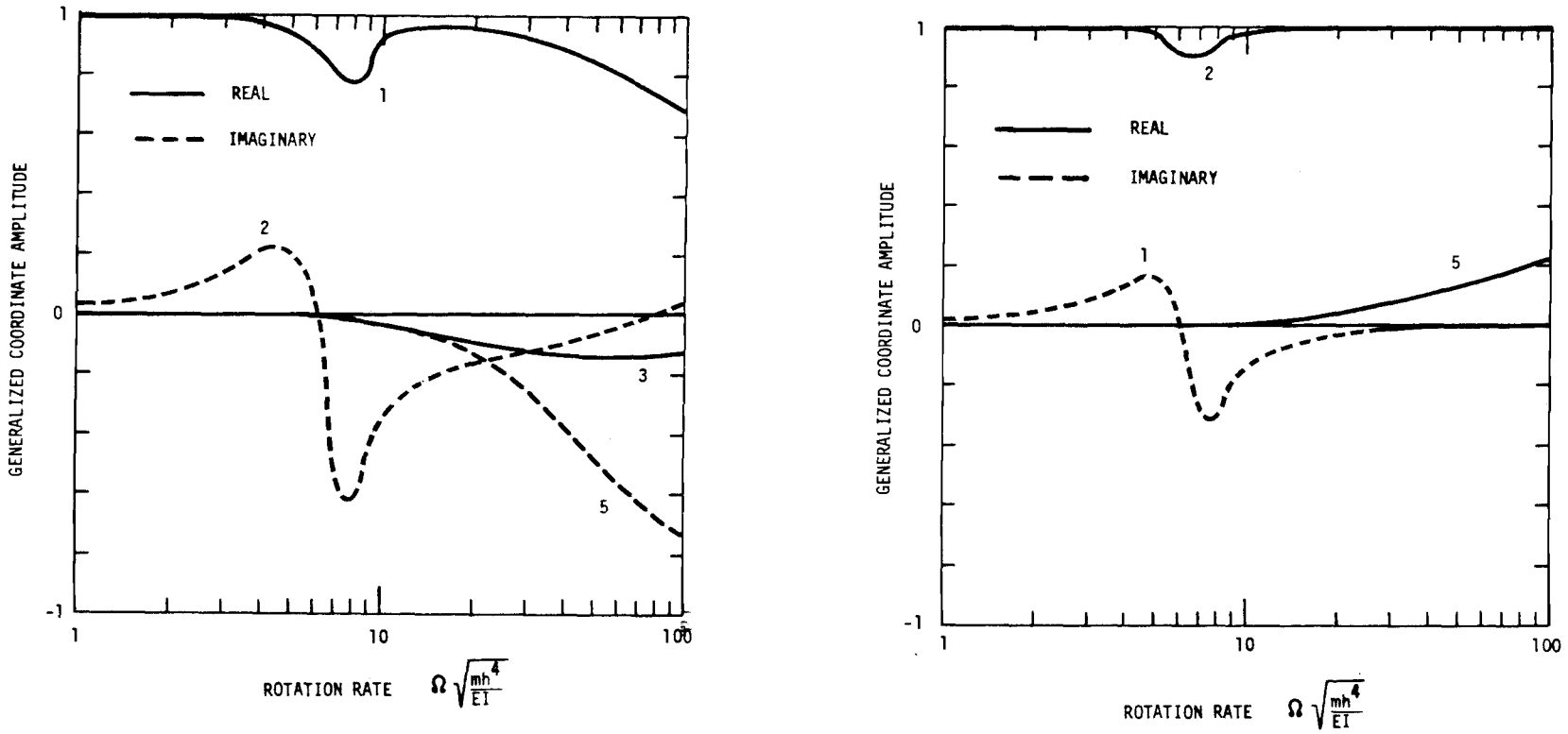

Figure 13. Generalized Coordinate Amplitudes

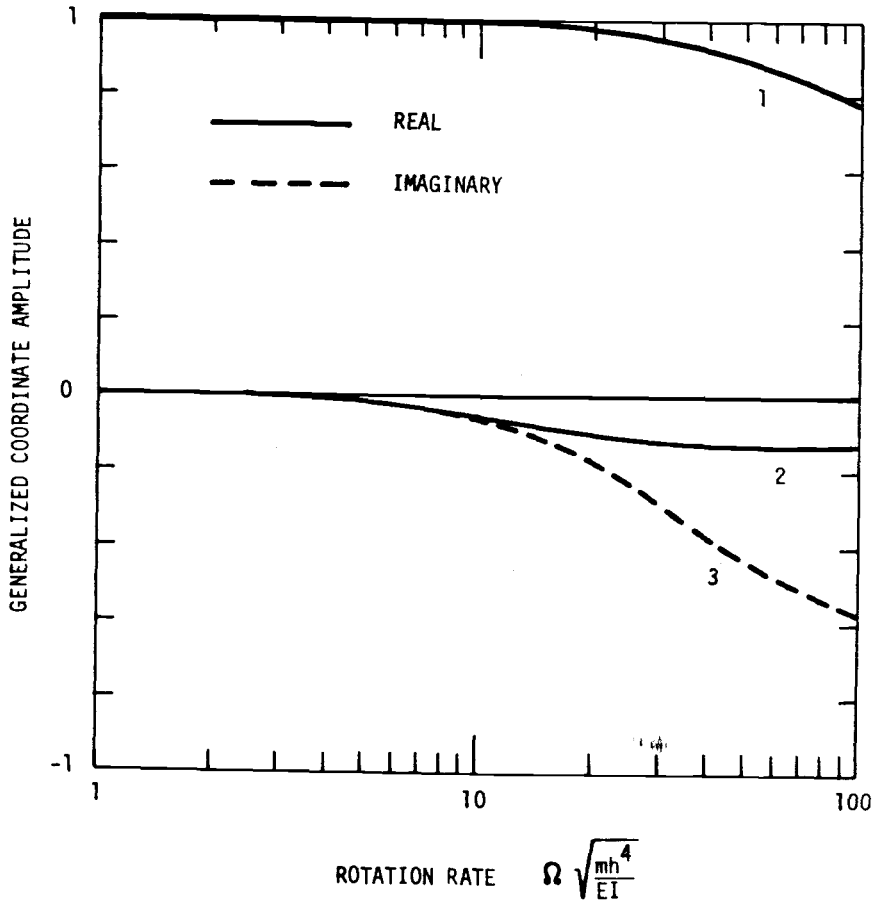

c) first antisymmetric mode

Figure 13 (cont)

representation of harmonic motion the physical displacement is obtained by multiplying the complex generalized coordinate by e^{pt} (using equation II.8.1) and taking the real part, we conclude that the free-vibration mode shape which corresponds to a real value of GC1 plus an imaginary value of GC2 must consist of bending in the x_3 direction (symmetric normal mode 2) followed ¼-cycle later by bending in the negative x_2 direction as in symmetric normal mode 1 (figure 11). That is, GC2 leads GC1. At the point where the frequency curves for modes 1 and 2 cross, approximately 6.5, the phase relationship between GC1 and GC2 suddenly changes by 180 degrees. This phenomenon can be explained by considering a simple spring-mass system with a harmonically-varying force. If the frequency of the forcing function is below the natural frequency of the spring-mass system, the response is in-phase with the force, whereas if the frequency is above the system's natural frequency the response is 180 degrees out-of-phase. If we think of the gyroscopic forces as the forcing function and GC2 as the spring-mass system, we see that this behavior is completely analogous. This behavior will prove to have important consequences in regards to the aeroelastic stability of the spinning blade.

IV.5 Stability of the Spinning Blade

Stability of the spinning blade can be determined from the flutter equations by simply examining the sign of the real part of the characteristic exponent: negative implies stable motion and positive implies instability. It should be pointed out that, strictly speaking, solutions to the flutter equations are valid only when the real part of the characteristic exponent is zero, implying steady harmonic oscillations. This is due to the fact that the aerodynamic forces were derived under the assumption of harmonic motion; it is generally agreed, however, that reasonable results are obtained even when the oscillations are growing or decaying (Reference 24).

Figure 14 shows the variation in growth rate of the oscillations with rotation rate for symmetric and antisymmetric motions. Recall that the growth rate is defined as

$$g = \frac{2Re(p)}{\omega} \qquad (1)$$

where Re(p) is the real part of the complex characteristic exponent p. Each curve represents a different mode of oscillation, known as an aeroelastic mode. At zero rotation rate the aeroelastic modes are just the normal modes of the blade. Figure 14 therefore illustrates the stability of motion in each aeroelastic mode. Typically, as the spin rate increases the growth rate becomes increasingly negative, indicating stable oscillations; at some point the growth rate for one of the modes begins increasing until it finally crosses the zero axis; at this point the oscillations are said to be neutrally stable, since the motion is neither growing nor

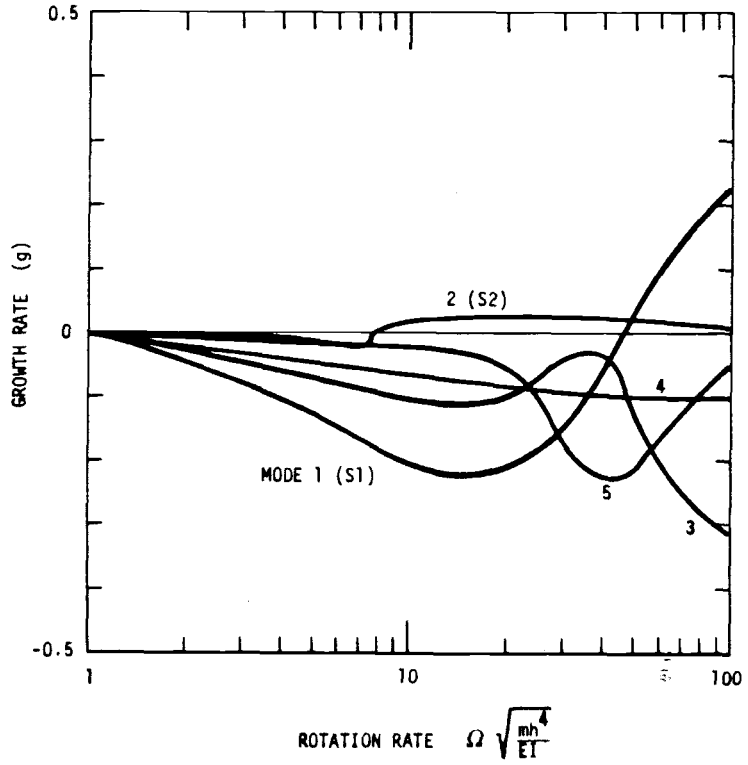

a) symmetric modes

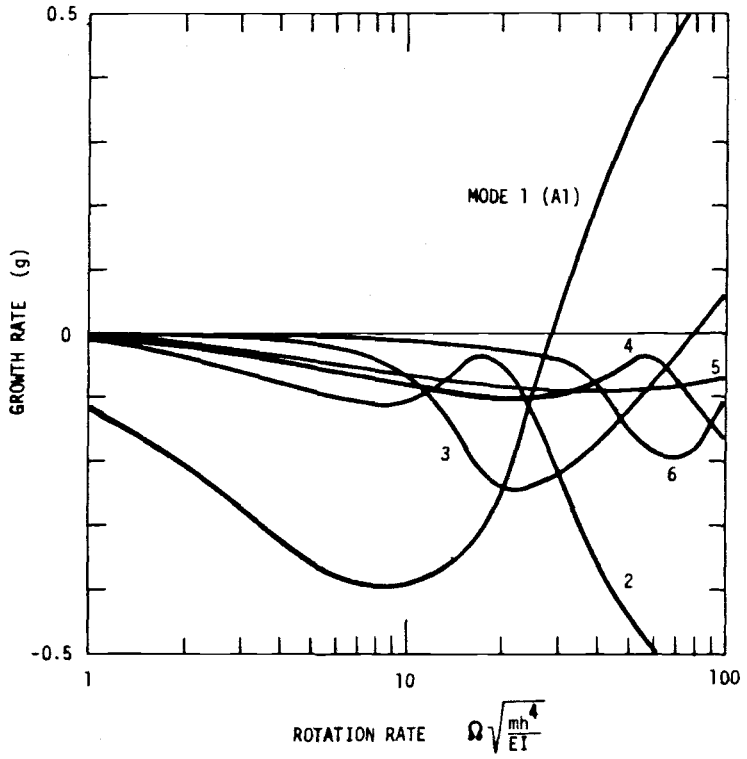

b) antisymmetric modes

Figure 14. Growth Rate of the Oscillations

decaying. These neutral stability points are also referred to as flutter points. Further increase in rotation rate causes the oscillations to grow, usually resulting in a catastrophic failure of the blade. Figure 14(a) shows that symmetric aeroelastic modes 1 and 2 flutter at dimensionless rotation rates of about 44 and 8, respectively. These two modes will be termed S1 and S2 for further discussion. In the antisymmetric case, figure 14(b) shows that aeroelastic mode 1 flutters at a rotation rate of about 27; for purposes of discussion this mode will be referred to as A1. These three modes, S1, S2 and A1 then are the most important modes of the system; the study of these modes will occupy the majority of the remainder of this chapter.

Mode S1 corresponds to normal coordinate 1, the first symmetric in-plane bending mode of the non-rotating blade. As shown in figure 14(a), S2 is quite stable up to about r = 40, at which point the growth rate rapidly changes sign, becoming increasingly unstable at higher rotation rates instead of stabilizing as S2 does. Since the growth rate (g) as defined here is approximately equal to the structural damping coefficient which would have to be subtracted from the system to result in steady harmonic oscillations as in a V-g flutter solution, we can conclude that this mode would be effected very little by the addition of structural damping.

To gain insight into the flutter mechanism it is helpful to study the variation in the mode shape with rotation rate. The mode shape at any rotation rate is merely the sum of the normal modes from figure 11 times their respective generalized coordinates times e^{pt}, bearing in mind that at any instant it is the real part of this complex mode shape which gives the physical configuration of the blade. The variation in mode

shape with rotation rate can therefore be visualized from plots of the generalized coordinate amplitudes as functions of rotation rate. Figure 15 illustrates the real and imaginary amplitudes of the generalized coordinates for aeroelastic mode S1 for a range of rotation rates. The generalized coordinates have been normalized in the following manner: at zero rotation rate the index of the generalized coordinate with the largest amplitude, say j_{max}, is determined; the generalized coordinates at any rotation rate are then normalized so that the sum of squares of the magnitudes equals one and the imaginary part of generalized coordinate j_{max} is zero. This figure should be compared with figure 13, the generalized coordinates for this mode in free-vibration. Note that in the free-vibration case the generalized coordinates are either pure real or pure imaginary, unlike non-gyroscopic systems where the generalized coordinates are always real; thus in a gyroscopic system the degrees of freedom may oscillate in-phase or 90 degrees out-of-phase with one another, whereas in a non-gyroscopic system the degrees of freedom all oscillate in-phase. With the addition of aerodynamic forces the phase differences are arbitrary; indeed, this phase difference between degrees of freedom is crucial to the stability of the system.

Referring to Figures 11 and 15 it can be seen that as the rotation rate is increased, gyroscopic coupling between in-plane and out-of-plane motion causes the contributions of the out-of-plane bending mode (GC2) and twisting mode (GC5) to increase. Note that the imaginary part of GC1 is always zero, on account of the normalization convention mentioned above. Below r = 6, the imaginary part of GC2 is positive while the real part is negative, so GC2 is said to <u>lead</u> GC1, since in a cycle of oscillation the displacement pattern in figure 11

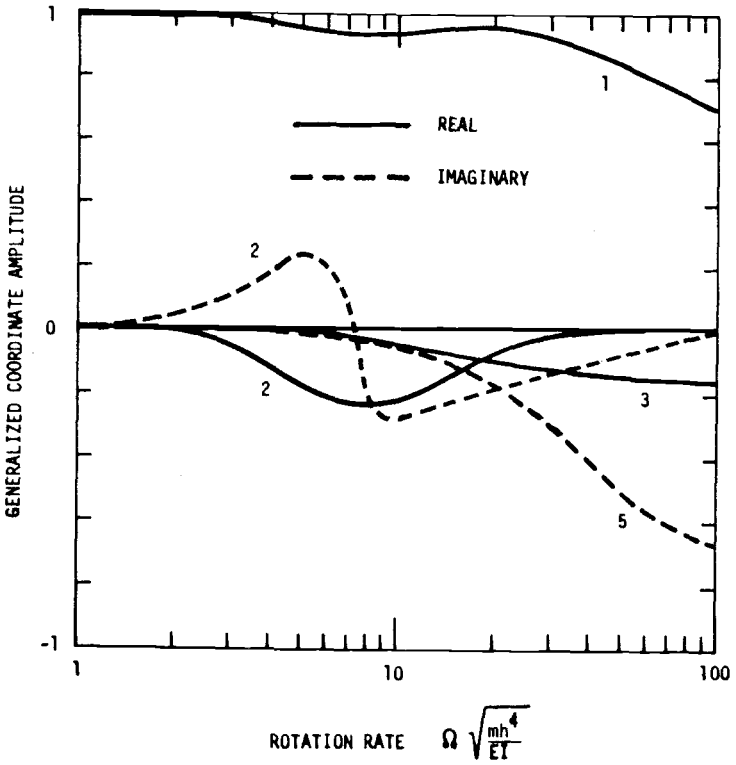

Figure 15. Generalized Coordinate Amplitudes for Mode S1

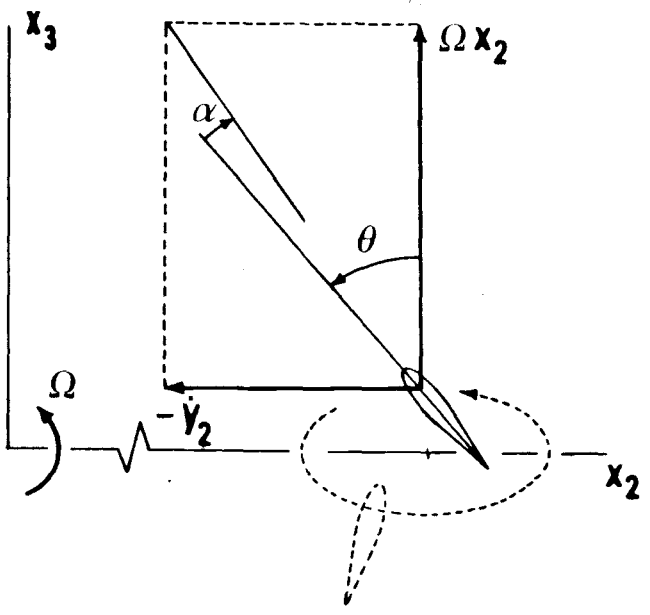

Figure 16. Effective Angle of Attack

corresponding to GC2 (normal mode 2) occurs before the displacement pattern corresponding to GC1 (normal mode 1). In the vicinity of r = 8 the imaginary part of GC2 suddenly changes sign, thus lagging GC1. As in the free-vibration case the cause of this abrupt change in phase is the increased centrifugal stiffening on the in-plane bending mode (GC1) and the accompaning crossing of the natural frequency curves seen in figure 12. In order to see what effect the aerodynamic forces have on the stability of the system, consider a section of the blade at mid-span, as shown in figure 16. The section has an effective angle of attack determined by the rotation rate and the velocity in the x_2 direction of approximately

$$\alpha = \theta + \frac{y_2}{\Omega x_2}$$

The lift induced by a positive effective angle of attack is in the negative x_2 direction. If the lift force is in phase with the velocity in the x_2 direction it will tend to destabilize the system; since the phasing of the lift is dependent on the phasing of y_2 and θ, it is the phasing between y_2 and θ which determines the stability of the oscillations. Note that this discussion applies to other sections of the blade with the velocity in the x_2 direction replaced with the velocity normal to the section. This view of the aerodynamic forces is greatly oversimplified, nevertheless it is the dominant mechanism controlling the aeroelastic stability of the blade.

In the case of aeroelastic mode S1, it can be seen that the phasing between the in-plane and out-of-plane motion below r = 8 is such that instability is possible; that is, the phasing is similar to the motion represented in figure 16. The reason this mode is stable below r = 8 is that the amplitude of

the twist in GC2 never becomes large enough to cause a positive effective angle of attack. Above r = 8 the phasing between GC1 and GC2 is such that an instability caused by interaction between these two coordinates is not likely. On the other hand, the amplitude of the twisting mode (GC5) steadily increases with a phase difference between GC1 and GC5 which makes instability possible. The amplitude of GC5 increases because of the gyroscopic coupling between the in-plane motion and the out-of-plane component of GC5. Finally, at a rotation rate of about 40, the effective angle of attack becomes positive over enough of the blade span to destabilize the motion.

The fact that GC5 is what destabilizes mode S1 can be further clarified by considering the work done by the aerodynamic forces as the blade goes through one cycle of oscillation. The advantage to measuring the influence of degrees of freedom on the stability of a system by the work done is that work is independent of any scaling of the coordinates; thus it is not necessary, for instance, to compare the amplitudes of angular deflections with linear displacements. Moreover, since work is a real, scalar quantity, the influence of phasing is automatically accounted for. A derivation of the expression for the work done on a fluttering system is contained in Appendix C. Figure 17 shows the work done (W_{jk}) on the system during one cycle of oscillation of each of the generalized coordinates (GCj) by forces induced by displacements in the generalized coordinates (GCk). Negative work indicates a stabilizing force, while positive work indicates destabilization. Thus the work done on GC1 by aerodynamic forces induced by displacement in GC5 are destabilizing, while the work done on GC1 by forces induced by

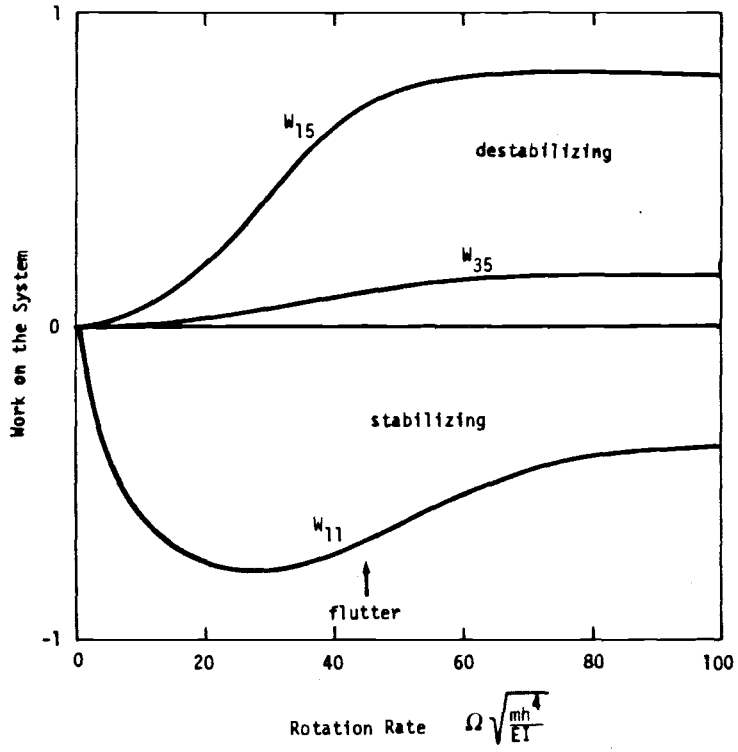

Figure 17. Work on the System - Mode S1

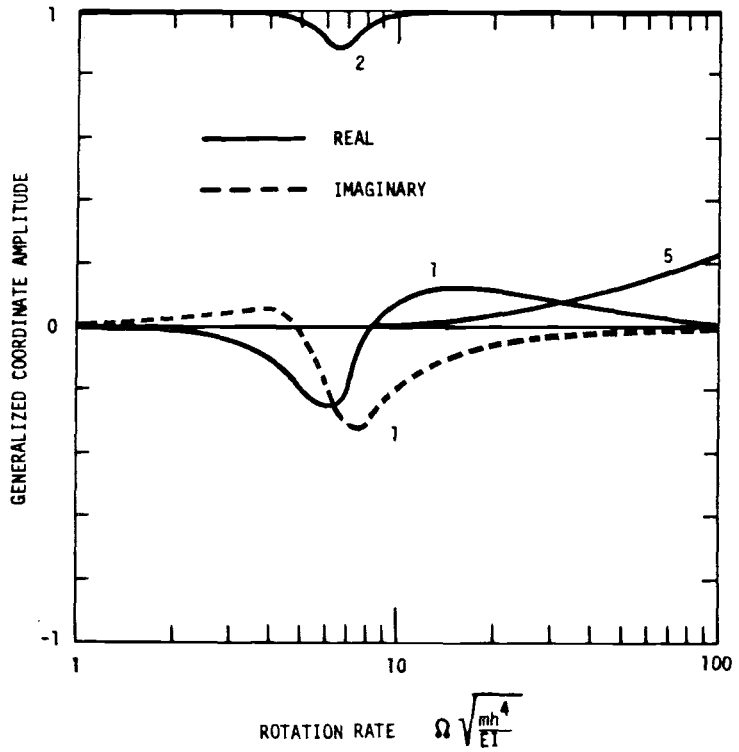

Figure 18. Generalized Coordinate Amplitudes for Mode S2

GC1 are stabilizing. A flutter instability which is due primarily to the interaction of two generalized coordinates is known as binary flutter.

Mode S2 corresponds to the first out-of-plane bending normal mode (GC2) of the non-rotating blade. Figure 14 shows that although this mode becomes unstable at a relatively low rotation rate, the instability is comparitively mild, as evidenced by the low growth rate. Evidently this mode would not flutter if the structural damping coefficient were greater than about .03. It is, however a potentially dangerous mode in regard to the fatique life of the blade since even with sufficient structural damping to prevent flutter this mode will have a relatively large gust response due to the low level of damping. Once again, looking at a plot of the generalized coordinate amplitudes (figure 18) we see that gyroscopic coupling between the out-of-plane bending mode (GC2) and the in-plane bending mode (GC1) increase the amplitude of GC1. As in mode S1, there is a sudden change in the phase relationship between GC1 and GC2, caused by the crossing of the natural frequencies of the corresponding free-vibration modes at about r = 8. The difference here is that, due to the higher frequency of oscillation, GC2 lags GC1 below r = 8, and leads GC1 above r = 8, opposite to the situation in S1. In this case the sudden phase change puts the two generalized coordinates in an unstable relationship, as evidenced by the change in sign of the growth rate (figure 14). The amplitude of GC1 does not continue to grow with increasing rotation rate, however, probably due to the fact that the frequency of the in-plane bending mode is increasing more rapidly than the out-of-plane bending mode (figure 12), resulting in decreased response to the lower-frequency oscillation of mode S2. At higher rotation

rates the amplitude of GC5 increases and serves to stabilize the motion further. This can be seen in figure 19 where the work on the system over one cycle of oscillation of mode S2 is presented. Here we see that the work done on GC2 by aerodynamic forces induced by motion of GC1 are destabilizing, while GC5 and GC1 are stabilizing.

Mode A1 is characterized by antisymmetric in-plane bending, primarily GC1, coupled gyroscopically with the first antisymmetric out-of-plane bending and twisting mode (GC3). At zero rotation rate aeroelastic mode A1 consists entirely of the first in-plane bending mode (GC1), as shown in figure 20. As was the case with mode S1, gyroscopic forces increase the amplitude of the out-of-plane bending and twist up to a point where the effective angle of attack over enough of the blade span becomes positive, resulting in a sudden change from stability to instability as the rotation rate is increased. Mode A1 flutters at a considerably lower rotation rate than S1, however, making it potentially more dangerous. A plot of the work done (figure 21) shows that the out-of-plane bending mode is destabilizing throughout the range of rotation rates, while GC1 is stabilizing.

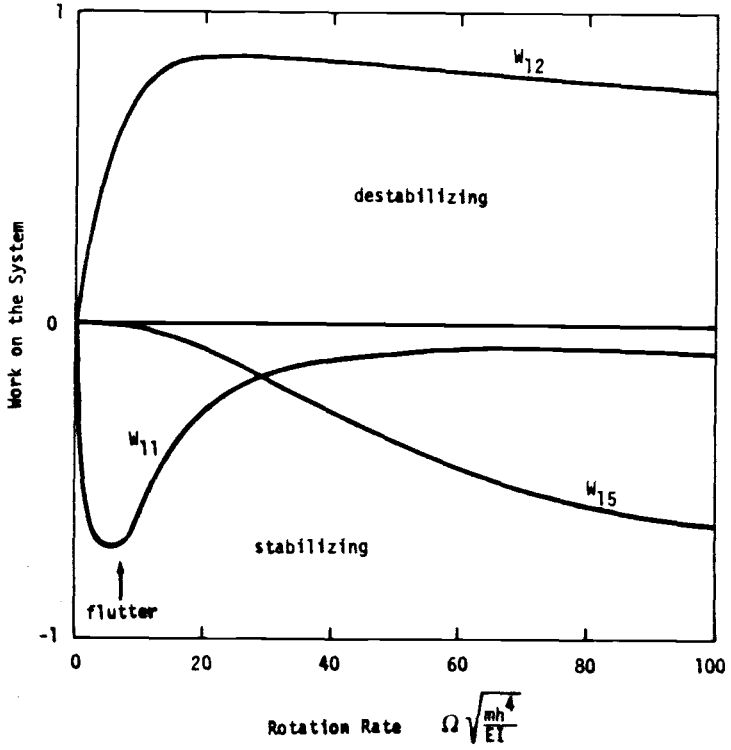

Figure 19. Work on the System - Mode S2

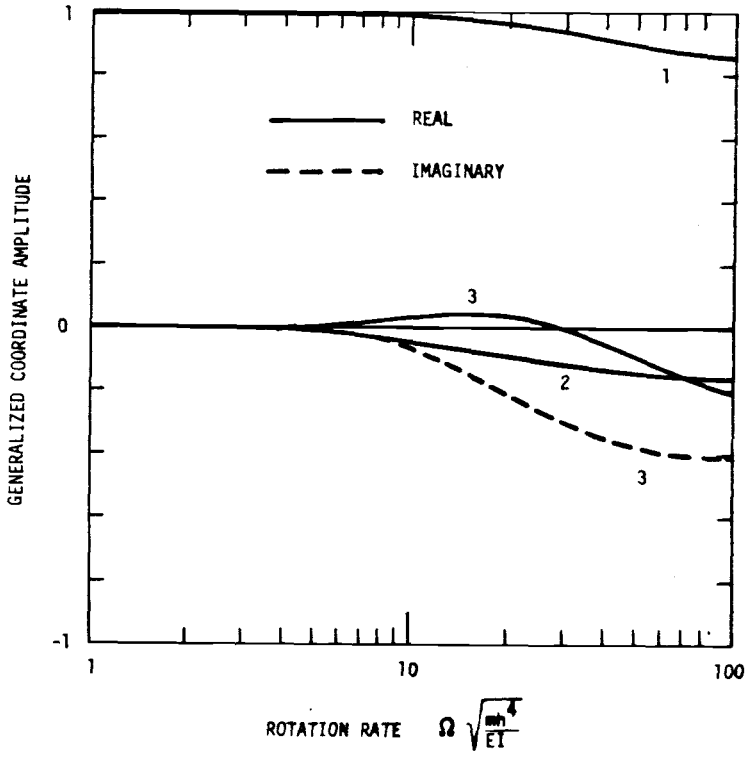

Figure 20. Generalized Coordinate Amplitudes for Mode A1

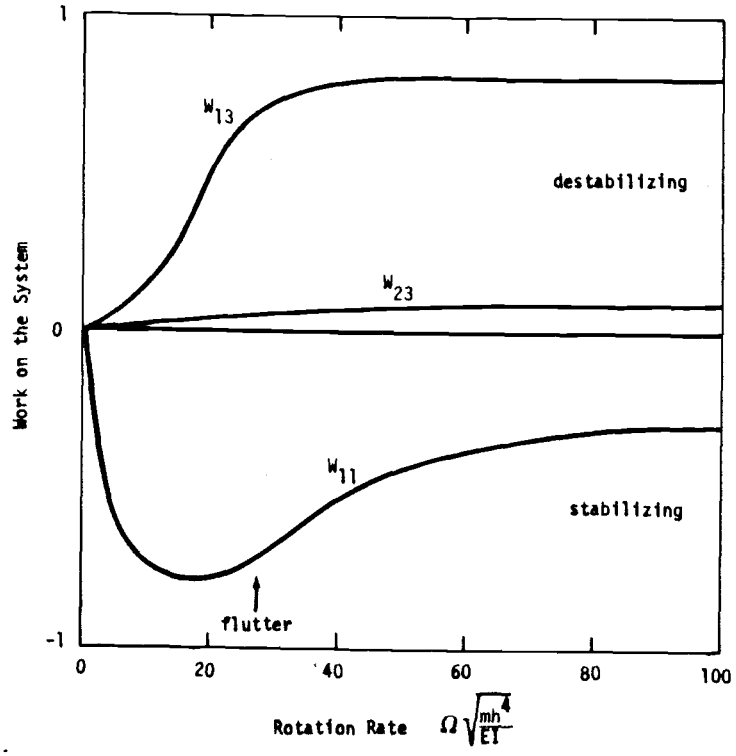

Figure 21. Work on the System - Mode A1

IV.6 Variation of Parameters

Now that we have looked at the causes of flutter instabilities in the Darrieus blade it is of interest to see what effect certain of the parameters have on the flutter rotation rates. In this section the effects of varying the location of the blade axis relative to the center of mass, the density of the blade, and the torsional and chordwise stiffnesses. In addition, the effect of assumptions in the aerodynamic model are examined.

Although the aerodynamic model used for this study accounts somewhat for the influence of shed vortices, it does not include such effects as the influence of the wake of previous blades or the aerodynamic interaction between sections of a blade. An indication of the sensitivity of the model to the aerodynamic theory is given by comparing the behavior of the model with and without the influence of shed vortices. The so-called quasi-steady aerodynamic theory is obtained from the theory used here by using a constant reduced frequency of zero; that is by setting Theodorsen's function to 1 in the expressions for aerodynamic forces (see section II.5). Figure 22 shows the results of the two theories for modes S1, S2, and A1. The fact that the differences are minor suggests that the neglected aerodynamic effects are probably not significant. This is supported by the fact that the generalized coordinate amplitudes are not greatly different with or without aerodynamic forces, suggesting that it is primarily the gyroscopic forces which determine the phase relationships which in turn determine the stability.

A parameter which is found to be very important in the

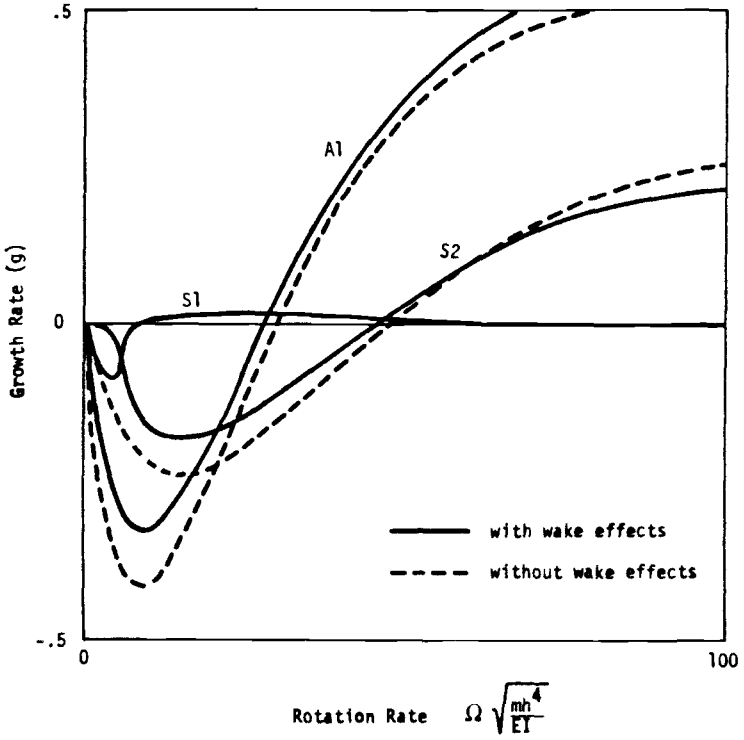

Figure 22. Effect of Aerodynamic Theory

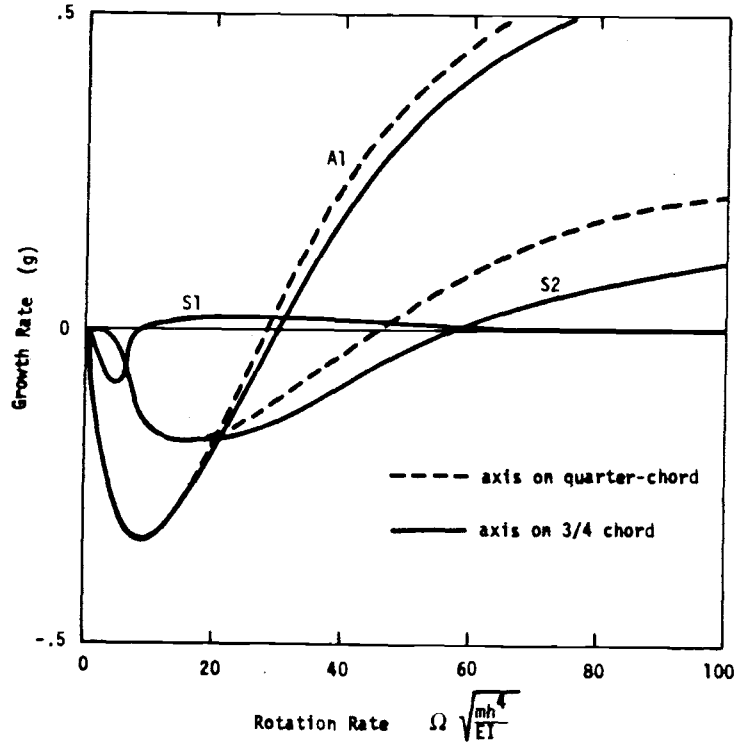

Figure 23. Effect of Axis Offset

study of the flutter of airplane wings is the location of the center of mass relative to the quarter-chord (also known as the aerodynamic center), and the elastic axis. To study this effect in the Darrieus, the blade axis was moved to the 3/4 chord, with the mass center on the ¼ chord. The results of this shift are shown in figure 23 for modes S1, S2, and A1. The offset apparently has little effect on modes S1 and A1. On the other hand, mode S2 flutters at a rotation rate which is about 30 percent higher than with the axis on the ¼ chord. Thus as far as the two most important modes (S1 and A1) are concerned, the locations of the mass center and elastic axis are of minor importance. This fact was also observed in Reference 4.

Another parameter which is important in the classical wing flutter problem is the density of the wing, or the density ratio m*. Since the blade density appears in the dimensionless rotation rate we might be tempted to conclude that the flutter rotation rate is proportional to the inverse square-root of the blade density; although it turns out that this conclusion is nearly correct, we cannot use the fact that the density appears in the dimensionless rotation rate as a justification since changing the blade density also changes the density ratio m*, which effects the aerodynamic forces. It is therefore necessary to study the effect of changes in the density ratio. Figure 24 shows the variation in flutter rotation rate with density ratio for modes S1, S2, and A1. Note that instead of the usual nondimensionalization of rotation rate we use

$$\frac{r}{m^*} = \Omega \sqrt{\frac{\pi \rho b^2 h^4}{EI}}$$

This plot can therefore be viewed as the effect of varying the blade density at a constant value of air density. Also shown

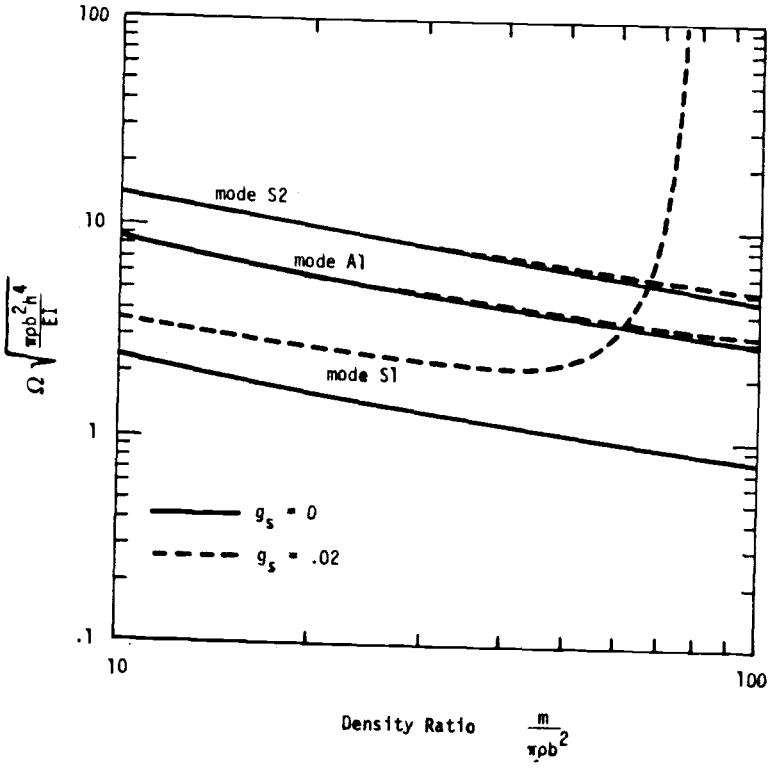

Figure 24. Density Variation

are the same modes with the addition of structural damping. With no structural damping the flutter rotation rates plot as nearly straight lines with slopes of $-\frac{1}{2}$; thus we may conclude that the flutter rotation rate is approximately proportional to the inverse square-root of the blade density. Moreover, this conclusion is not changed significantly for modes S1 and A1 with the addition of a small amount of structural damping. Mode S2, on the other hand, shows a drastic change in sensitivity to density ratio with the addition of structural damping. This is not surprising however in view of the lightly damped nature of mode S2 as shown in figure 14.

Perhaps the most important parameters determining the stability of the Darrieus blade are the stiffness ratios k_1 and k_2. Recall that k_1 is the ratio of out-of-plane or chordwise bending stiffness to in-plane bending stiffness, and k_2 is the ratio of torsional to in-plane stiffness. These two parameters were varied over a wide range and the corresponding flutter rotation rates computed using the same basic solution technique as outlined in Appendix B. Since changing the stiffness parameters can be expected to make significant changes in the normal modes of the blade, it was felt necessary to modify the set of non-rotating normal modes used as generalized coordinates in the stability calculations of the previous section. Instead of the 5 symmetric and 6 antisymmetric modes used previously, 9 symmetric and 9 antisymmetric modes were used. For both the symmetric and antisymmetric cases these modes consisted of 6 in-plane bending modes and 3 out-of-plane bending and twisting modes. In addition, 3 more symmetric and 3 antisymmetric modes were created from the 3 out-of-plane normal modes. These 3 additional modes consisted of the torsional portion of the 3 out-of-plane normal modes, with all other

displacements set to zero. The purpose in adding these 3 degrees of freedom was to allow changes in the coupling between out-of-plane bending and twist, changes which are bound to occur with variations in the stiffness parameters. Numerical experiments with this set of 12 generalized coordinates confirmed that they represent the structure very well over the range of stiffness parameters used.

The results of these variations are presented in figures 25, 26, and 27 for modes S1, S2, and A1, respectively. In each figure is shown a) the results of varying k_1 holding k_2 constant, and b) the results of varying k_2 holding k_1 constant. Each curve represents neutral stability: rotation rates above the curves are unstable, and below the curves are stable regions. Figure 25(a) shows the effect of varying the chordwise stiffness for four different values of torsional stiffness for mode S1. Looking at figure 25(a) we see that for low values of k_2 (.01 or .1), the critical flutter speed increases with increasing chordwise stiffness. On the other hand for higher values of k_2 (1 or 5) it is desirable to have k_1 relatively low to avoid flutter. Figure 25(b) shows the effect of varying k_2 for three values of k_1. For a particular value of k_1, say 10, this mode is completely stabilized if k_2 is greater than a certain value, about 1 in this case.

There is a great deal of similarity between the behavior of mode S1 and mode A1, shown in figure 27, except that the critical rotation rates for A1 are lower than S1. Thus adjusting the stiffness parameters to increase the flutter speed for one mode will have much the same effect in the other mode.

The effect of varying the stiffness parameters on mode S2 has a much different effect, as shown in figure 26. Recall that

mode S2 has a relatively mild instability at a rotation rate of about 8 (k_1 = 5 and k_2 = 1) which could be removed with the addition of a small amount of structural damping. Evidently this instability is relatively mild over the range of stiffness parameters studied here, as no instability was found with the addition of a structural damping coefficient of .03. Figure 26 shows that this mode is generally unstable at lower rotation rates for lower values of the stiffness parameters. In the last section we saw that the cause of flutter in this mode was the crossing of frequencies of the in-plane bending and out-of-plane bending modes due to the stronger centrifugal stiffening of the in-plane mode. Reducing the torsional and chordwise stiffnesses then results in lower frequencies for the out-of-plane mode, hence the in-plane mode frequency crosses at a lower rotation rate. Unlike modes S1 and A1, this mode does not have regions in the k_1-k_2 plane which are flutter-free.

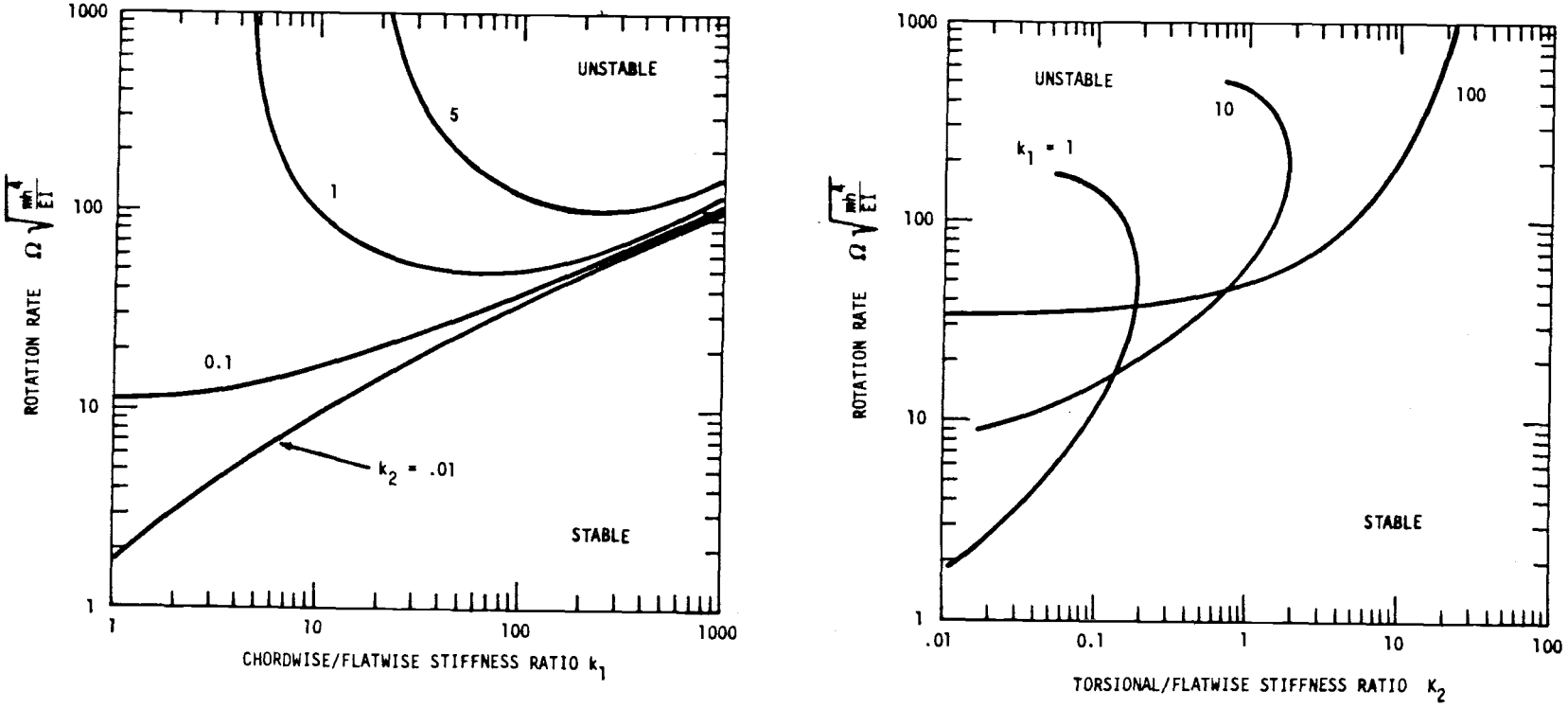

Figure 25. Stiffness Variation for Mode S1

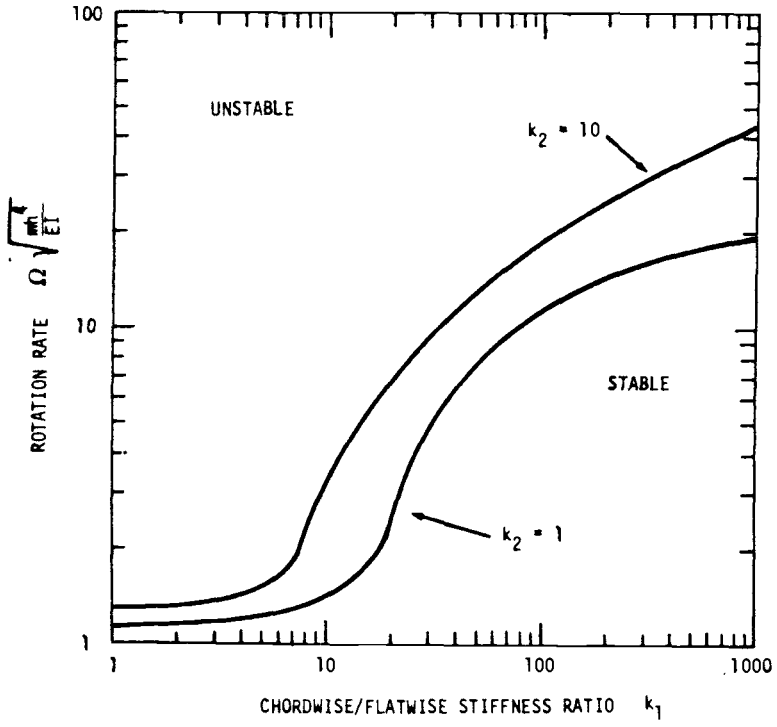

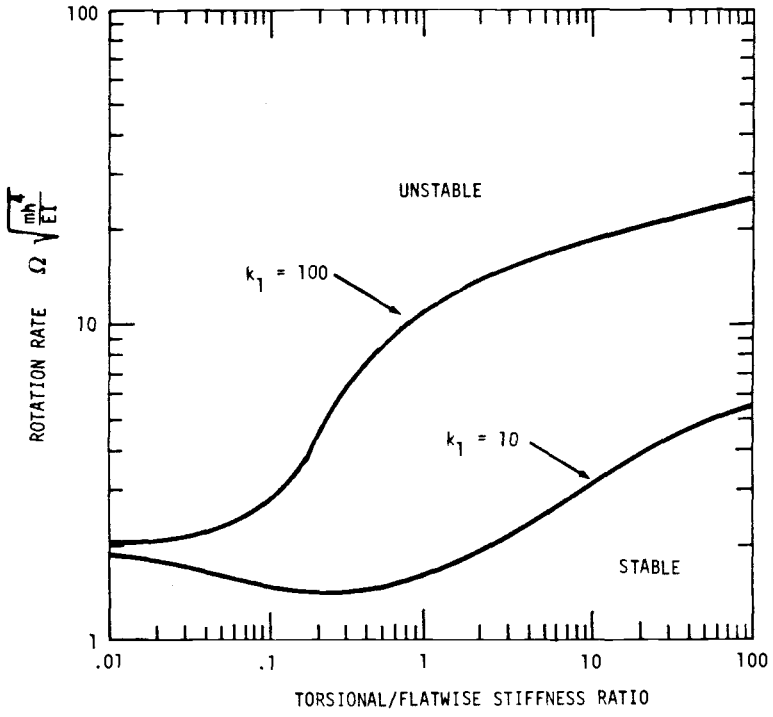

Figure 26. Stiffness Variation for Mode S2

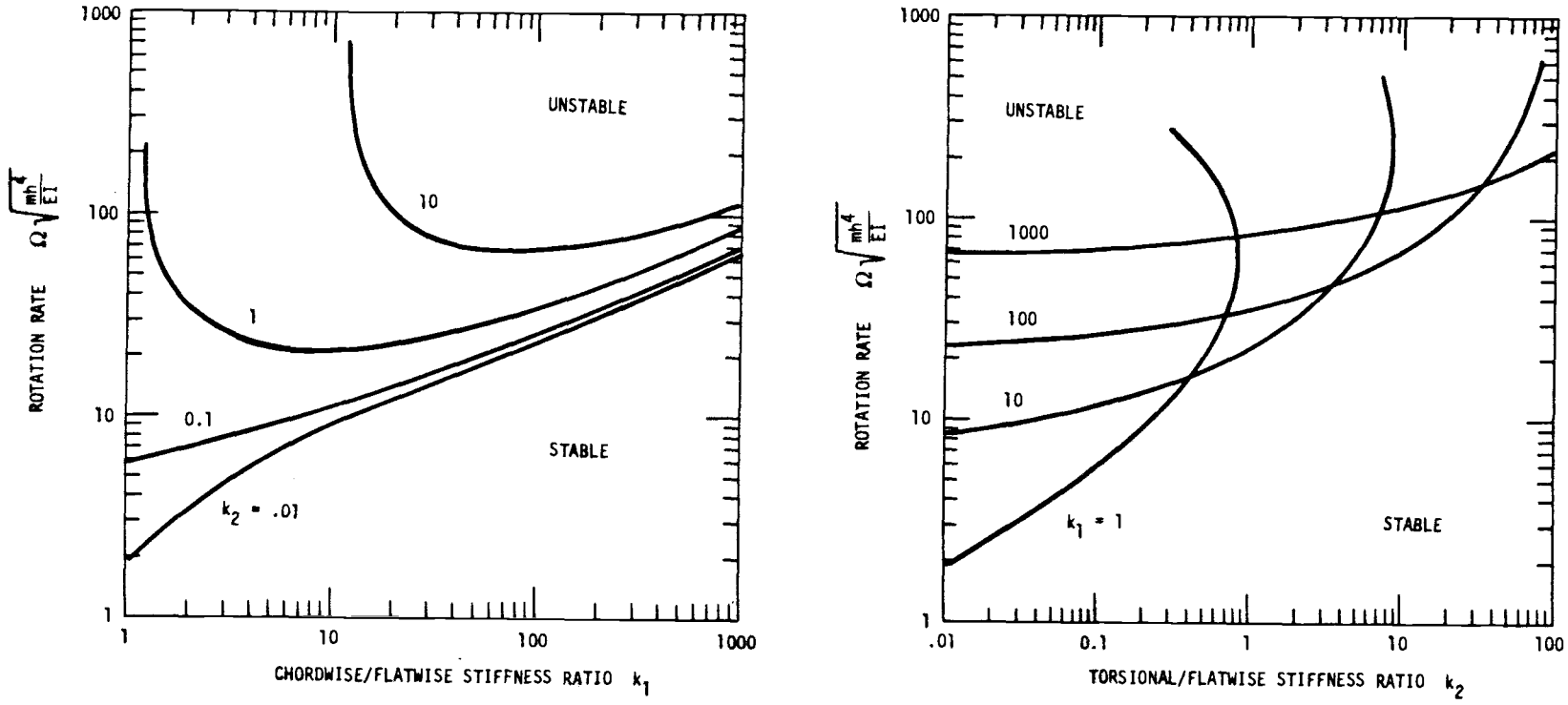

Figure 27. Stiffness Variation for Mode A1

V. CONCLUSIONS

In previous sections it has been shown that small oscillations in the Darrieus wind turbine can, under certain conditions, become unstable. Although this study considered only a single Darrieus blade spinning in the absence of wind, stability in this case is clearly a prerequisite for stability in the case of a multi-blade turbine spinning in the presence of wind.

The primary cause of the flutter instabilities was shown to be the gyroscopic coupling between motion in the plane of the blade and motion perpendicular to the plane of the blade. The strength of this coupling is directly dependent on the spin rate of the turbine. Furthermore, the nature of the gyroscopic coupling, particularly the phase difference between in-plane and out-of-plane motions, is dependent on the frequency of the oscillations, which in turn is also depenent on the rotation rate. The phase difference between the in-plane and out-of-plane motions was shown to have a decisive influence on the stability of small oscillations of the blade.

Three modes of oscillation were identified as the primary flutter modes of the Darrieus. The mode which becomes unstable at the lowest spin rate is a mildly unstable mode which is very similar to the second symmetric free-vibration mode of the spinning blade, which consists of out-of-plane bending and torsion coupled with in-plane bending. Because this instability is very mild, it is easily stabilized with a small amount of

structural damping; this is not to say that this mode is of no concern, however. Even with enough structural damping to alleviate the flutter problem, it is likely that oscillations caused by, for instance, gusts would decay relatively slow. These lighly-damped oscillations could shorten the fatique life of the blade.

As the rotation rate is increased, the second unstable mode encountered is comparatively violent. This mode was identified as being very close to the first antisymmetric free-vibration mode of the spinning blade. Although this instability occurs at a rotation rate which is roughly three times as great as the first flutter mode, it is potentially more dangerous since it is evidently not stabilized by structural damping.

The third flutter mode was identified as a symmetric torsion mode coupled with in-plane bending. Although for the nominal case studied here this mode flutters at a rotation rate approximately 60 percent higher than the second mode, at certain combinations of in-plane, out-of-plane, and torsional stiffnesses, the flutter rotation rates for these two modes become nearly equal. Like the second mode, this flutter mode also occurs abruptly and leads to violently unstable oscillations.

The fact that in all three instabilities the modes were identified as being close to free-vibration modes suggests that instabilities in the Darrieus are caused more by inertia forces, particularly the gyroscopic forces, than aerodynamic forces as in classical airplane wing flutter. This conclusion was supported by showing the effect of varying the ratio of blade mass to air mass.

As mentioned above, it is the phasing between in-plane and out-of-plane motions which plays a decisive role in the sta-

bility or instability of the Darrieus blade. This phasing is largely dependent on the frequency of the oscillations by way of the gyroscopic coupling. The fact that in-plane motions are effected much more by centrifugal forces than out-of-plane motions causes abrupt changes in the phasing in both free-vibation modes and the corresponding aeroelastic modes. This is the primary cause of the second instability; the cause of the other two is the increased gyroscopic coupling as rotation rate is increased. Both of these mechanisms were shown to be be strongly influenced by the in-plane, out-of-plane and torsional stiffness of the blade. Moreover, these flutter modes were shown to be relatively independent of the location of the mass center and elastic axis in a cross-section of the blade.

VI. BIBLIOGRAPHY

1. Blackwell, B. F., and Reis, G. E., "Blade Shape for a Troposkein type of Vertical-Axis Wind Turbine", SLA-74-0154, Sandia Laboratories, Albuquerque, New Mexico, 1974.

2. Darrieus, G. J. M., "Turbine Having its Rotating Shaft Transverse to the Flow of the Current", United States Patent No. 1,835,018, December 8, 1931.

3. South, P., and Rangi, R. S., "Preliminary Tests of a High Speed Vertical Axis Windmill Model", National Research Council of Canada, LTR-LA-74, March 1971.

4. Ham, N. D., "Aeroelastic Analysis of the Troposkien-Type Wind Turbine", Sandia Laboratories Report SAND 77-0026, April 1977.

5. Meirovitch, L., Analytical Methods in Vibrations, MacMillan and Co., 1967.

6. Strang, G., and Fix, G., An Analysis of the Finite Element Method, Prentice-Hall, 1973.

7. Bisplinghoff, R., Ashley, H., and Halfman, R., Aeroelasticity, Addison-Wesley, 1955.

8. Sokolnikoff, I. S., Tensor Analysis, John Wiley and Sons, Inc., N.Y., 1964.

9. Ojalvo, I. U., "Coupled Twist-Bending Vibrations of Incomplete Elastic Rings", Int. J. Mech. Sci., **4**, pp. 53-72, 1962.

10. Fettahlioglu, O. A., "Consistent Treatment of Extensional Deformations for the Bending of Arches, Curved Beams and Rings", ASME Journal of Pressure Vessel Technology, Vol. 99, pp. 2-11, Feb. 1977.

11. Archer, R. R., "Small Vibrations of Thin Incomplete Circular Rings", International Journal of Mechanical Science, Vol. 1, pp. 45-56, 1962.

12. Meirovitch, L., Methods of Analytical Dynamics, McGraw-Hill, 1970.

13. Fung, Y. C., An Introduction to the Theory of Aeroelasticity, John Wiley, 1955.

14. Ortega, J. M., and Rheinboldt, W. C., Iterative Solution of Nonlinear Equations in Several Variables, Academic Press, New York, 1970.

15. Powell, M. J. D., "A Fortran Subroutine for Solving Systems of Nonlinear Algebraic Equations", in Numerical Methods for Nonlinear Algebraic Equations, P. Rabinowitz (ed.), Gordon and Breach, London, 1970.

16. Prenter, P. M., Splines and Variational Methods, John Wiley and Sons, New York, 1975.

17. Dawe, D. J., "Curved Finite Elements for the Analysis of Shallow and Deep Arches", Computers and Structures (4), pp. 559-580, 1974.

18. Mitchell, A. R., and Wait, R., The Finite Element Method in Partial Differential Equations, John Wiley and Sons, London, 1977.

19. Parlett, B. N., The Symmetric Eigenvalue Problem, Prentice-Hall, Englewood Cliffs, N. J., 1980.

20. Demarais, R. N., and Bennett, R. M., "An Automated Procedure for Computing Flutter Eigenvalues", Journal of Aircraft, Vol. 11, pp. 75-80, Feb. 1974.

21. Smith, B. J., et. al., Matrix Eigensystem Routines: EISPACK Guide, Springer-Verlag, Berlin, 1974.

22. Rakowski, J. E., and Renard, M. L., "A Study of the Nutational Behavior of a Flexible Spinning Satellite Using Natural Frequencies and Modes of the Rotating Structure", presented as Paper 70-1046 at the AIAA Astrodynamics Conference, Santa Barbara, Ca., 1970.

23. Meirovitch, L., "A Stationarity Principle for the Eigenvalue Problem for Rotating Structures", AIAA Journal (14) 10, pp. 1387-1394, Oct. 1976.

24. Hassig, H. J., "An Approximate True Damping Solution of the Flutter Equation by Determinant Iteration", Journal of Aircraft Vol. 8 (11), pp. 885-889, Nov. 1971

25. Dahlquist, G., and Bjork, A., Numerical Methods, Prentice-Hall, Englewood Cliffs, N. J., 1974.

26. Dongarra, J. J., et. al., LINPACK Users' Guide, SIAM, 1979..

27. Meirovitch, L., "A New Method of Solution of the Eigenvalue Problem for Gyroscopic Systems", AIAA Journal (12) 10, pp. 1337-1342, Oct. 1974.

28. Hagedorn, P., "On the Stability of Steady Motions in Free and Restrained Dynamical Stystems", ASME Journal of Applied Mechanics (46), June 1979.

29. Huseyin, K., and Plaut, R. H., "Transverse Vibrations and Stability of Systems with Gyroscopic Forces", Journal of Structural Mechanics (3) 2, pp. 163-177, 1974.

30. Mantagazza, C.C., "Continuation and Direct Solution of the Flutter Equation", Computers and Structures, **8**, 185-192, 1978.

31. Jocelyn Lawrence, A., and Jackson, P., "Comparison of Different Methods of Assessing the Free Oscillatory Characteristics of Aeroelastic Systems", Current Papers, C.P.N 1084, Dec. 1968, Aeronautical Research Council, London, England.

32. Rheinboldt, W.C., "Numerical Analysis of Continuation Methods for Nonlinear Structural Problems", Computers and Structures **13**, 103-113, 1981.

33. Keller, H.B., "Global Homotopies and Newton Methods", in Recent Advances in Numerical Analysis, C. deBoor and G. H. Golub (eds), Academic Press, New York, 1978.

34. Broyden, C. G., "A Class of Methods for Solving Nonlinear Simultaneous Equations", Math. Comp. **19**, 577-593, 1965.

35. Schmidt, W. F., "Adaptive Step Size Selection for Use with the Continuation Method", Int. J. Num. Meth. Eng. **12**, 677-694, 1978.

36. Rheinboldt, W. C., "Solution Fields of Nonlinear Equations and Continuation Methods", SIAM J. Numer. Anal. **17** (2), 221-237, 1980.

37. Den Heijer, C., and Rheinboldt, W. C., "On Steplength Algorithms for a Class of Continuation Methods", SIAM J. Num. Anal. **18** (5), 1981.

38. Lanczos, C., The Variational Principles of Mechanics, University of Toronto Press, 1970 (4^{th} edition).

39. Crisp, J. D. C., "The Equations of Energy Balance for Fluttering Systems with some Applications in the Supersonic Regime", J. of Aero/Space Sciences **26** (11), pp. 703-716, 738, Nov. 1959.

APPENDICES

APPENDIX A. MATRIX TERMS

In this section the terms of the various matrices arising from discretization of the strain energy, kinetic energy, and aerodynamic forces will be listed. In section II.8 the flutter equations were written as

$$\left[p^{*2}\mathbf{M} + p^{*}r\mathbf{G} + r^{2}\mathbf{C} + k_1\mathbf{K}_1 + k_2\mathbf{K}_2 + k_3\mathbf{K}_3 + \mathbf{K}_4 - \frac{r^2}{m^*}\mathbf{A}(k^*) \right] \mathbf{u} = \mathbf{0} \qquad (1)$$

Each of these matrices is the result of substituting the discretized variables y_1, y_2, y_3 and θ into the expressions for potential energy, kinetic energy, and aerodynamic forces, and integrating from $s^* = -1$ to $s^* = 1$. Each matrix has a form which is typified by the mass matrix:

$$\mathbf{M} = \int \mathbf{M}' ds^*$$

where

$$\mathbf{M}' = \begin{bmatrix} \mathbf{M}_{11} & \mathbf{M}_{12} & \mathbf{M}_{13} & \mathbf{M}_{14} \\ \mathbf{M}_{21} & \mathbf{M}_{22} & \mathbf{M}_{23} & \mathbf{M}_{24} \\ \mathbf{M}_{31} & \mathbf{M}_{32} & \mathbf{M}_{33} & \mathbf{M}_{34} \\ \mathbf{M}_{41} & \mathbf{M}_{42} & \mathbf{M}_{43} & \mathbf{M}_{44} \end{bmatrix} \qquad (2)$$

$\mathbf{M}_{ij}$ is an (n_i, n_j) rectangular matrix relating inertia forces on the i^{th} variable to displacements of the j^{th} variable,

$$n_1 = \underline{n} + 1$$
$$n_2 = \underline{n} + 1$$
$$n_3 = \underline{n} - 1$$
$$n_4 = \underline{n} + 1,$$

and $\underline{n}$ is the number of spline intervals.

It will prove useful to look at what happens to the various matrices when Lagrange's equations are used to derive the equations of motion. In general the Lagrangian for a linear system has the form

$$L = T - V = \tfrac{1}{2}\mathbf{z}^T\mathbf{M}\mathbf{z} + \mathbf{z}^T\mathbf{B}\mathbf{z} + \tfrac{1}{2}\mathbf{z}^T\mathbf{C}\mathbf{z} - \tfrac{1}{2}\mathbf{z}^T\mathbf{K}\mathbf{z}$$

which, when substituted into Lagrange's equation

$$\frac{d}{dt}\left[\frac{\partial L}{\partial \dot{\mathbf{z}}}\right] - \frac{\partial L}{\partial \mathbf{z}} = \mathbf{0}$$

results in

$$\tfrac{1}{2}(\mathbf{M} + \mathbf{M}^T)\mathbf{z} + (\mathbf{B} - \mathbf{B}^T)\mathbf{z} + \tfrac{1}{2}(\mathbf{C} + \mathbf{C}^T)\mathbf{z} + \tfrac{1}{2}(\mathbf{K} + \mathbf{K}^T)\mathbf{z} = \mathbf{0}$$

Thus we see that $\mathbf{M}$, $\mathbf{C}$, and $\mathbf{K}$ are symmetric matrices and $\mathbf{G} = (\mathbf{B} - \mathbf{B}^T)$ is skew-symmetric. These properties will be taken into account below in writting expressions for the matrix terms.

The mass matrix $\mathbf{M}$ arises from kinetic energy terms which are quadratic in the velocities. The terms of $\mathbf{M}_{ij}$ are given explicitly by

$$\mathbf{M}_{11} = \mathbf{q}_1\mathbf{q}_1^T$$

$$\mathbf{M}_{12} = \mathbf{0}$$

$$\mathbf{M}_{13} = \tfrac{1}{2} e_m b^* x_1^{*\prime} \mathbf{q}_1 \mathbf{q}_3'$$

$$\mathbf{M}_{14} = -\tfrac{1}{2} e_m b^* x_2^{*\prime} \mathbf{q}_1 \mathbf{q}_4$$

$$\mathbf{M}_{21} = \mathbf{M}_{12}^T$$

$$\mathbf{M}_{22} = \mathbf{q}_2 \mathbf{q}_2^T$$

$$\mathbf{M}_{23} = \tfrac{1}{2} e_m b^* x_2^{*\prime} \mathbf{q}_2 \mathbf{q}_3'^T$$

$$\mathbf{M}_{24} = \tfrac{1}{2} e_m b^* x_1^{*\prime} \mathbf{q}_2 \mathbf{q}_4^T$$

$$\mathbf{M}_{31} = \mathbf{M}_{13}^T$$

$$\mathbf{M}_{32} = \mathbf{M}_{23}^T$$

$$\mathbf{M}_{33} = \mathbf{q}_3 \mathbf{q}_3^T + e_r^2 b^{*2} \mathbf{q}_3' \mathbf{q}_3'^T$$

$$\mathbf{M}_{34} = \mathbf{0}$$

$$\mathbf{M}_{41} = \mathbf{M}_{14}^T$$

$$\mathbf{M}_{42} = \mathbf{M}_{24}^T$$

$$\mathbf{M}_{43} = \mathbf{M}_{34}^T$$

$$\mathbf{M}_{44} = e_r^2 b^{*2} \mathbf{q}_4 \mathbf{q}_4^T$$

The gyroscopic matrix

$$\mathbf{G} = \int \mathbf{G}' ds^*$$

where the terms of G' are

$$G'_{11} = G'_{12} = G'_{13} = G'_{14} = 0$$

$$G'_{21} = G'_{22} = G'_{24} = 0$$

$$G_{23} = 2q_2q_3^T$$

$$G_{31} = 0$$

$$G_{32} = - G_{23}^T$$

$$G_{33} = 2e_m b^* x_2^{*\prime}(q'_3q_3^T - q_3q_3'^T)$$

$$G_{34} = - 2e_m b^* x_1^{*\prime} q_3q_4$$

$$G_{41} = G_{42} = 0$$

$$G_{43} = - G_{34}^T$$

$$G_{44} = e_m b^* x_2^* q_4q_4^T - (e_m b^* x_2^* q_4q_4^T)^T = 0$$

The matrix of centrifugal force terms is

$$C = M_0 + K_0 = \quad C'ds^*$$

where the terms of C' are

$$C_{11} = P^* q'_1q_1'^T$$

$$C_{12} = C_{13} = C_{14} = 0$$

$$C_{21} = 0$$

$$C_{22} = q_2 q_2^T + P^* q_2' q_2'^T$$

$$C_{23} = \tfrac{1}{2} e_m b^* x_2^{*\prime} q_2 q_3'^T$$

$$C_{24} = \tfrac{1}{2} e_m b^* x_1^{*\prime} q_2 q_4^T$$

$$C_{31} = C_{13}^T$$

$$C_{32} = C_{23}^T$$

$$C_{33} = q_3 q_3^T + P^* q_3' q_3'^T$$

$$C_{34} = 0$$

$$C_{41} = C_{14}^T$$

$$C_{42} = C_{24}^T$$

$$C_{43} = C_{34}^T$$

$$C_{44} = 0$$

The stiffness matrix

$$K = k_1 K_1 + k_2 K_2 + k_3 K_3 + K_4 = \int K' ds^*$$

where the terms of K' are

$$K_{11} = x_2^{*\prime 2} q_1'' q_1''^T - 2c^* x_1^{*\prime} x_2^{*\prime} (q_1' q_1''^T + q_1'' q_1'^T)$$

$$+ c^{*2} x_1^{*\prime 2} q_1' q_1'^T + k_3 x_1^{*\prime 2} q_1' q_1'^T$$

$$\mathbf{K}_{12} = - x_1^{*\prime} x_2^{*\prime} q_1'' q_2''^T + c^*(x_1^{*\prime 2} q_1' q_2''^T - x_2^{*\prime 2} q_1'' q_2'^T)$$

$$+ c^{*2} x_1^{*\prime} x_2^{*\prime} q_1' q_2'^T + k_3 x_1^{*\prime} x_2^{*\prime} q_1' q_2'^T$$

$$\mathbf{K}_{13} = \mathbf{K}_{14} = \mathbf{0}$$

$$\mathbf{K}_{21} = \mathbf{K}_{12}^T$$

$$\mathbf{K}_{22} = x_1^{*\prime 2} q_2'' q_2''^T + c^* x_1^{*\prime} x_2^{*\prime} (q_2' q_2''^T + q_2'' q_2'^T)$$

$$+ c^{*2} x_2^{*\prime 2} q_2' q_2'^T + k_3 x_2^{*\prime 2} q_2' q_2'^T$$

$$\mathbf{K}_{23} = \mathbf{K}_{24} = \mathbf{0}$$

$$\mathbf{K}_{31} = \mathbf{K}_{13}^T = \mathbf{0}$$

$$\mathbf{K}_{32} = \mathbf{K}_{23}^T = \mathbf{0}$$

$$\mathbf{K}_{33} = k_1 q_3'' q_3''^T + k_2 c^{*2} q_3' q_3'^T$$

$$\mathbf{K}_{34} = k_1 c^* q_3'' q_4^T - k_2 c^* q_3' q_4'^T$$

$$\mathbf{K}_{41} = \mathbf{K}_{14}^T = \mathbf{0}$$

$$\mathbf{K}_{42} = \mathbf{K}_{24}^T = \mathbf{0}$$

$$\mathbf{K}_{43} = \mathbf{K}_{34}^T$$

$$\mathbf{K}_{44} = k_1 c^{*2} q_4 q_4^T + k_2 q_4' q_4'^T$$

Finally, the terms of the aerodynamic matrix are

$$\mathbf{A}_{11} = - x_2^{*\prime} \left[k^{*2} b^* x_2^{*\prime} - 2k^* x_2^* C(k) \right] \mathbf{q}_1 \mathbf{q}_1^T$$

$$\mathbf{A}_{12} = x_2^{*\prime} \left[k^{*2} b^* x_1^* + 2k^* x_1^{*\prime} x_2^* C(k) \right] \mathbf{q}_1 \mathbf{q}_2^T$$

$$\mathbf{A}_{13} = \mathbf{0}$$

$$\mathbf{A}_{14} = x_2^{*\prime} \left[k^{*2} b^* e_a + k^* x_2^* b^* + 2x_2^{*2} C(k) + k^* b^* (\tfrac{1}{2} + e_a) \right] \mathbf{q}_1 \mathbf{q}_4^T$$

$$\mathbf{A}_{21} = x_1^{*\prime} \left[k^{*2} x_2^{*\prime} b^* + 2k^* x_2^* x_2^{*\prime} C(k) \right] \mathbf{q}_2 \mathbf{q}_1^T$$

$$\mathbf{A}_{22} = - x_1^{*\prime} \left[k^{*2} x_1^{*\prime} b^* + 2k^* x_2^* C(k) \right] \mathbf{q}_2 \mathbf{q}_2^T$$

$$\mathbf{A}_{23} = \mathbf{0}$$

$$\mathbf{A}_{24} = - x_1^{*\prime} \left[k^{*2} b^* e_a + k^* x_2^* b^* + x_2^{*2} C(k) + k^* (\tfrac{1}{2} b^* + e_a) \right] \mathbf{q}_2 \mathbf{q}_4^T$$

$$\mathbf{A}_{31} = \mathbf{A}_{32} = \mathbf{A}_{33} = \mathbf{A}_{34} = \mathbf{0}$$

$$\mathbf{A}_{41} = - x_2^{*\prime} \left[k^{*2} e_a b^{*2} + 2b^* (\tfrac{1}{2} - e_a) k^* x_2^* C(k) \right] \mathbf{q}_4 \mathbf{q}_1^T$$

$$\mathbf{A}_{42} = x_1^{*\prime} \left[k^{*2} e_a b^{*2} + 2b^* (\tfrac{1}{2} - e_a) k^* x_2^* C(k) \right] \mathbf{q}_2 \mathbf{q}_2^T$$

$$\mathbf{A}_{43} = \mathbf{0}$$

$$\mathbf{A}_{44} = - k^{*2} (e_a^2 b^* + b^{*3}/8) \mathbf{q}_4 \mathbf{q}_4^T$$

$$+ k^* \left[2x_2^* b^* (\tfrac{1}{2} - e_a)(\tfrac{1}{2} + e_a) C(k) - b^{*2}(\tfrac{1}{2} + e_a) \right] \mathbf{q}_4 \mathbf{q}_4^T$$

$$+ b^* (\tfrac{1}{2} - e_a) x_2^{*2} C(k) \mathbf{q}_4 \mathbf{q}_4^T$$

Theodorsen's function is a complex-valued function of the so-called reduced frequency $k = \omega b / \Omega x_2$; hence the terms of $\mathbf{A}$ are in general complex. Note also that steady harmonic motion has been assumed in deriving the aerodynamic forces, as discussed in section II.5.

In terms of these matrices the kinetic energy , potential energy and generalized forces may be written as

$$T = \tfrac{1}{2} m_p h^3 \mathbf{u}^T \mathbf{M} \mathbf{u} + \Omega p m h^3 \mathbf{u}^T \mathbf{G} \mathbf{u}^T + \Omega^2 m h^3 \mathbf{u}^T \mathbf{M}_0 \mathbf{u}$$

$$V = \frac{EI}{2h} \mathbf{u}^T (k_1 \mathbf{K}_1 + k_2 \mathbf{K}_2 + k_3 \mathbf{K}_3 + \mathbf{K}_4) \mathbf{u}$$

$$+ \Omega^2 m h^3 \mathbf{u}^T \mathbf{K}_0 \mathbf{u}$$

$$\mathbf{f} = \pi \rho \Omega^2 b h^4 \mathbf{A} \mathbf{u}$$

Substituting these expressions into Lagrange's equation and dividing by EI/h then results in (1).

APPENDIX B. FLUTTER EQUATION SOLUTION TECHNIQUE

Perhaps the most commonly used method for solving the flutter equations is the so-called V-g technique (Reference 24). The most attactive feature of the V-g method is the fact that it consists of solving a number of eigenvalue problems, for which there are very efficient techniques. There are, however, several disadvantages to the V-g method, most of which are related to the fact that in the V-g method the flutter equations are formulated as an eigenvalue problem, which places severe restrictions on the form of the equations. For our purposes the biggest drawback is that V-g solutions often give poor indications of the response of a system except at the critical flutter point; in order to explain the cause of the flutter instabilities it is necessary to have a reasonably clear picture of the behavior of the critical modes all the way from zero rotation rate up to the critical flutter speed. It is generally agreed (References 24, 30, and 31) that a superior formulation of the flutter equations is the so-called p-k formulation, in which the characteristic exponent p is solved for, rather than the added structural damping coefficient. The difficulty with the p-k formulation is that it involves the solution of a system of nonlinear equations. The techniques available for the solution of nonlinear equations are far less reliable than those for solving the V-g eigenvalue problem. Moreover, the cost of a p-k solution is likely to be much greater than the corresponding V-g solution simply because a V-g solution tracks all n aeroelastic modes simultaneously, whereas in a p-k solution each mode must be tracked individually.

An example of the problems encountered in solving the Darrieus flutter equations using the V-g technique is shown in

figure 28. The V-g solution not only shows far greater levels of damping before flutter, but also exhibits a physically unrealistic loop-back accompanied by a rapid change in the mode. The V-g mode began at zero rotation rate as mode 1, but switches during the loop to become mode 2 at flutter, unlike the p-k solution curve which shows no such drastic changes. This type of behavior, while not typical of a V-g solution, is not uncommon either; Hassig (Reference 24) gives a similar example.

Various authors have proposed methods which overcome some of these difficulties. Hassig (Reference 24) discussed the differences between the V-g method and the so-called "British" or p-k method and presented a method based on computing roots of the determinant of the dynamic matrix. Mantegazza (Reference 30) differentiates the flutter equation with respect to velocity and uses an initial-value ordinary differential equation solver to compute the solution curve; this type of continuation method will be discussed in the next section. The fundamental difference between the V-g method and methods such as presented in Reference 30 is that instead of viewing the flutter equations as an eigenvalue problem, they are treated as a set of nonlinear algebraic equations, allowing far more general definitions of the terms in the flutter equations. In this appendix we discuss a class of methods which have been developed in several fields for the solution of nonlinear equations, known collectively as continuation methods.

Continuation methods are a class of methods for the solution of nonlinear equations which have been used extensively in nonlinear structural mechanics, among other fields. In general, continuation methods are used to compute solutions to systems of underdetermined nonlinear equations over a specified

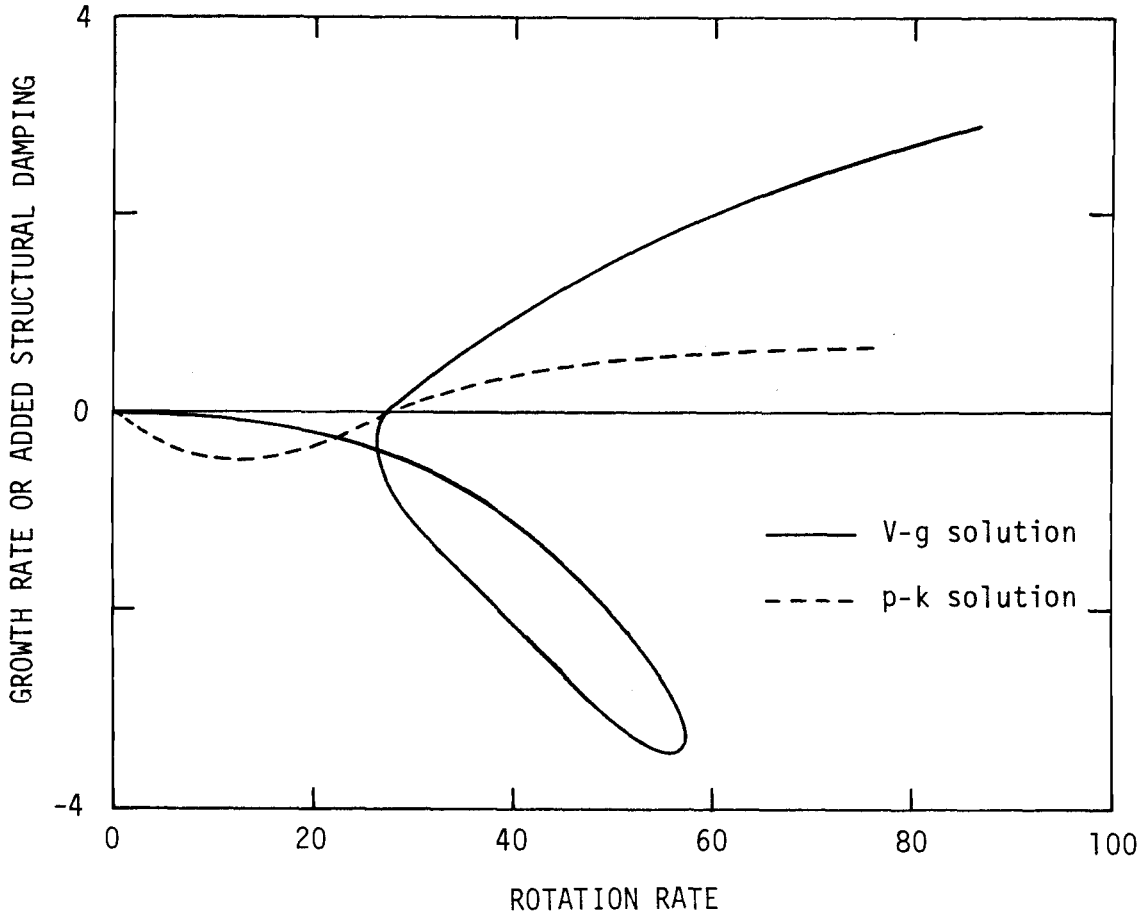

Figure 28. Comparison Between p-k and V-g Solution Techniques

range. In structural mechanics the underdetermined system is a result of imbedding an exactly determined system of equations in a one-parameter family of equations for which a known solution exists when the parameter is zero, while the solution to the original pro blem exists at some other value of the parameter. Using discrete steps in the parameter and solving the nonlinear equations at each step results in a series of nonlinear equations which are solved using a predictor-corrector process, analagous to the predictor-corrector methods used to solve initial-value ordinary differential equations.

The interest in solving the flutter equations is usually to find the critical flutter speed, at which point the body experiences self-sustained neutrally stable oscillations, due to the interaction with the fluid; also of interest is how this flutter speed varies with changes in certain of the system parameters. Both of these problems are amenable to solution using the contination methods. The purpose of this appendix then is to give a brief review of continuation processes in general, to describe a new contination process, and to show how it may be applied to solutions of the flutter equations.

The Linear Flutter Equation

The problem of primary interest here is the linear flutter equation

$$\mathbf{D}(p,r)\mathbf{u} = \mathbf{r} = \mathbf{0} \tag{1}$$

where $\mathbf{r}$ is the residual vector. Commonly the interest is in finding values of the variables p, r, and $\mathbf{u}$ such that p is

purely imaginary, indicating neutral stability of the system. Often it is also necessary to analyze the variation of these neutral-stability points with a system parameter such as the fluid density or an element of the stiffness matrix. These two types of solution will be termed NS (neutral stability) and PV (parameter variation) solutions.

Since (1) is linear and homogeneous in $\mathbf{u}$ it is necessary to eliminate the trivial solution $\mathbf{u} = \mathbf{0}$. This is usually done by adding a normalization equation of the form

$$r_{n+1} = \mathbf{e}_j^T \mathbf{u} - 1 = 0 \tag{2}$$

where $\mathbf{e}_j$ is the j^{th} column of the identity matrix.

The flutter equations may be formulated as an equivalent real system of 2n equations in the 2n+3 unknowns r, l, g, Re($\mathbf{u}$), and Im($\mathbf{u}$). The main reason for doing this is because the terms flutter equation are not, in general, analytic functions of complex variables. The rotation rate, for instance, is not a complex variable, and the aerodynamic matrix is not an analytic function of p.

Continuation Methods

Continuation methods deal with problems of the form

$$\begin{aligned} &\mathbf{y}(\mathbf{x}) = \mathbf{0} \\ &\mathbf{y}(\mathbf{x}_0) = \mathbf{0} \end{aligned} \tag{3}$$

where $\mathbf{y}$ is in R^m, $\mathbf{x}$ is in R^{m+1}, and $\mathbf{x}_0$ is a known solution. (3) is therefore an underdetermined system of nonlinear equa-

tions which has, in general, an infinity of solutions. Solutions to 34) are curves in m+1-dimensional space.

Starting with the known solution $\mathbf{x}_0$, continuation methods usually compute solutions at increments of the continuation parameter using a predictor-corrector process similar to those used in the solution of ordinary differential equations. Indeed, ODE solvers are commonly used to compute solutions to continuation problems of the form (Reference 14)

$$\begin{aligned} &\mathbf{z}(\mathbf{x};t) = \mathbf{0} \\ &\mathbf{x} = \mathbf{x}(t) \\ &\mathbf{x}_0 = \mathbf{x}(0) \end{aligned} \tag{4}$$

where $\mathbf{z}$ and $\mathbf{x}$ are in R^m and t is a parameter. In many cases it is possible to transform a problem which is in the form (3) into this form; for example, as mentioned earlier Mantegazza (Reference 30) does this with the flutter equations by setting t = V (or r in our case). Differentiation of (4) with respect to t then yeilds

$$d\mathbf{z}/dt = \mathbf{J}\mathbf{x}'(t) + \mathbf{z}_t \tag{5}$$

where $\mathbf{J}$ is the Jacobian matrix of partial derivatives of z with respect to $\mathbf{x}$ and $\mathbf{z}_t$ is the partial of $\mathbf{z}$ with respect to t. The solution curve is then described by solutions to the system of ordinary differential equations

$$\mathbf{x}'(t) = -\mathbf{J}^{-1}\mathbf{z}_t(\mathbf{x},t) \tag{6}$$

$$\mathbf{x}(0) = \mathbf{x}_0$$

which can be computed using any of the ODE solvers. As an example of this technique, a common method for solving (3) is to pick an arbitrary vector $\mathbf{x}_0$ and define

$$\mathbf{z}(\mathbf{x},t) = \mathbf{y}(\mathbf{x}) + (t-1)\mathbf{y}(\mathbf{x}_0) \tag{7}$$

Note that when $t = 0$, $\mathbf{x}_0$ is a solution to $\mathbf{z}(x,t) = \mathbf{0}$, while at $t = 1$, the solution to (7) is also a solution to (3). Differentiating (7) with respect to the continuation parameter t results in the initial-value problem

$$\mathbf{x}'(t) = -\mathbf{J}^{-1}(\mathbf{x})\mathbf{y}(\mathbf{x}_0) \tag{8}$$

$$\mathbf{x}(0) = \mathbf{x}_0$$

which can be integrated from $t = 0$ to $t = 1$ using any of a number of methods (Reference 25). The desired solution to (3) is obtained when $t = 1$.

There are, however important differences between continuation problems and initial-value ODEs. The most important difference, as pointed out by Rheinboldt (Reference 32), is that with ODE solvers the error in the solution at each point on the curve is dependent upon the solution errors at all previous points on the curve, hence on the size of each previous step in the continuation parameter; in a continuation process this is not the case since the error at each point is dependent only on the termination criteria for the corrector. The step size in a continuation method is therefore limited only by the convergence properties of the corrector, and in general it is desirable to use as large a step-size as possible while still obtaining convergence in the corrector process.

Parameterization of the Underdetermined System

To some extent the choice of the parameter t depends on the requirements of the problem. Some problems contain a variable which would appear to be a natural choice for t. For instance, in nonlinear structural mechanics (Reference 32) the interest is in solutions to equations of the form

$$\mathbf{K}(\mathbf{x})\mathbf{x} = \mathbf{p} \tag{9}$$

where $\mathbf{K}$ is the (n,n) nonlinear stiffness matrix, $\mathbf{x}$ is an n-vector of generalized coordinates, and $\mathbf{p}$ is the load vector. This equation is usually recast in the form

$$\mathbf{K}(\mathbf{x})\mathbf{x}(t) = t\mathbf{p} \tag{10}$$
$$\mathbf{x}(0) = \mathbf{0}$$

That is, the continuation parameter t is chosen as a scalar multiplier of the load vector and the solution is found when $t = 1$. The main problem with this formulation is that there may be points on the solution curve where $\mathbf{x}'(t)$ is unbounded; that is, the solution curve might contain limit points or bifurcation points.

In the case of the flutter equations a natural choice for the continuation parameter for an NS solution is the rotation rate, and for a PV solution the system parameter which is varied. Here again, however, it is possible that the solution curve may contain limit points with respect to r or p, so we are interested in other choices for the continuation parameter which do not have this potential problem.

A parameter which avoids the problem of limit points is

the arc-length along the solution curve (References 32, 33). Since we compute solutions at discrete points on the solution curve we can only compute approximations to the arc-length segments as the norm of the secant vector

$$\mathbf{s}_{k+1} = \mathbf{x}_{k+1} - \mathbf{x}_k \tag{11}$$

where $\mathbf{x}_k$ is the solution on the k^{th} increment along the curve. The fact that $t_{k+1} = (\mathbf{s}_{k+1}^T \mathbf{s}_{k+1})^{\frac{1}{2}}$ is only an approximation to the arc-length is not important since we are not usually concerned with the actual values of the arc-length; it is merely a convenient continuation parameter. By using arc-length as the continuation parameter t, $\mathbf{x}'(t)$ becomes the tangent to the solution curve, which for flutter solution curves is almost always well-behaved.

The tangent vector is the vector $\mathbf{v}_k$ such that

$$\mathbf{J}_k \mathbf{v}_k = \mathbf{0} \tag{12a}$$

$$\mathbf{v}_k^T \mathbf{v}_k = 1 \tag{12b}$$

$$\mathbf{v}_{k-1}^T \mathbf{v}_k \quad 0 \tag{12c}$$

Hence $\mathbf{v}_k$ lies in the null space of $\mathbf{J}_k$, the Jacobian matrix evaluated at $\mathbf{x}_k$. The condition (12c) ensures that the tangent vector has the same orientation relative to the curve that the previous tangent vector had. Thus an additional piece of information required to start the process is an approximate starting tangent vector which determines the direction along the curve the solution will trace. Usually it is sufficient to set $\mathbf{v}_0 = \pm \mathbf{e}_j$ with the sign and the index j chosen to reflect

the desired direction along the curve.

The tangent vector given by (12) is unique provided J_k has rank m; if the Jacobian has rank less than m it is still possible to compute a tangent vector, although it will not necessarily be unique; this problem is discussed in more detail below.

From a known solution point $\mathbf{x}_k$, an approximation to the next solution point is obtained from the Euler predictor

$$\mathbf{x}_{k+1}^0 = \mathbf{x}_k + t_k^0 \mathbf{v}_k \tag{13}$$

where t_k^0 is the desired arc-length for this step and $\mathbf{v}_k$ is the tangent to the solution curve at $\mathbf{x}_k$. Using the predicted value of $\mathbf{x}_{k+1}$, a correction process is applied to compute the solution $\mathbf{x}_{k+1}$. The approximate arc-length for this step then is given by (11).

A New Corrector Process

Dropping subscripts and concentrating on the corrector process, we are faced with the problem of finding a solution to the underdetermined system of equations $\mathbf{y}(\mathbf{x}) = \mathbf{0}$ using $\mathbf{x}^0 = \mathbf{x}_k + t^0\mathbf{v}_k$ as an initial guess to the solution $\mathbf{x}^*$. Normally this system of m equations in m+1 unknown is augmented with an $(m+1)^{st}$ equation of the form $\mathbf{e}_j^T\mathbf{x} = 0$, which fixes the value of one of the variables for the corrector iterations. The resulting $(m+1)^{st}$ order system can then be solved using, for instance, Newton's method, which in our notation may be written as

$$\mathbf{x}^{i+1} = \mathbf{x}^i - \mathbf{J}^{-1}(\mathbf{x}^i)\mathbf{y}(\mathbf{x}^i) \tag{14}$$

Here we choose to solve the underdetermined system directly, rather than augmenting the equations. Naturally since the underdetermined system has an infinity of solutions it is necessary to somehow restrict the solution; this added flexibility is perhaps the most attractive feature of this method. Denoting the Jacobian matrix evaluated at $\mathbf{x}^i$ by $\mathbf{J}^i$ and $\mathbf{y}(\mathbf{x}^i)$ by $\mathbf{y}^i$, a linear approximation to $\mathbf{y}$ at $\mathbf{x}^i$ is

$$\mathbf{y}(\mathbf{x}^i+\mathbf{h}) = \mathbf{y}^i + \mathbf{J}^i\mathbf{h} \tag{15}$$

As in Newton's method we require the next iterate to satisfy

$$\mathbf{J}^i\mathbf{h} = -\mathbf{y}^i \tag{16}$$

$$\mathbf{h} = \mathbf{x}^{i+1} - \mathbf{x}^i$$

This underdetermined linear system has an infinity of solutions; indeed, if $\mathbf{h}$ satisfies (16) and $\mathbf{v}$ is in the null space of $\mathbf{J}^i$, then $\mathbf{h} + a\mathbf{v}$ also satisfies (16) for any a. A natural choice for $\mathbf{h}$ is the shortest vector (in some sense) which satisfies (16). That is, we want to pick the $\mathbf{h}$ which solves the minimization problem (dropping superscripts)

$$\begin{aligned} &\text{minimize} \quad \mathbf{h}^T\mathbf{h} \\ &\quad \mathbf{h} \\ &\text{subject to} \quad \mathbf{Jh} = -\mathbf{y} \end{aligned} \tag{17}$$

Using a lagrange multiplier $\mathbf{l}$ we can rewrite the problem as

$$\begin{aligned} &\text{minimize} \quad \mathbf{h}^t\mathbf{h} - 2\mathbf{l}^T(J\mathbf{h} + \mathbf{y}) \\ &\quad \mathbf{h} \\ &\text{subject to} \quad J\mathbf{h} = -\mathbf{y} \end{aligned} \tag{18}$$

A necessary condition for a minimum is that the derivative with respect to $\mathbf{h}$ be zero. This requirement leads to

$$\begin{bmatrix} I & J^T \\ J & 0 \end{bmatrix} \begin{bmatrix} \mathbf{h} \\ \mathbf{l} \end{bmatrix} = \begin{bmatrix} 0 \\ -\mathbf{y} \end{bmatrix} \tag{19}$$

which has the solution

$$\begin{bmatrix} \mathbf{h} \\ \mathbf{l} \end{bmatrix} = \begin{bmatrix} I-J^T(JJ^T)^{-1}J & J^T(J^{-1}J^T)^{-1} \\ (J^{-1}J^T)^{-1}J & -(JJ^T)^{-1} \end{bmatrix} \begin{bmatrix} 0 \\ -\mathbf{y} \end{bmatrix} \tag{20}$$

Thus the shortest $\mathbf{h}$ which satisfies (16) is

$$\mathbf{h} = -J^T(J^{-1}J^T)^{-1}\mathbf{y} \tag{21}$$

and the corrector iteration process (with superscripts) is

$$\mathbf{x}^{i+1} = \mathbf{x}^i + \mathbf{h}^{i+1} = \mathbf{x}^i - J^T(JJ^T)^{-1}\mathbf{y}^i \tag{22}$$

Note that if both $\mathbf{x}$ and $\mathbf{y}$ are in R^m, the iteration reduces to Newton's method.

Computational Aspects

Computationally speaking, the corrector process in the form (22) requires far more work than the Newton iteration

(14). In order to make the iterations (22) more efficient, we introduce the QR decomposition of the Jacobian (Reference 25). Any (m,n) rectangular matrix may be decomposed into the product of an (m,n) matrix **Q**, the columns of which are orthonormal, times an (n,n) upper-triangular matrix **R**. Also, in the case where m n, there is associated with the QR decomposition an (m,m-n) matrix **N**, the columns of which span the null space of **X**; that is

$$\mathbf{X} = \begin{bmatrix} \mathbf{Q} & \mathbf{N} \end{bmatrix} \begin{bmatrix} \mathbf{R} \\ \mathbf{0} \end{bmatrix}$$
$$\mathbf{XN} = \mathbf{0} \tag{23}$$

For our purposes we write

$$\mathbf{J}^T\mathbf{E} = \mathbf{QR} = \begin{bmatrix} \mathbf{Q} & \mathbf{n} \end{bmatrix} \begin{bmatrix} \mathbf{R} \\ \mathbf{0} \end{bmatrix} \tag{24}$$

where **E** is a permutation matrix which reflects column pivoting done during the decomposition for numerical stability, and **n** is the null space vector. The relationship between the null space vector **n**, which is a by-product of the QR decomposition, and the tangent vector defined by (12) can be seen by writing

$$\mathbf{R}^T\mathbf{Q}^T\mathbf{n} = \mathbf{E}^T\mathbf{J}\mathbf{n} = \mathbf{0}$$

from which we conclude that $\mathbf{v} = \pm \mathbf{n}$, where the sign is chosen to satisfy (12c).

Substituting (24) into (22) and using the fact that **E** is an orthogonal matrix and the columns of **Q** are orthonormal,

$$\mathbf{h} = -\mathbf{Q}(\mathbf{Q}^T\mathbf{Q})^{-1}\mathbf{R}^{-T}\mathbf{E}^T\mathbf{y} = -\mathbf{Q}\mathbf{R}^{-T}\mathbf{E}^T\mathbf{y} \tag{26}$$

The additional effort involved in this iteration procedure over Newton's method comes from the fact that the QR decomposition requires approximately twice as many operations as the LU factorization normally used with Newton's method. However, the QR facorization offers the advantage that it is more stable than the LU factorization. If pivoting is used in the factorization it is possible to isolate singularities in the Jacobian; if the rank of **J** is r n, matrix **R** will have the form

$$\mathbf{R} = \begin{bmatrix} \mathbf{R}_{11} & \mathbf{R}_{12} \\ \mathbf{0} & \mathbf{0} \end{bmatrix} \tag{27}$$

where $\mathbf{R}_{11}$ is (r,r) upper-triangular, and (24) becomes

$$\mathbf{J}^T\mathbf{E} = \begin{bmatrix} \mathbf{Q}_1 & \mathbf{N} \end{bmatrix} \begin{bmatrix} \mathbf{R} \\ \mathbf{0} \end{bmatrix} \tag{28}$$

where the null space matrix **N** now has n - r + 1 columns. Thus it is possible to continue the iterations using $\mathbf{Q}_1\mathbf{R}_{11}$ instead of **QR** and the vector **h** defined by (26) is still the shortest vector which satisfies (16). In this rank-deficient case the tangent vector is no longer unique, due to the fact that the null space matrix has (n-r+1) columns. A natural condition to place on the tangent vector to ensure uniqueness in this case is to pick the vector which is closest to the tangent vector from the previous step; that is we pick the tangent vector as the projection of the previous tangent vector onto the current null space. This leads to (Reference 26)

$$\mathbf{v}_{k+1} = \pm c\mathbf{N}\mathbf{N}^T\mathbf{v}_k \tag{29}$$

where c is a normalizing factor chosen to satisfy (12b) and the sign is chosen to satisfy (12c).

Step Size Selection

Perhaps the most important, yet at the same time the most difficult aspect of a continuation process is the choice of the predictor step size t_k. If the step size is too large the corrector iterations may not converge or may converge to the wrong root, while small steps require extra computational effort. Recently Den Heijer and Rheinboldt (Reference 37) presented a set of algorithms both for the case of a Newton corrector, and for the general corrector process. We present here a somewhat modified version of the step-length algorithm for the general corrector process as presented in Reference 37.

Evidently what is needed in a step-length algoritm is a way to tell if the corrector is likely to converge from a predicted point, which in turn requires that we can estimate the distance between the predicted point and the solution. An estimate of the distance between the predicted point and the solution in the case of the Euler predictor (13) is simply given by the norm of the third term in the Taylor's series expansion of $\mathbf{x}(t)$ about the previous solution

$$d = \tfrac{1}{2}t^2 \left\| \mathbf{x}''(t) \right\| = \tfrac{1}{2}t^2 \left\| \mathbf{v}'(t) \right\| \tag{30}$$

If the rate of change of the tangent vector is approximated by

$$\mathbf{v}'(t) \doteq \frac{2}{t_k}\left(\mathbf{v}_k - \frac{1}{t_k}\mathbf{s}_k\right) \tag{31}$$

then for a desired distance d^0 between the predicted and corrected solutions

$$t_{k+1}^{0} = \frac{d^{0} t_k}{\sqrt{2(1 - \frac{1}{t_k} \mathbf{v}_k^T \mathbf{s}_k)}} = f t_k \tag{32}$$

If we knew the convergence radius for the corrector we could use it for d^0 and thus obtain the maximum permissible step-size. Here we take a sligthly different approach and attempt to pick a step-size which will result in a pre-selected number of iterations. If the number of iterations required on the previous step was i_k and the distance between the predicted and converged solutions was d_k, then by setting

$$d^0 = \frac{i_m}{i_k} d_k \tag{33}$$

the number of iterations at each step will tend to be i_m provided the convergence behavior is the same at each step. In order to stabilize the step-length selection process it is necessary to limit the change in step-size by requiring that

$$1/b < f < b \tag{34}$$

where b is some number greater than 1, say 2 or 3. Furthermore, if the curvature is small, the distances d_k will tend to become small, and the step-length algorithm will tend to be the ratio of two small numbers. Recognizing that (30) represents only an approximation to the distance between the predicted and corrected solutions, we allow for error in this quantity by introducing a lower threshold on the quantity

$$q = (1 - \frac{1}{t_k} \mathbf{s}_k^T \mathbf{v}_k)^{\frac{1}{2}}, \tag{35}$$

or equivalently, on the angle between the secant and tangent

vectors. That is let

$$t^0_{k+1} = \frac{d^0 t_k}{\sqrt{\max\,(q,\ q_{min})}} \tag{36}$$

Updating the QR Factorization

Rather than evaluate and decompose the Jacobian with each iteration, it is more usually economical to use the QR factors for more than one iteration. Implicit in the changes in **x** and **y** with each iteration is information about the Jacobian, and changes in the Jacobian. Exploiting this information to modify the Jacobian so that it more closely approximates the true Jacobian is the idea behind the update or quasi-Newton methods.

Update methods modify the Jacobian its factors using low-rank matrices for computational convenience. Broyden (Reference 34) gives a number of rank-one and rank-two update formulas suitable for square matrices. Since we are working here with a rectangular Jacobian the choice is limited to a rank-one formula of the form

$$\mathbf{J}^{i+1} = \mathbf{J}^i + \mathbf{a}\mathbf{b}^T \tag{37}$$

where **a** is in R^m and **b** is in R^{m+1}. It can be readily verified that choices for **a** and **b** which satisfy the so-called "divided difference" requirement

$$\mathbf{J}^{i+1}\mathbf{h} = \mathbf{y}^{i+1} - \mathbf{y}^i \tag{38}$$

are

$$\mathbf{a} = q\mathbf{y}^i, \qquad q = 1/\mathbf{y}^{iT}\mathbf{y}^i, \qquad \mathbf{b} = \mathbf{h}. \tag{39}$$

Rather than modify the Jacobian it is more economical to modify the QR factors directly. Substituting (35) and (37) into (24)

$$\mathbf{J}^{i+1T}\mathbf{E} = \mathbf{QR} + \mathbf{E}^T\mathbf{ba}^T = \begin{pmatrix}\mathbf{Q} & \mathbf{v}\end{pmatrix}\begin{bmatrix}\mathbf{R}\\ \mathbf{0}\end{bmatrix} + \mathbf{wa}^T$$

where $\mathbf{w} = \begin{pmatrix}\mathbf{Q} & \mathbf{v}\end{pmatrix}^T\mathbf{E}^T\mathbf{b}$. Next, using a sequence of Givens rotations we can pick an orthogonal matrix G such that $\mathbf{Gw} = \mathbf{we}_1$, where $\mathbf{e}_1$ is the first column of the identity matrix. Thus

$$\mathbf{J}^{i+1T}\mathbf{E} = \mathbf{QG}^T\begin{bmatrix}\mathbf{GR}\\ \mathbf{0}\end{bmatrix} + \mathbf{e}_1\mathbf{a}^T.$$

From the properties of the Givens transformations (Reference 26) it is easily shown that GR is in upper-Hessenberg form, and therefore the matrix $\mathbf{GR} + \mathbf{e}_1\mathbf{a}^T$ is also in upper-Hessenberg form. Now we pick another sequence of Givens transformations which comprise a matrix H such that $\mathbf{H}(\mathbf{GR} + \mathbf{e}_1\mathbf{a}^T)$ is upper-triangular, hence is the updated R factor. The updated Q factor is then $\mathbf{QG}^T\mathbf{H}^T$.

Application to the Flutter Equation

The continuation process described in the preceding sections can be used for either NS or PV solutions of the flutter equations by setting

$$\mathbf{y}(\mathbf{x}) = \begin{Bmatrix} \mathrm{Re}(r_1) \\ \mathrm{Im}(r_1) \\ \cdot \\ \cdot \\ \mathrm{Re}(r_{2n+1}) \\ \mathrm{Im}(r_{2n+1}) \end{Bmatrix}$$

where in the case of an NS solution

$$\mathbf{x} = \begin{Bmatrix} r \\ \omega \\ g \\ \mathrm{Re}(u_1) \\ \mathrm{Im}(u_1) \\ \cdot \\ \cdot \\ \mathrm{Re}(u_n) \\ \mathrm{Im}(u_n) \end{Bmatrix}$$

and for a PV solution in which some parameter w, such as mass density or a stiffness parameter, is varied over a specified range,

$$\mathbf{x} = \begin{Bmatrix} r \\ \omega \\ w \\ \mathrm{Re}(u_1) \\ \mathrm{Im}(u_1) \\ \cdot \\ \cdot \\ \mathrm{Re}(u_n) \\ \mathrm{Im}(u_n) \end{Bmatrix}$$

Although we do not treat the case of nonlinear flutter here we note in passing that this case is readily accounted for by writting

$$\mathbf{y}(\mathbf{x}) = \mathbf{D}(p,r,\mathbf{u})\mathbf{u}$$

In the case of a neutral-stability solution, the Jacobian matrix has the form

$$\mathbf{J} = \begin{bmatrix} \mathbf{D}_1\mathbf{u} & \mathbf{D}_2\mathbf{u} & \mathbf{D}_3\mathbf{u} & \mathbf{D} \end{bmatrix}$$

where $\mathbf{D}_1$, $\mathbf{D}_2$ and $\mathbf{D}_3$ are the partials of $\mathbf{D}$ with respect to r, ω, and g, respectively.

Starting points for the continuation process in an NS solution are found by solving the free-vibration eigenvalue problem at r = 0,

$$(p^2\mathbf{M} + \mathbf{K})\mathbf{u} = \mathbf{0}$$

This generalized eigenvalue problem yeilds n pair of eigenvalues and eigenvectors, each of which may be used as the starting point for a continuation solution curve. Normally, the aerodynamics matrix is only defined within certain ranges of reduced frequency (k*). Solutions outside these ranges, for instance from zero velocity up to the minimum velocity, can be obtained by using a fixed value of the aerodynamics matrix evaluated at the nearest valid point. Starting points for PV solutions are the neutral-stability points found in an NS solution.

APPENDIX C. WORK AND ENERGY

For an oscillating conservative system the integral of the total energy leads to the law of the conservation of energy (Reference 38). On the other hand, for a nonconvservative system such as a fluttering system the energy integral leads to an equation relating the change in total energy of the system to the work done on the system by external forces. Here we take external forces to mean internal damping forces as well as external aerodynamic forces. The rate of decay or growth of oscillations depends on the rate at which work is done on the structure by the surrounding air. If the net work done on the system by the air over one cycle of oscillation is positive, the amplitude of the oscillations will grow, while if the work is negative the oscillations will decay. At the same time the kinetic and potential energies of the system are changing in response to the work done by external forces. An analysis of the mechanism by which work is done on the system can give insight into the causes of flutter. Two aspects of the analysis of the work done on the system are the genesis of the forces and the way in which these forces contribute to the total work.

The external forces associated with linear flutter equations are always homogeneous and linear in the generalized coordinates, hence there is a one-to-one correspondence between the external forces and the generalized coordinates which give rise to them. Thus by identifying which forces cause the flutter instability we can further identify the generalized coordinates which give rise to these destabilizing forces.

In general, motion of the system involves displacements in

each of the generalized coordinates. Thus the total work on the system may be broken down according to the contributions of the external forces acting through displacements of each of the generalized coordinates. Some of these contributions may be positive and therefore destabilizing, while others may be negative or stabilizing. While it is the sum of all the contributions to the total work which determines whether or not the motion is stable or unstable, the individual contributions show which generalized coordinates are responsible for absorbing or dissipating energy to the airstream.

The total energy of the system, taken here to be the sum of the kinetic and potential energies, can likewise be broken down into contributions from each of the generalized coordinates. If the generalized coordinates are completely uncoupled the change in energy associated with each generalized coordinate is stricly due to a change in the amplitude of oscillation of that coordinate; on the other hand if the generalized coordinates are coupled an additional part of the change in energy associated with a particular coordinate will be due to changes in amplitudes of the other coordinates. In either case the total change in energy is due to changes in the amplitudes of oscillation of the generalized coordinates, and is therefore related to the rate of growth or decay of the oscillations and the complex vector of generalized coordinate amplitudes obtained in the solution of the flutter equations.

Expressions for Work and Energy

In Reference 39 Crisp derived expressions for the work done by aerodynamic forces on a linear system undergoing steady

oscillations (flutter); here we extend this to include systems in which the oscillations are growing or decaying. It is customary when discussing periodic solutions to linear systems to use the complex representation of the generalized coordinates and forces, where it is understood that it is only the real part which is of interest. At a particular rotation rate the flutter equations may be written as

$$(p^2\mathbf{M} + p\mathbf{G} + \mathbf{K})\mathbf{u} = -(\mathbf{A} + ig_s\mathbf{K})\mathbf{u}$$

$$= \mathbf{f}(\mathbf{u}) \tag{1}$$

in which $\mathbf{f}$ is a complex vector representing nonconservative forces due to the aerodynamics and structural damping, the generalized coordinates as functions of time are given by

$$\mathbf{z}(t) = \mathrm{Re}(\mathbf{u}e^{pt}) \tag{2}$$

and $p = \omega(\frac{1}{2}g + i)$ is the characteristic exponent. For a differential change in the coordinates the work done on the system by these forces is

$$\begin{aligned} dW &= \mathrm{Re}(f_1)dz_1 + \mathrm{Re}(f_2)dz_2 + \ldots + \mathrm{Re}(f_n)dz_n \\ &= (\mathrm{Re}(f_1)z_1 + \mathrm{Re}(f_2)z_2 + \ldots + \mathrm{Re}(f_n)z_n)dt \end{aligned} \tag{3}$$

and the work done on the system between time t_1 and t_2 is

$$W = \sum \sum W_{jk} \tag{4}$$

where

$$W_{jk} = \int \mathrm{Re}(z_j F_{jk} z_k)\,dt \tag{5}$$

is the work done on the system by the nonconservative forces resulting from displacement of the k^{th} coordinate acting through displacement of the j^{th} coordinate, and

$$\mathbf{F} = -(\mathbf{A} + ig_s\mathbf{K}) \tag{6}$$

is a matrix relating the generalized coordinates to the nonconservative forces. Substituting (2) into (5) and integrating over one cycle of oscillation results in

$$\begin{aligned}\frac{4gW_{jk}}{e^{2\pi g}-1} &= 2\,\mathrm{Im}(\bar{u}_j F_{jk} u_k) \\ &\quad + g\,\mathrm{Re}(\bar{u}_j F_{jk} u_k) \\ &\quad + g\,\mathrm{Re}(u_j F_{jk} u_k)\end{aligned} \tag{7}$$

where $\bar{(\ )}$ indicates complex conjugate. At flutter, $g = 0$ and (7) reduces to

$$W_{jk} = \pi\,\mathrm{Im}(u_j F_{jk} u_k) \tag{8}$$

which is equivalent to the result in Reference 39.

Each term W_{jk} in (7) may be interpreted as the contribution to the total work done on the system by forces arising from a displacement in the k^{th} coordinate, acting on the j^{th} coordinate through one cycle of oscillation. Thus, for example in figure (17) the total work on the system in

aeroelastic mode S1 is primarily due to forces induced by coordinates 1, 3, and 5. The resulting work on coordinate 1 due to forces induced by motion in coordinate 5 (W_{15}) is destabilizing, while the work on coordinate 1 due to forces induced by motion in coordinate 1 (W_{11}) is stabilizing.